ACOUSTIC EMISSION MONITORING

OF

ELECTRICAL DISCHARGE MACHINING

ACOUSTIC EMISSION MONITORING

OF

ELECTRICAL DISCHARGE MACHINING

By

ALEXANDER W. GOODLET, B.ENG.MGT

A Thesis

Submitted to the School of Graduate Studies

In Partial Fulfillment of the Requirements

For the Degree

Master of Applied Science

McMaster University

MASTER OF APPLIED SCIENCE (2013)	McMaster University
(Department of Mechanical Engineering)	Hamilton, Ontario

TITLE:	Acoustic Emission Monitoring of Electrical Discharge Machining
AUTHOR:	Alexander W. Goodlet, B.Eng.Mgt (McMaster University)
SUPERVISOR:	Dr. Philip Koshy
NUMBER OF PAGES:	116

Abstract

Electrical discharge machining (EDM) is a non-conventional machining process in which material removal is accomplished through spark erosion between a workpiece and tool electrode. Process stability is of great importance to the productivity of the EDM process, especially in the wire EDM configuration where an unstable process could lead to wire breakage having a detrimental effect on productivity. This thesis investigates the application of acoustic emission (AE) in EDM as a process monitoring technique. AE techniques have been applied to almost all machining processes; however its benefit as applied to EDM has not been investigated yet. The AE signal from the EDM process is related to various EDM parameters including, electrical parameters, tool materials, flushing and some process modifications, such as dispersing metallic powder into the gap. Using this knowledge, the benefits of using an AE sensor for a real-time process monitoring technique have been proven.

Acknowledgements

First and foremost, I would like to thank my supervisor, Dr. Philip Koshy. With his innovative ideas and constant strive to pursue exciting new research areas, it made working with him a rewarding experience. Through many of the roadblocks that have been encountered over the past two years, Dr. Koshy was always there to provide support and encouragement. Where others would simply accept hitting a dead end, Dr. Koshy would find a way to make a new route. The level of trust given to me over the past two years by Dr. Koshy has allowed to me to mature greatly as an engineer and as an individual. By being a part of his research group that promotes creative thinking, or just brainstorming over coffee with him, I could not have asked for a better supervisor!

I would like to thank the technicians in the department; Terry, Ron, Mark, Jim, Joe and Mike for their help with purchasing materials and providing advice with everyday situations such as machining or using new equipment.

Most importantly, I would like to thank my family. They have always supported me in everything that I do, and I am extremely grateful to have such an amazing family.

Finally, if you did not get mentioned but are taking the time to read my thesis, then I would like to thank you as well!

Table of Contents

List of Figures

List of Tables

1 Introduction

In today's machining industry, process monitoring plays a vital role in the research and development of several machining processes. Process stability, surface quality, and material removal rates are all important aspects of machining that are in constant demand for improvement. In conventional machining processes such as milling and turning, several process monitoring techniques have been extensively researched and employed. In the case of the non-conventional electrical discharge machining (EDM), very few process monitoring techniques have been investigated. Currently EDM is monitored by only the voltage and current signals, and lacks a reliable tool to monitor the process stability.

This thesis will explore the use of an acoustic emission (AE) sensor as a real-time monitoring tool for EDM. The intent is to use acoustic emission to improve process stability and enhance material removal rates. This chapter will provide a general introduction and background to electrical discharge machining and acoustic emission, in terms of how they relate to the scope of this thesis.

1.1 Electrical Discharge Machining

Electrical discharge machining (EDM) is a non-conventional machining process in which material removal is accomplished through spark erosion between a workpiece and a tool electrode. Conventional machining processes utilize a traditional cutting edge to remove material through direct contact whereas in EDM, the workpiece and tool (or "electrode") are separated by a gap of several micrometres (~10-100 μm) [1]. In conventional machining, the tool needs to be harder than the workpiece unlike in EDM where the electrode can be made from any electrically conductive material, most commonly, copper or graphite. The EDM process takes place in a dielectric fluid that acts as an insulator between the workpiece and electrode. A voltage is applied to the electrode and workpiece as shown in Figure 1.1a. As the electrode approaches the workpiece, the electric field intensifies and the dielectric begins to breakdown as plasma formation begins (Figure 1.1b). The discharge between the electrode and workpiece leads to a flow of current between the electrode and workpiece through this plasma channel. The temperature in this channel can reach 8000-10,000 K [2] which results in melting and vaporization of both the tool and electrode (Figure 1.1c). The plasma channel implodes and ejects material from the molten pool. The molten metal solidifies and is now flushed away as shown in Figure 1.1d.

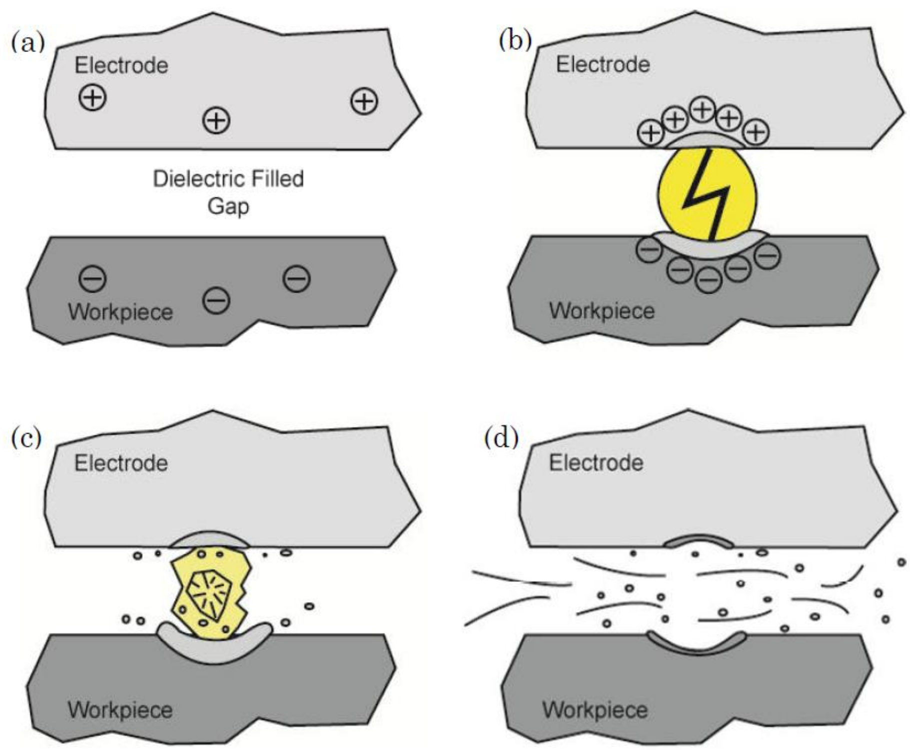

Figure 1.1: Material removal mechanism in EDM process
a) Voltage Applied b) Dielectric Breakdown c) Melting and Vaporization d) Flushing

The material removal mechanism can be represented by a distinct waveform in the voltage and current signal. This desired 'spark' waveform is shown in Figure 1.2, along with three other undesirable waveforms: arcs, short circuits, and open circuits. The desired waveform consists of an ignition time delay (t_d), which is the time taken for the dielectric to break down so the current flow can be initiated. After the ignition time delay, the voltage drops to the working voltage where it remains for the duration of the spark. An arc occurs when the gap is not properly flushed causing local contamination of debris which causes discharge localization due to the spark taking the path of least resistance. Arcing can ultimately lead to scrapping of a part due to this localized material removal. Short circuits occur in the extreme case of arcing when the debris in the gap creates a chain between the electrode and workpiece. Short circuits can leave burn marks on the workpiece greatly affecting surface quality. Current still flows during arcs and sparks, meaning discharge differentiation is difficult with the current signal alone. Finally, open circuits occur when the gap width is too large or the dielectric fluid is not given enough time to ionize, and no current flows. Open circuits do not harm the surface; however they are reducing the material removal rate when they occur.

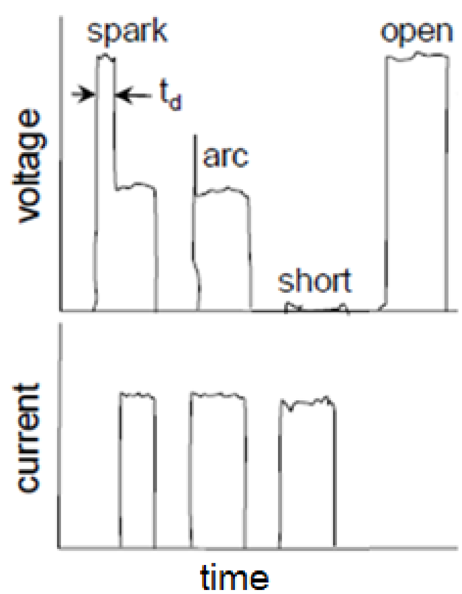

Figure 1.2: Current and voltage waveforms

Due to the high plasma temperatures achieved in EDM discharges, the hardness of the workpiece material is not an issue. These EDM discharges occur rapidly at frequencies from $10^3 - 10^6$ Hz [1], however each discharge removes only $10^{-6} - 10^{-4}$ mm^3 [3] of material from the workpiece, with typically less than 5% of this volume being removed from the electrode [4]. This results in material removal rates up to the order of 100 mm^3/min, which is relatively low compared to traditional machining processes. Due to the small volume removed with each discharge, a surface roughness as fine as Rz 0.4 μm can be achieved [1]. Therefore, while EDM material removal rates are a disadvantage, EDM has the advantage of high accuracy, fine surface finishes, and the ability to machine intricate geometries in hard-to-machine materials as long as they are electrically conductive. EDM is consequently used in aerospace, medical, and tool/die industries.

There are three main different configurations of electrical discharge machining, each with a specific purpose. The three types include ram/sink EDM, wire EDM and fast hole EDM which will now be discussed.

1.1.1 Sink EDM

Sink EDM, also known as ram EDM is generally used to produce cavities in a workpiece that complement the shape of the electrode. An electrode is first machined to the desired shape and then used to reproduce its shape in the workpiece as shown in Figure 1.3. Alternatively, an electrode could be CNC controlled to sweep out the desired shape into the workpiece. In sink EDM, the most common electrode materials are copper and graphite. This is due to the high conductivity of copper and the high melting point of graphite. Unlike conventional machining, the feed rate of the tool electrode is not constant in EDM. A servo control feed maintains the gap width between the electrode and workpiece. If the gap width is too large, the ignition time delay increases which could lead to open circuit, while if the gap width is too small, the ignition time delay decreases which could lead to discharge localization and arcing. An issue with sink EDM is discharge localization occurring in areas that are not exposed to adequate flushing which has a detrimental effect on the material removal rate and surface finish.

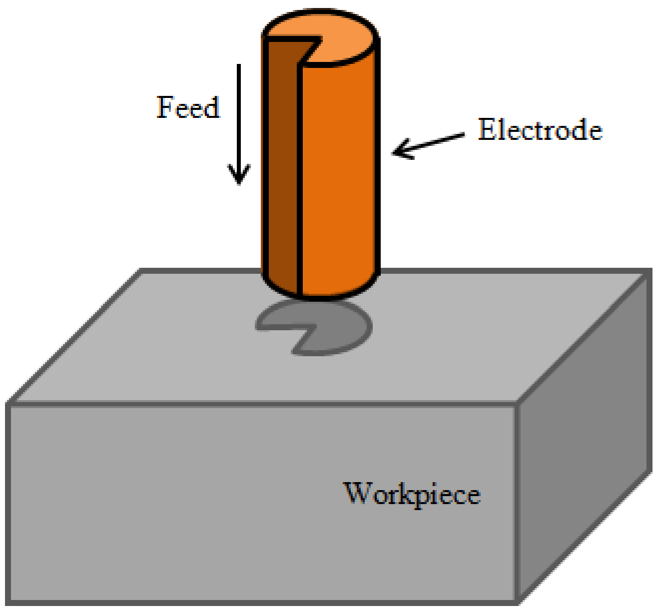

Figure 1.3: Sink EDM

1.1.2 Wire EDM

In wire EDM, a wire held in tension acts as the electrode and is fed through a workpiece to cut out a desired shape as shown in Figure 1.4. The wire is generally a diameter of 0.02 – 0.33 mm and is usually made from brass or in the case of very thin wires, tungsten or molybdenum. Brass or steel wires coated in zinc are also commonly used [1]. Deflection and vibration of the wire, which cause dimensional inaccuracies, are reduced by keeping the wire in tension between the wire guides. New wire is fed through the wire guides to constantly introduce new electrode material to prevent wire breakage and to ensure consistent surface quality. Wire breakage can lead to scrapped parts by ruining the surface finish and also leads to lost machining time. Due to the low material removal rate, wire EDM machines are usually run unattended for large periods of time, therefore a wire breakage can have a detrimental effect on productivity.

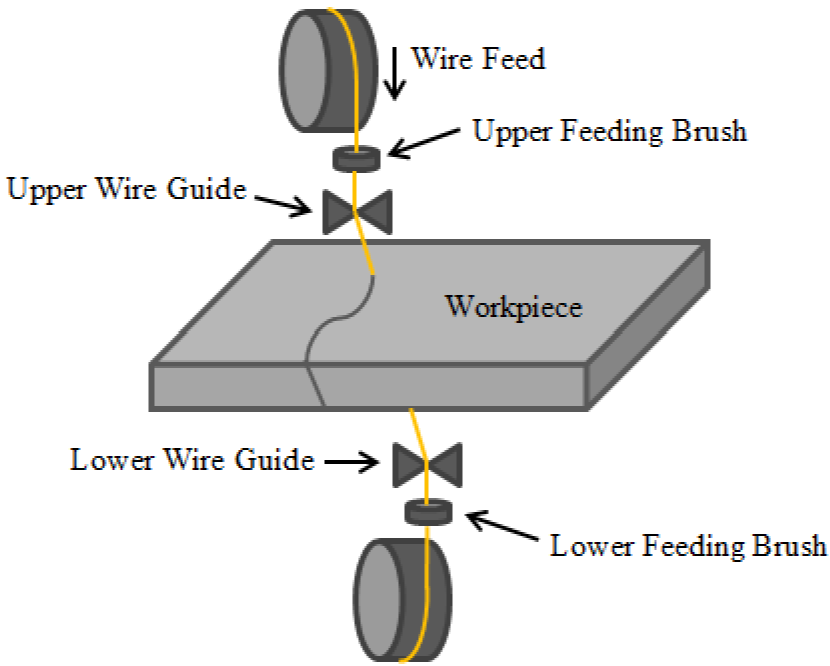

Figure 1.4: Wire EDM

1.1.3 Fast Hole EDM

Fast hole EDM, also known as small hole EDM is used for 'drilling' very small holes into hard metals. Holes are generally a diameter of 0.15 – 3 mm and can have a length-to-diameter ratio of 150:1 [5]. The hollow electrode is plunged into the workpiece while spinning and a dielectric fluid is pumped through the electrode as shown in Figure 1.5. The rotation is to ensure uniform wear and to assist in flushing while the dielectric fluid is pumped through the centre of the hollow electrode to flush out debris and to increase stiffness of the electrode.

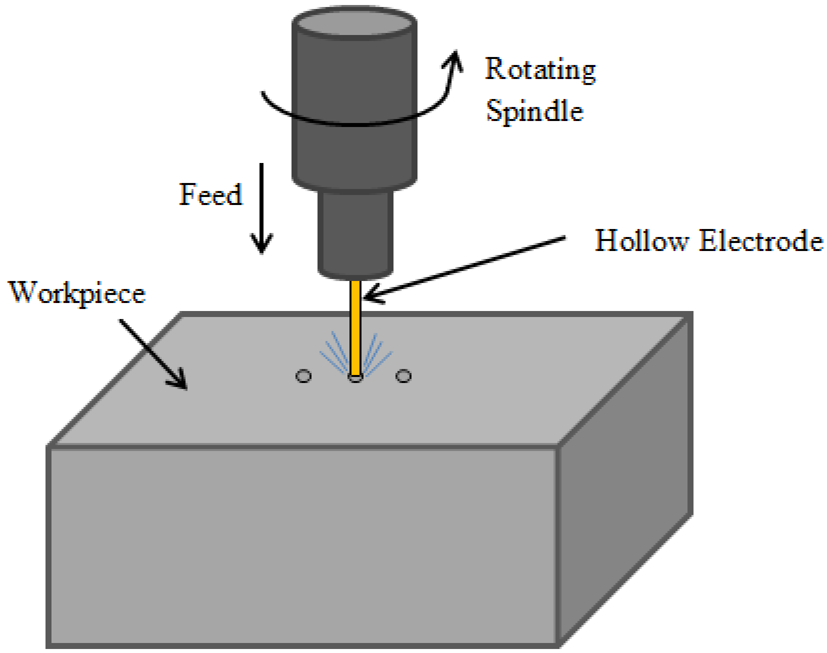

Figure 1.5: Fast hole EDM

1.2 Acoustic Emission (AE)

Acoustic emission testing is a form of non-destructive testing that is applied during loading of a structure as opposed to before or after loading like many testing methods. AE is used to detect fractures at a very early stage long before a structure actually fails, which is done by detecting the elastic waves that propagate from a growing fracture. The detected waves are above the human acoustic range, in the ultrasonic frequency range of 20 kHz to several megahertz. The source of these elastic waves can be from inhomogeneities in phase transformations, melting or solidification, crack growth, surface degradation, etc. [6]. In the manufacturing industry, experienced EDM operators listen to the process to interpret whether the EDM process is stable or not. The issue with this is that it is subjective monitoring and the operators are limited to audible frequencies. This project plans to improve on this technique by removing the human element and 'listen' to the process at much higher frequencies. The heat generated from the EDM process releasing energy into the workpiece provides a source of elastic waves in the workpiece material, making AE a logical method for monitoring the EDM process.

The main advantage of AE is that the workpiece can be observed during the entire process without any disturbance to either the workpiece or the process. A disadvantage with AE is that each AE wave cannot be perfectly repeated due to the random behaviours of crack formations and small inhomogeneities in the workpiece material [7].

1.2.1 Acoustic Wave Modes

In order to use acoustic emission to monitor the EDM process, the various acoustic wave modes should be understood. In solids, there are four principal ways in which sound waves can propagate: longitudinal waves, shear waves, surface waves, and plate waves. In ultrasonics, longitudinal (P-wave) and shear waves (S-wave) are the most common modes used. Longitudinal waves, also known as pressure or compression waves, have the oscillations occur in the same direction as the wave propagation. Shear waves, also known as transverse waves, have the oscillations occur perpendicular to the direction of wave propagation. The particle movements in longitudinal and shear waves are illustrated in Figure 1.6 below.

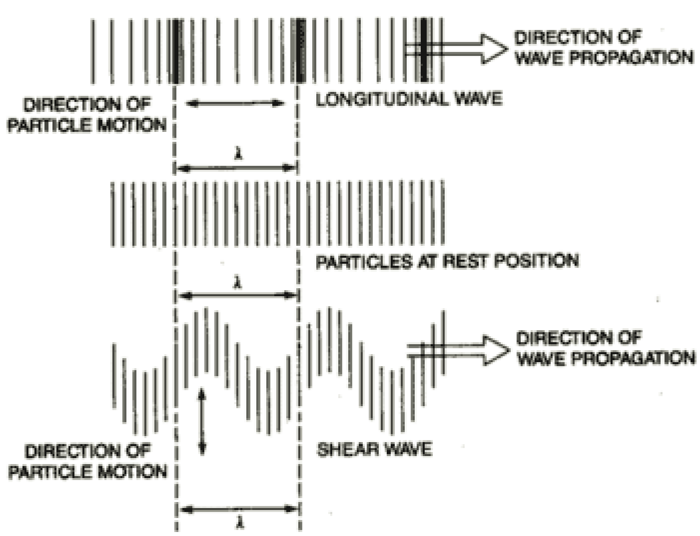

Figure 1.6: Longitudinal and Shear Wave Modes [8]

Surface waves (Rayleigh waves) combine both longitudinal and shear wave modes. The motion becomes an elliptical orbit that creates a rolling motion as illustrated in Figure 1.7. Rayleigh waves travel along the surface of the workpiece and penetrate to a depth of one wavelength [8].

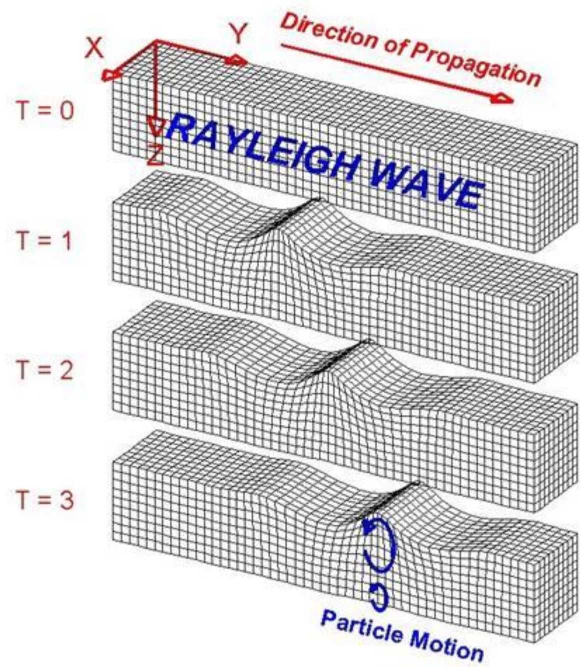

Figure 1.7: Rayleigh Wave Mode [9]

In the case of very thin workpieces, Lamb waves (plate waves) can occur. Lamb waves propagate parallel to the surface and throughout the thickness of the workpiece, with an elliptical orbit motion similar to Rayleigh waves [8]. The Lamb waves occur on both sides of the thin workpiece and there are consequently different modes of particle vibration, most commonly, asymmetric and symmetric as shown in Figure 1.8.

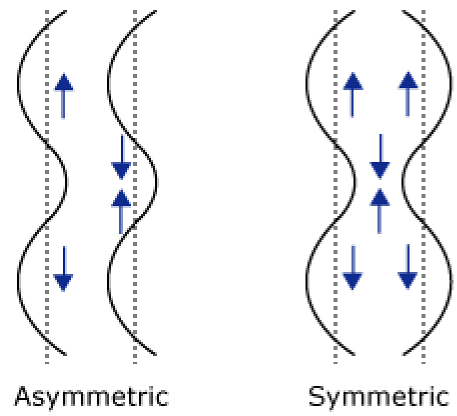

Figure 1.8: Lamb Wave Modes [8]

The four principal wave modes can also be distinguished by their velocity and by their energy. The Rayleigh wave is the slowest and is 0.87 – 0.95 times the speed of the shear wave [8]. The longitudinal wave is the fastest, and the Lamb wave lies in between the longitudinal and shear wave. In regards to the total energy, about 67% is carried by the Rayleigh wave, 26% is carried by the shear wave, and 7% is carried by the longitudinal wave [10]. By looking at a typical AE signal shown in Figure 1.9, the various wave modes can be distinguished by the amplitude changes and by the time it takes them to reach the sensor.

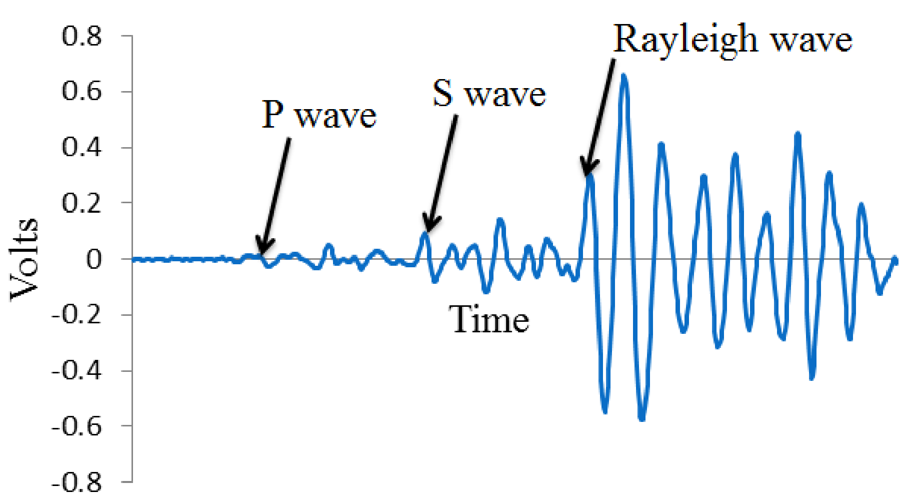

Figure 1.9: Typical AE Signal [10]

1.2.2 Attenuation

Attenuation of sound waves within a material is an important aspect that must be taken into consideration when using an AE sensor. Attenuation refers to the decay rate of the sound wave as it propagates through the workpiece material. Attenuation is due to scattering and absorption of the sound wave. The amplitude of an attenuating wave can be represented by the equation:

$$A(z) = A_0 e^{-\alpha z} \qquad \textbf{Equation 1.1}$$

Where A_0 is the initial amplitude of the wave at the source location, z is the distance travelled, and α is an experimentally determined attenuation constant that depends on the workpiece material [8].

1.2.3 Electromagnetic Interference (EMI)

Electromagnetic interference (EMI) is a phenomenon which causes a high frequency disturbance in the acoustic emission signal at the instant of discharge in EDM. In a typical EDM discharge, the current rises from zero to several amperes in ~ 200 ns [11]. This rapid current rise is associated with an EMI that disturbs the acoustic signal as can be seen in Figure 1.10. In the case of a high amplitude acoustic signal as in Figure 1.10, the EMI can be neglected. In the case of a low amplitude acoustic signal, the EMI amplitude can match or even be larger than the amplitude of the desired acoustic wave and cause issues with the processing of the acoustic signal.

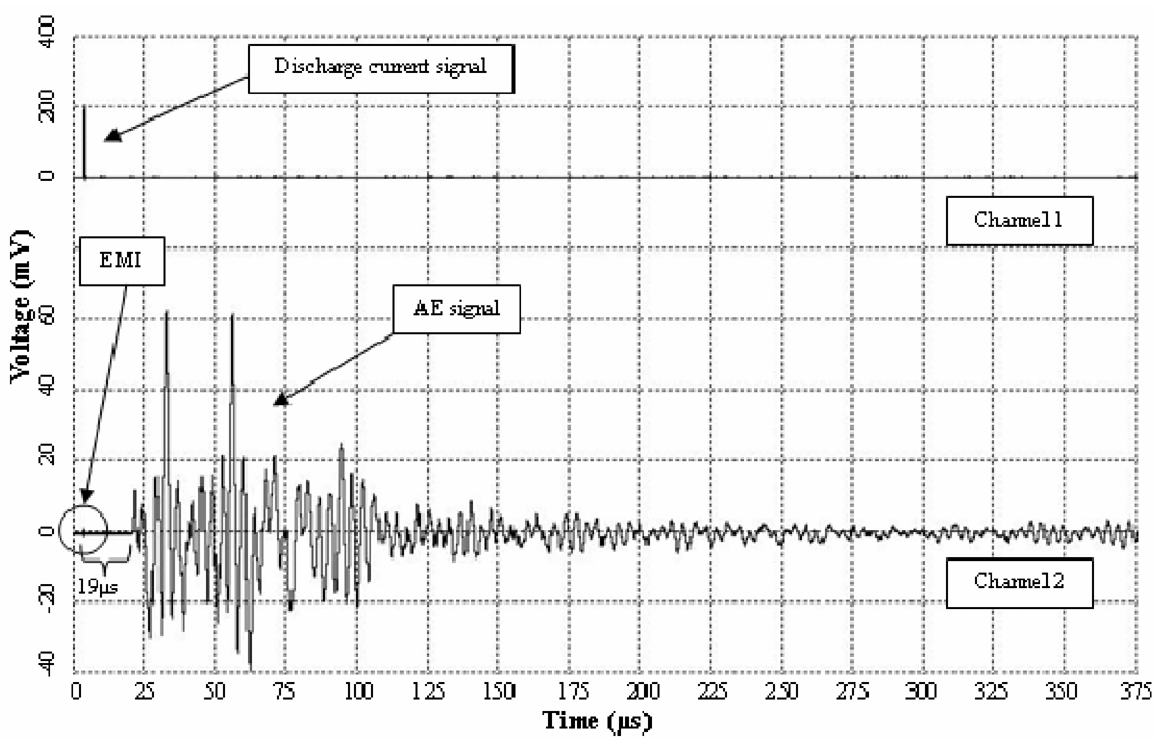

Figure 1.10: Electromagnetic Interference [12]

Knowing that the EMI occurs at the instant of discharge while the desired acoustic wave occurs after the surface wave propagates from the discharge location to the sensor, the EMI can be analyzed separately. Smith [13] determined that the EMI generally occurred at frequencies above 500 kHz while the desired acoustic wave remains in the frequency range below 500 kHz. With this knowledge, the unwanted EMI can be filtered out of the AE signal.

1.3 Scope of Thesis

Acoustic emission sensors have long been utilized as a process monitoring tool for conventional machining processes such as milling and grinding, as well as non-conventional machining processes, such as waterjet machining. For example, examination of the RMS of raw AE data has been used to monitor tool wear in milling [14], monitor workpiece burn in grinding [15], and monitor material removal in waterjet cutting [16]. To date, there has been little research performed employing AE sensors in EDM. This is surprising, considering the well-known fact that experienced EDM operators gauge the stability of the process by ‘listening’ to the sound emitted during operation. The goal of this research is to determine the capabilities and benefits of using an acoustic emission sensor as a monitoring tool for the EDM process. Currently, voltage and current signals are analyzed to monitor EDM. There are aspects of EDM that cannot be monitored accurately using the voltage and current signals alone. For example, the material removal rate and the effectiveness of flushing are difficult to measure in-process with only the voltage and current signals. Improper flushing can cause catastrophic surface finishes and in the case of wire EDM, can lead to wire breakage which has a negative effect on productivity. The benefit of utilizing a real-time monitoring tool for the EDM process could be seen in all three types of EDM by improving process stability, surface quality and material removal rates.

2 Literature Review

In order to provide a background for the elements of this research, a review of the state of the art was conducted. The information below presents different flushing techniques and process monitoring techniques in EDM. Examples of current applications of AE sensors in other manufacturing processes, as well as electrical transformers are also reviewed.

2.1 Flushing Techniques in EDM

Flushing of the workpiece gap is an extremely important component of the EDM process. As mentioned earlier, if flushing is inadequate, too much debris collects in the discharge gap and arcing and ultimately short circuits can occur. The effect of arcing on the surface finish can be seen in Figure 2.1. Alternatively, if the level of flushing is too high, the dielectric fluid in the discharge gap will not have enough time to ionize before it is removed and subsequently open circuits will occur. In order to monitor the process with acoustic emission, flushing must be first understood as it has a significant effect on the process and potentially the acoustic emission signal.

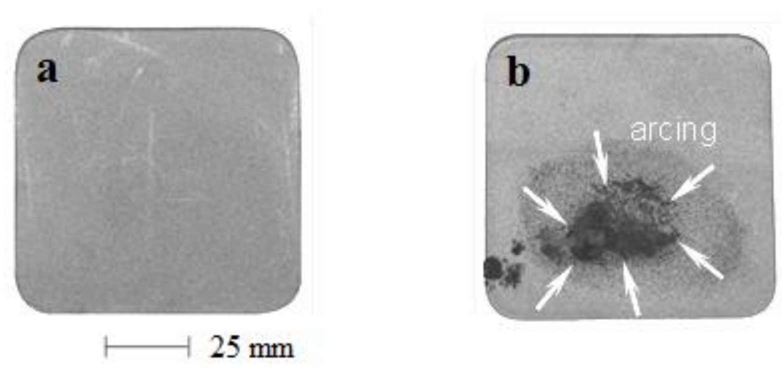

Figure 2.1: Effect of flushing a) Adequate flushing b) Inadequate flushing

2.1.1 Jet Flushing

Jet flushing is the oldest and remains the most popular type of flushing for EDM due to its simplicity. A nozzle is directed towards the machining area and a pressurized dielectric fluid jet ensues from the nozzle. The issue with jet flushing is that the most appropriate location for the nozzle or nozzles is difficult to determine, and is usually decided just on operator's experience. Without proper nozzle placement, debris uniformity and a stable process cannot be ensured. Masuzawa et al. [17] studied the effect of nozzle placement on the surface profile of the workpiece. The resulting surface profiles of three different nozzle configurations run for 8 hours between two flat surfaces are presented in Figure 2.2. In Figure 2.2a two nozzles are placed on one side of the workpiece and it can be seen that with this method, the density of debris particles increases downstream resulting in an uneven gap width. In Figure 2.2b two nozzles are placed on one side and another nozzle on the opposite side. With this configuration, the debris appears to collect in the centre resulting in geometrical inaccuracies. The last configuration shown in Figure 2.2c has three nozzles on one side and the sides are alternated every 3 minutes. Even with this alternating flow, it can be seen that the distribution of debris is still not uniform across the surface.

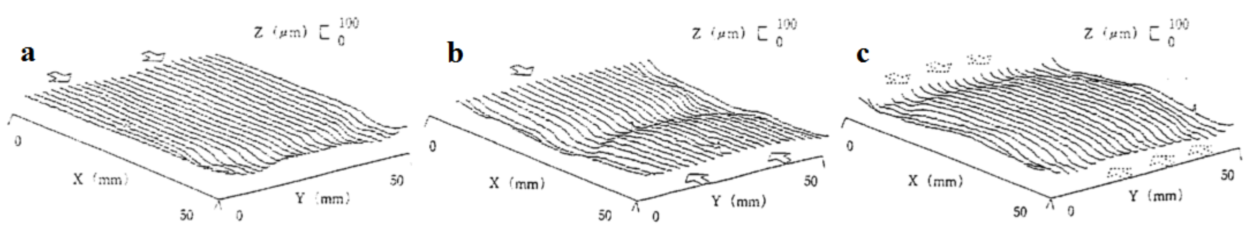

Figure 2.2: Surface profile of workpiece
a) Flushing from one side, b) Flushing from both sides, c) Alternate flushing [17].

Masuzawa et al. improved jet flushing by developing a sweeping jet flushing design. The design involves two parallel nozzles spaced 10 mm apart on each side of the workpiece which move along the outline of the machining area. The jets on each side have a phase shift of 90 degrees to avoid interference of the jets. The results from the sweeping jet flushing method are evident in Figure 2.3. The flatness of the surface profile considerably improved from the basic jet flushing techniques meaning a uniform distribution of debris was achieved.

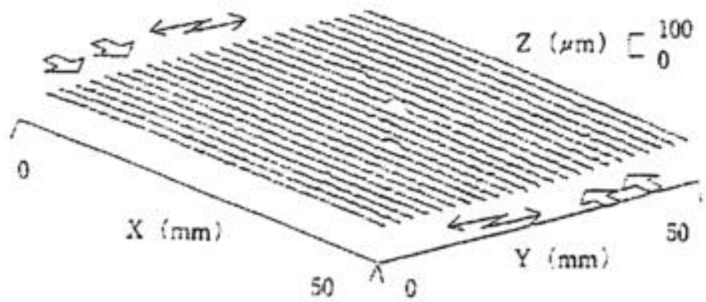

Figure 2.3: Surface profile of the workpiece (sweeping jet) [17]

2.1.2 Self-Flushing Method

Jet flushing can prove to be ineffective in clearing out debris in EDM applications that require deep cavities to be machined into the workpiece. Masuzawa and Heuvelman [18] have developed a fast additive movement of the electrode to the workpiece known as the self-flushing method. The method uses a driving system which can control the electrode in at least two axes in order to construct a pumping action between the electrode and the workpiece. One of the simplest movements can be seen in Figure 2.4. The electrode moves in a rectangular pattern which allows fluid to come in the gap at one side and leave out the other side.

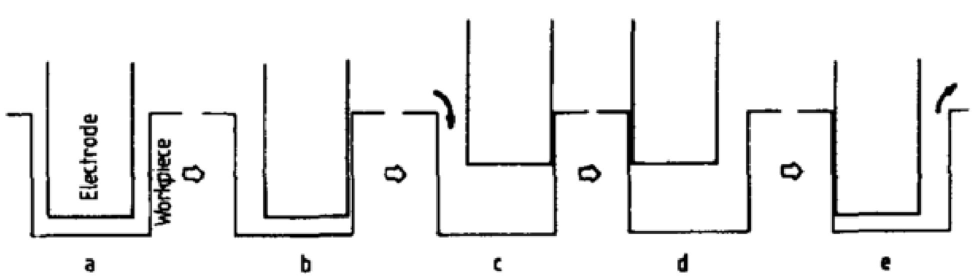

Figure 2.4: Basic movements of the Self Flushing method [18]

The self-flushing method is compared against two basic electrode movements, 'normal' and 'z-only'. In 'normal', no flushing is applied and the z-axis only moves for gap control. In 'z-only', the z-axis is lifted periodically at various distances. The results of the three methods can be seen in Figure 2.5 below. The black dots indicate the occurrence of arcing and further machining with these conditions was impossible. During the 'normal' electrode movement (x = 0, z = 0), arcing occurred very early and machining is almost impossible. With the 'z-only' electrode movement, it was seen that the larger the pull-up distance, the longer the machining could be continued as indicated by the 3 black dots along the top line. The lower line refers to the self-flushing method and shows that with just a small amount of x-displacement, the machining rate is increased and the machining is free from interruption. The self-flushing method, however, has an increase in electrode wear at the edges and corners.

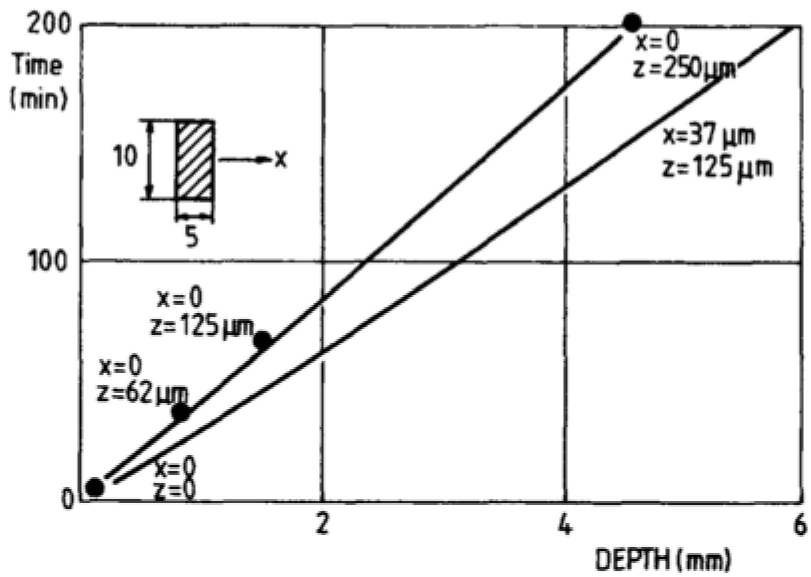

Figure 2.5: Relation between machining time and depth [18]

2.1.3 Rotating Electrode

An issue with flushing methods that require special movements like the self-flushing technique is that the generator is switched off during the special movement and machining time is lost reducing the average MRR of the process. Koshy et al. [19] investigated the use of a rotating disk electrode in which the electrode is rotated and sunk simultaneously into a plate workpiece. The rationale for this method is the rotation of the disk imparts a velocity to the dielectric fluid in the gap and effectively flushes out the debris. The goal of this technique is to increase MRR and improve surface finish through effective flushing, as well as better reproduction of corners due to the fact that the tool wear will not be localized and is evenly spread over the circumference of the disk. The results of this technique can be seen in Figure 2.6. At a constant current, the MRR increases as the peripheral speed increases and eventually reaches a plateau. It can also be seen that an increase in current also increases the MRR. Due to this higher rate of debris formation at higher pulse currents, a small velocity increase of the electrode imparts a more significant increase in MRR which explains the difference in the slope of the three curves.

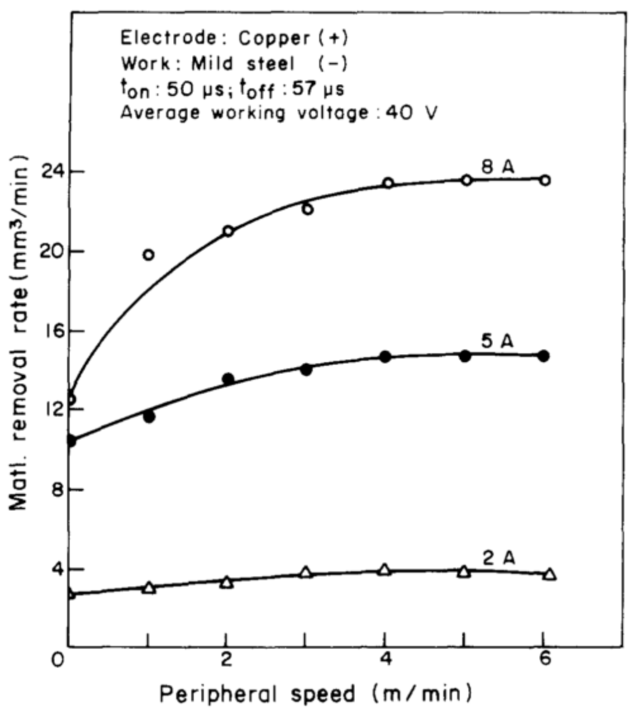

Figure 2.6: Variation of MRR with peripheral speed of electrode [19]

It can be seen in Figure 2.7 that the roughness value decreases with increasing peripheral speed at a constant pulse current. This relationship can be explained using the following energy (E) equation:

$$E = \int_{t_d}^{t_p} I(t)V(t)dt \qquad \textbf{Equation 2.1}$$

Where $I(t)$ is the gap current, $V(t)$ is the working voltage, t_d is the ignition time delay, and t_p is the pulse on-time. As the peripheral speed increases, the ignition time delay increases which in turn decreases the energy of the individual discharges allowing a smaller crater to be formed. As well, with improved flushing conditions, the possibility of resolidification of debris on the surface is reduced providing a better surface finish.

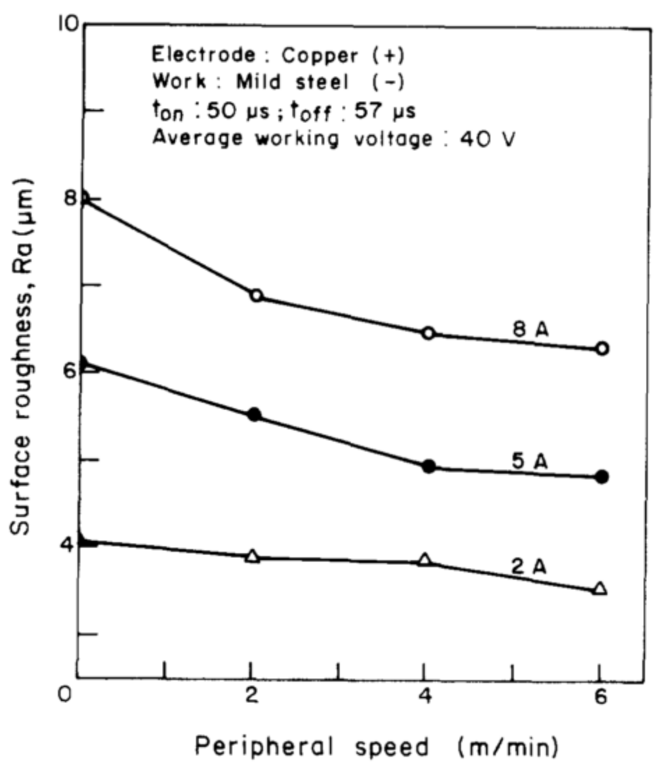

Figure 2.7: Variation of surface roughness with peripheral speed of electrode [19]

The final goal of the rotating electrode technique was to improve the corner reproduction accuracy. The reproduction achieved with a rotating copper electrode can be seen in Figure 2.8, where r_t is the radius of the corner of the electrode before machining and r_w is the corresponding radius generated on the workpiece after machining. It can be seen that the corner reproduction index (r_w/r_t) increases as the current increases. The corners machined with an electrode peripheral speed of 6 m/min show a remarkable improvement in corner reproduction, so much that the corner reproduction index at 8 A with a rotating electrode is still significantly better than at 2 A with a stationary electrode.

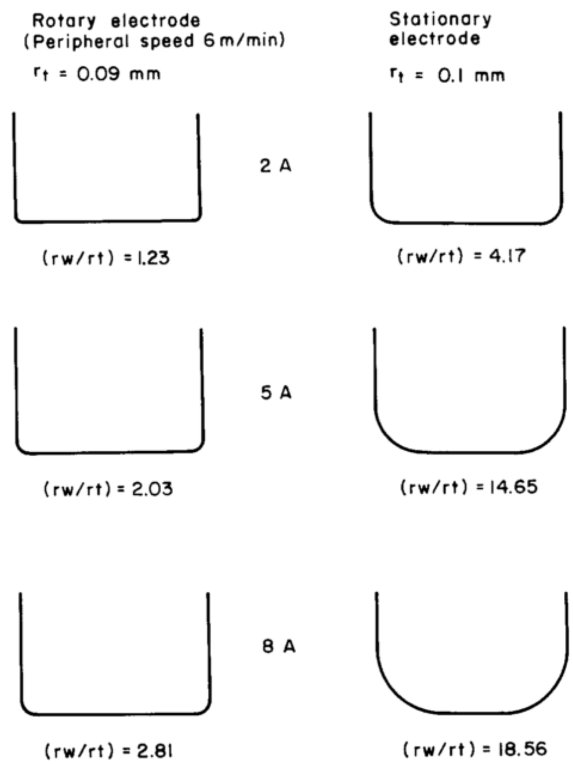

Figure 2.8: Typical profiles machined by copper electrode [19]

The results of the rotating electrode flushing technique therefore show improvements in not only MRR and surface finish but also show better reproduction of corners making the rotating electrode a desirable flushing method. This method, however, is limited to the specific geometries which can accommodate a rotating electrode. The use of a rotating electrode for this thesis will be discussed in further detail later on.

2.2 Acoustic Emission Monitoring of Power Transformers

Acoustic emissions have proved to be useful for areas outside of machining such as for insulation diagnostics of power transformers. The insulating system of a power transformer holds an essential role in the safe operation of the unit. Without careful monitoring of the insulating system, the system can fail from short circuits, lightning strokes or transients from switching operations [20]. A diagnostic tool for power transformers is to analyze the AE signal generated by partial discharges. Partial discharges are formed in power transformers at the point of junction of three phases: a copper wire of which a winding is made, a solid dielectric and insulation oil [21]. Research on partial discharges in transformers is highly related to the background of this thesis because of the fact that the partial discharges occur along the same mechanism as EDM discharges. “A partial discharge can be defined as localized electrical discharge in insulating media which only partially bridges the insulation between conductors” [22].

Cichon [21] conducted research on partial discharges using three different geometric configurations of spark-gaps: point-point, point-plane, and surface. The acoustic sensor used had a frequency band from 100 kHz to 1 MHz and was passed through an amplifier and a filtering system with a high-pass filter of 10 kHz and a low-pass filter of 700 kHz. Cichon realized the fact that partial discharges could occur in multiple spark-gap configurations simultaneously. It was therefore chosen to use an experimental setup that would apply partial discharges in two different configurations simultaneously in the attempt to distinguish the discharge type from the resulting AE signal. Spectrograms were created to present the time-frequency analysis using a short-time Fourier transform. Using the spectrograms shown in Figure 2.9, the dominant frequency bands in the acoustic emission signal were able to be correlated to the corresponding partial discharge configuration. It was determined that the point-point configuration has a discharge with a frequency from 70-300 kHz, the point-plane configuration is in the range of 20-100 kHz, and the surface configuration can occur from 20-500 kHz.

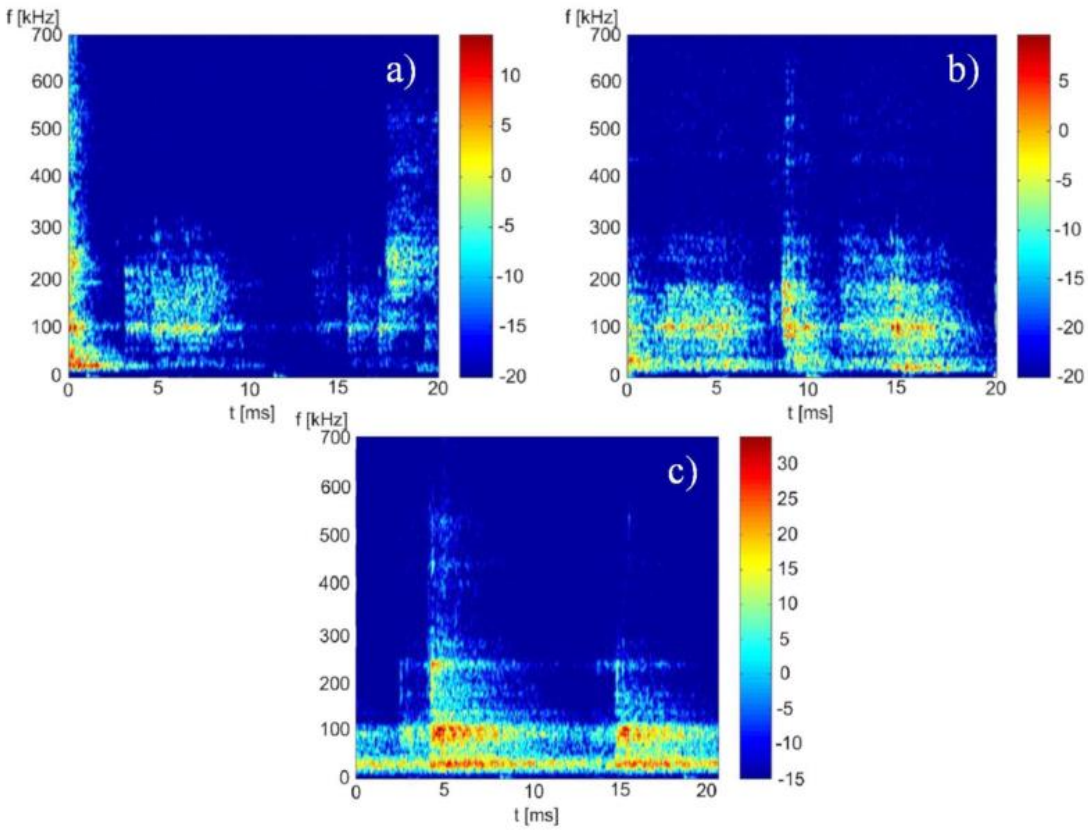

Figure 2.9: Two-dimensional spectrograms of AE signals for multi-source partial discharges
a) point-point and point-plane, b) point-point and surface, c) point-plane and surface [21]

2.3 Acoustic Emission in Machining Processes

As mentioned earlier, acoustic emission sensors have been utilized in most machining processes. Inasaki gives some examples of basic uses of AE in cutting processes with single-point and multipoint tools and also grinding [23]. In a turning operating, where a single-point tool is in constant contact with the workpiece, an AE sensor can be attached to the tool shank and can be used to distinguish between continuous and discontinuous chips. With discontinuous chips, the number of large amplitude spikes in the AE signal is increased as shown in Figure 2.10 below.

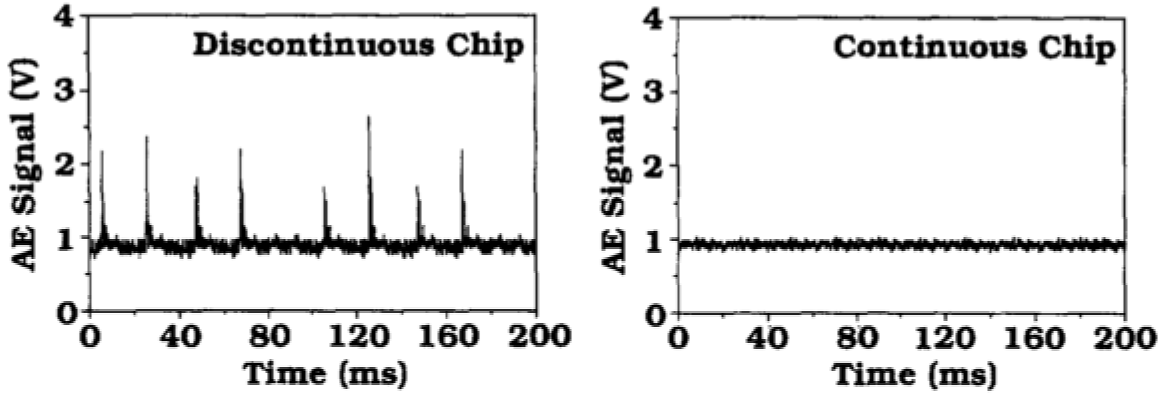

Figure 2.10: AE Signal during cutting with discontinuous and continuous chips [23]

Even with a fairly consistent AE signal as in the case of a continuous chip, much can be learned from analyzing the frequency domain of the AE signal. With the same setup, the frequency domain of the AE signal can be used to detect chatter vibration. Chatter vibration is detected by large amplitude peaks in the frequency domain as shown in Figure 2.11. The chatter frequency can change depending on the structural dynamics and therefore the exact frequency is not considered and only the occurrence of a peak is necessary to determine whether the process is sustains chatter.

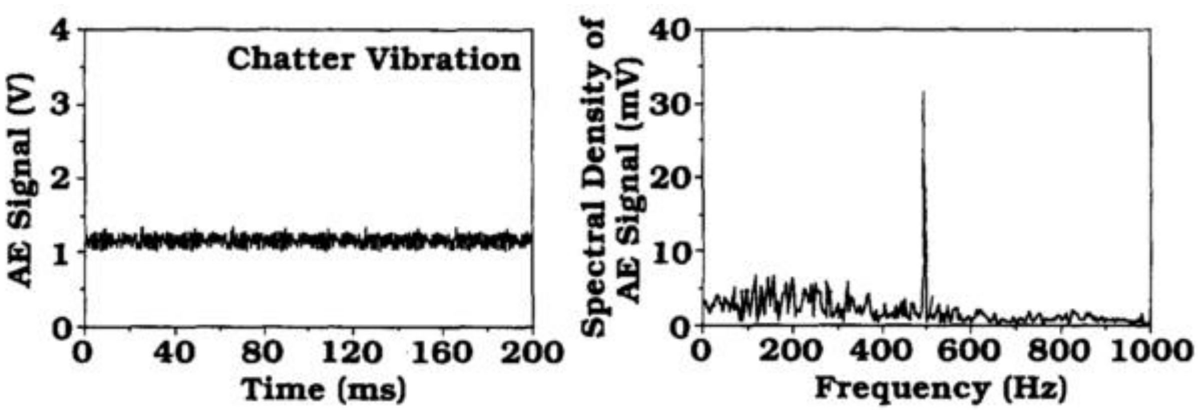

Figure 2.11: AE Signal and resulting spectral density sampled during chatter condition [23]

Ravindra et al. [24] found that an acoustic sensor could be used as a sensitive tool for the on-line monitoring of failure of a cutting tool. Chipping of the cutting tool causes a substantial change in the RMS of the AE signal with a steep decrease in rise time. Rise time refers to the time taken to reach peak amplitude from the first threshold crossing of the AE signal.

In the case of using multipoint milling tools, tool breakage and chipping are problematic to detect because of the nonconstant chip thickness and the fact that more than one cutting edge might be in contact with the workpiece. The AE signal of a multipoint cutting tool produces two characteristic peaks in the power spectrum as shown in Figure 2.12. Peak P_s, refers to the rotational speed of the spindle while peak P_c refers to the rotational frequency of the spindle times the number of cutting edges. A chipping coefficient, k, is calculated as P_s/P_c. Figure 2.12a and Figure 2.12b show the power spectrum of the AE signal for a new tool and a chipped tool respectively. It can be seen in Figure 2.12d that the chipping coefficient increases from Figure 2.12c in amplitude and variability with the chipped tool, which is believed to be due to the increased chip thickness for the engaged tooth that follows the chipped tooth [23].

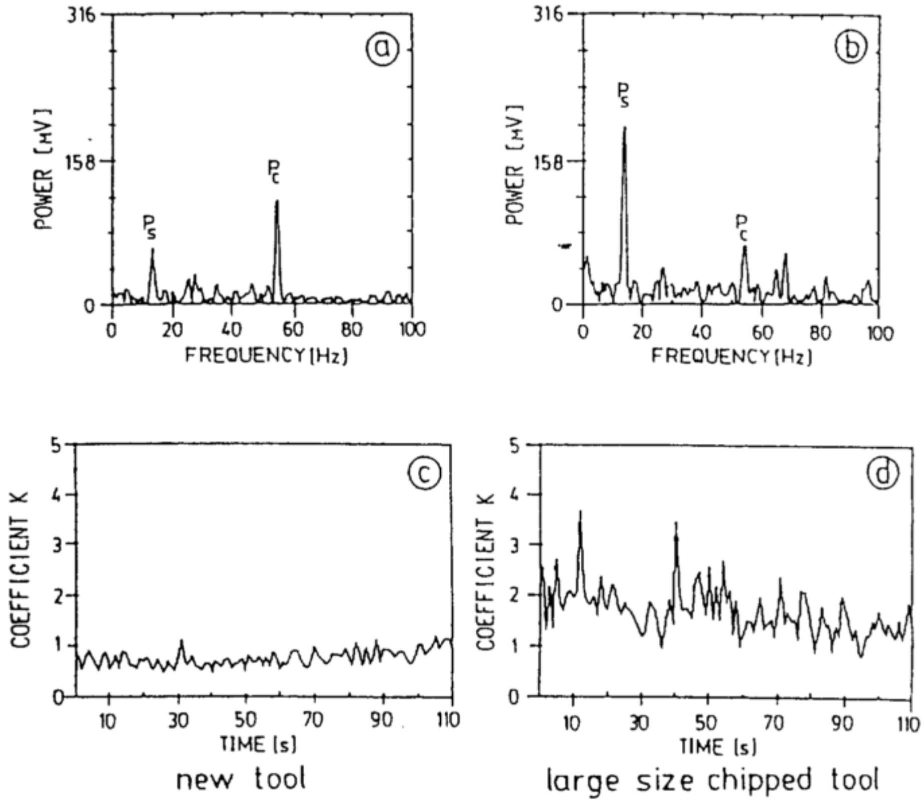

Figure 2.12: AE power spectrum and corresponding chipping coefficient [23]

An issue with using an AE sensor in milling to monitor tool condition is the inability to mount the sensor on a rotating tool. Kayaba and Inasaki proposed a novel idea to address this issue [25]. By coupling the AE sensor with the cutting fluid supply system, the cutting fluid acts as a medium to transmit the AE signal.

Mounting an AE sensor to a rotating object is also an issue with a grinding wheel. Wakuda et al. dealt with this issue by using a grinding wheel with a built-in AE sensor [26]. The grinding wheel contains batteries, a preamplifier and a FM transmitter which sends the signal to a receiver outside the wheel. By continuously monitoring the AE signal in the frequency domain, the development of a particular frequency component can be attributed to chatter vibrations from self-excited vibrations or from forced vibration due to out-of-roundness of the wheel. As well, by monitoring the AE amplitude level, the amplitude standard deviation, and the cumulative workpiece removal, a relationship could be established with the surface roughness [23]. Using a simpler setup, Webster et al. [15] mounted the AE sensor to the bottom side of the workpiece and were able to make a correlation between the RMS of the AE signal, normal force and workpiece burn. As shown in Figure 2.13a, the RMS of the AE signal appears to be proportional to the normal force, and in Figure 2.13b, the RMS of the AE signal increases during workpiece burn.

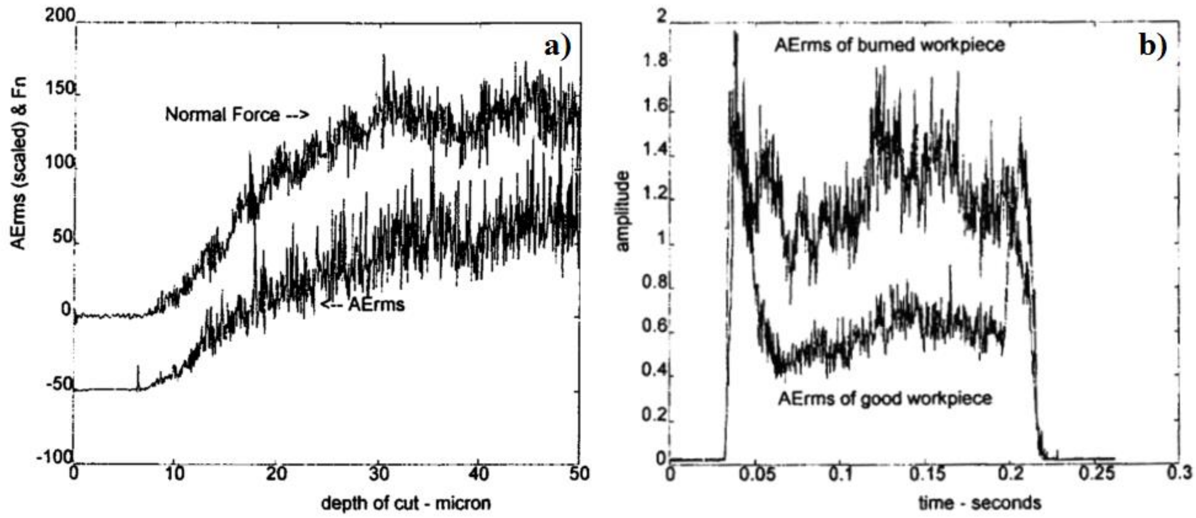

Figure 2.13: RMS AE signal in grinding condition
a) Normal force and RMS AE correlation, b) Effect of a burned workpiece on RMS AE [15]

Mechanical damage to sliding components is commonly caused by sliding friction resulting in mechanical wear. Hase et al. [27] were able to correlate the AE signal to the two main wear mechanisms, adhesion and abrasion. For adhesive wear, the frequency peak of the AE signals occurs around 1.1 MHz, whereas in abrasive wear the frequency peaks are distributed between 0.25 and 1 MHz. The amplitude of the AE signal is influenced by the transfer of particles in adhesive wear and influenced by the removal capability of the abrasive grains in abrasive wear.

Acoustic emissions have not only been used in conventional machining processes like turning, milling, and grinding, they have also been used in non-conventional machining processes such as waterjet machining. Momber et al. [16] determined that in cutting concrete, material removal dominated by intergranular fracture can be characterized by a continuous type AE signal, whereas material removal dominated by transgranular fracture can be characterized by burst type AE signals. To come to this conclusion, the samples shown in Figure 2.14 were prepared. Figure 2.14a was prepared to be a low strength matrix with fine inclusion grains and Figure 2.14b was prepared to be a high strength matrix with coarse inclusion grains. The samples were prepared with these properties to ensure one would be dominated by intergranular fractures when waterjet machined, while the other one would be dominated by transgranular fracture.

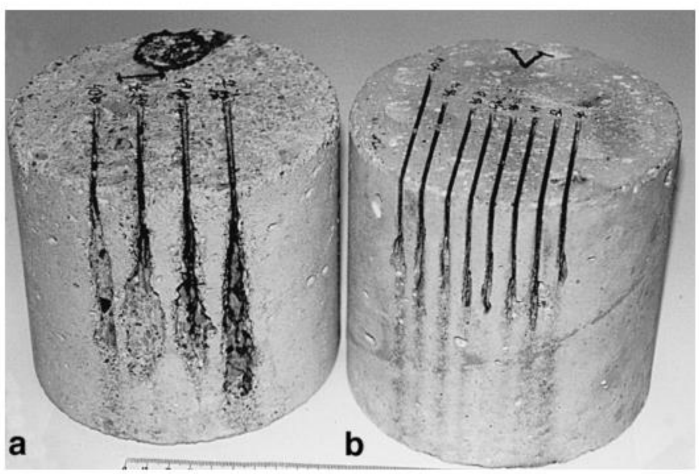

Figure 2.14: Concrete samples indicating different material removal mechanisms
a) Low matrix strength b) High matrix strength [16]

An AE sensor was fixed directly on the concrete samples and a section of the AE signal resulting from the waterjet process can be seen in Figure 2.15. Figure 2.15a occurred during the machining of the low matrix strength sample and typically shows a continuous AE signal. Figure 2.15b occurred during the machining of the high matrix strength sample and shows an AE signal characteristic of burst type signals as well as higher amplitudes.

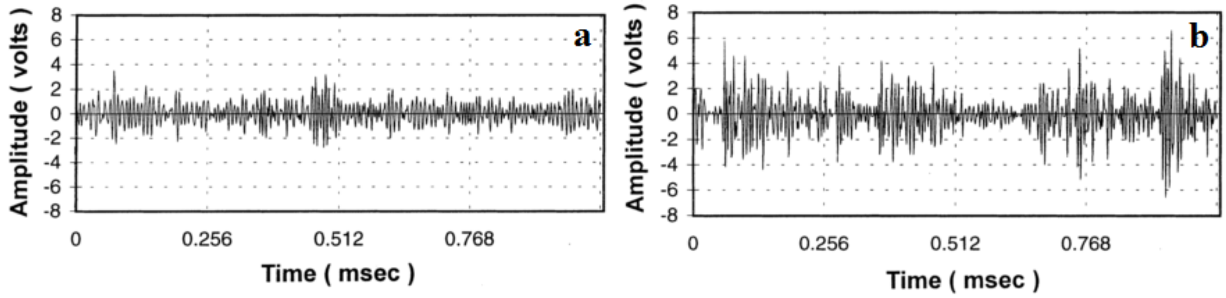

Figure 2.15: Resulting raw AE signal
a) Continuous type AE signal, b) Burst type AE signal [16]

Just a few examples of the extensive uses of AE sensors in the majority of conventional and non-conventional machining processes have been discussed above. Consequently, it would appear to be a valid assumption that AE sensors could benefit the EDM machining process as well.

2.4 EDM Process Monitoring Techniques

The ability to identify and correct process instabilities as they occur is essential to maintaining the efficiency of any machining process. This requirement of process monitoring is particularly important for the EDM process. Unlike majority of other machining processes, the EDM process occurs in a fluid and is not directly visible to the human eye. Due to the slow material removal rate in EDM, the product may not be seen for several hours, therefore requiring a reliable process monitoring technique. Some of the process monitoring techniques that have been used for EDM are discussed below.

2.4.1 Voltage and Current Signals

A real-time monitoring technique for the EDM process is to measure the voltage and current signals between the electrode and the workpiece. The voltage and current signals can be used to discriminate the EDM pulses as sparks, arcs, shorts, and open circuits which can be related to the material removal rate (MRR), the surface finish, and the accuracy of the component. Kao and Tarng [28] proposed a neural-network approach for the on-line monitoring of the EDM process. Due to the fact that the spark and arc discharges have similar voltage and current waveforms, they are first separated into a group called the discharge pulse. These pulses then go through the flowchart shown in Figure 2.16 to distinguish between spark and arc pulses.

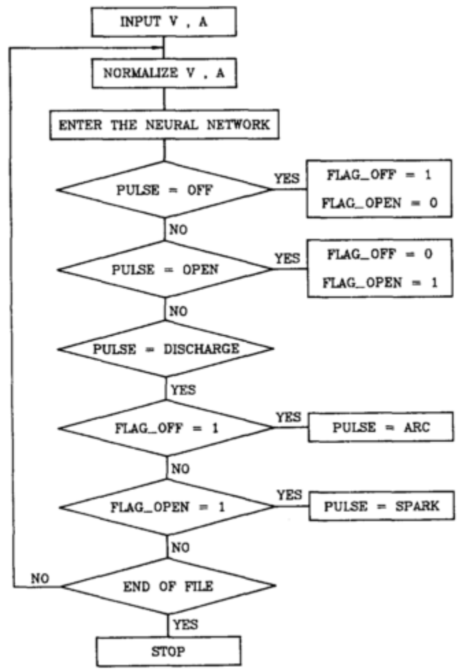

Figure 2.16: Flow chart to separate the spark pulse from the arc pulse [28]

The neural network method was tested with a cylindrical copper electrode on a SKD11 steel workpiece. The tests were done with a no-load voltage of 90 V and a peak current of 40 A. The voltage and current recorded are shown in Figure 2.17a and Figure 2.17b, respectively, and the classification results of the pulses can be seen in Figure 2.17c.

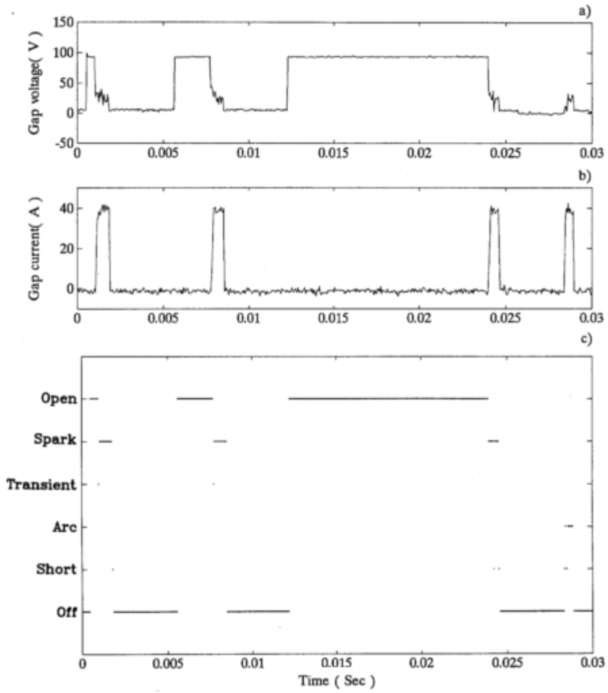

Figure 2.17: a) Gap voltage, b) Gap current, c) Classification results [28]

The neural network approach developed by Kao and Tarng has not been widely embraced because it is not efficient in terms of computational requirements and cannot be easily implemented using common programmable integrated circuits that are used in industry. Pey Tee et al. [29] propose a method that is simpler in terms of computational requirements. The current waveforms are nearly the same for a normal discharge, an arc, and a short circuit. Therefore the voltage signal is compared with a threshold. Four thresholds are set for the gap voltage and one is set for analyzing the gap current (Figure 2.18). The voltage is very close to zero for a short circuit, whereas an arc is larger but still lower than a normal pulse. An open circuit is detected when the gap voltage remains above the open circuit threshold V_{Toc} for longer than the pre-set time while the gap current is below the current threshold I_T.

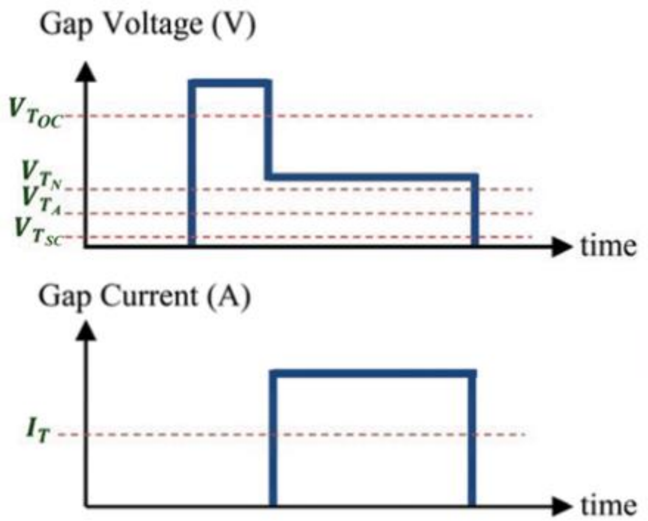

Figure 2.18: Voltage and current thresholds [29]

This method is a straightforward technique that is viable for real-time operation. The thresholds used for this technique however, depend on the workpiece material along with the pre-set voltage and current, and must be determined through multiple trial and error experiments.

2.4.2 Ignition Time Delay

Currently, the most used real-time monitoring and control of the EDM process is based on the ignition delay time which has a direct influence on the MRR, surface roughness and accuracy. For example, Weck and Dehmer [30] used the ignition delay time to estimate the material removal on both the workpiece and the electrode. More specifically, they used a summation of the rising time (t_r), ignition delay time (t_d), and the fall time (t_f), which they referred to as the measured time (t_{df}) as illustrated in the voltage waveforms shown in Figure 2.19.

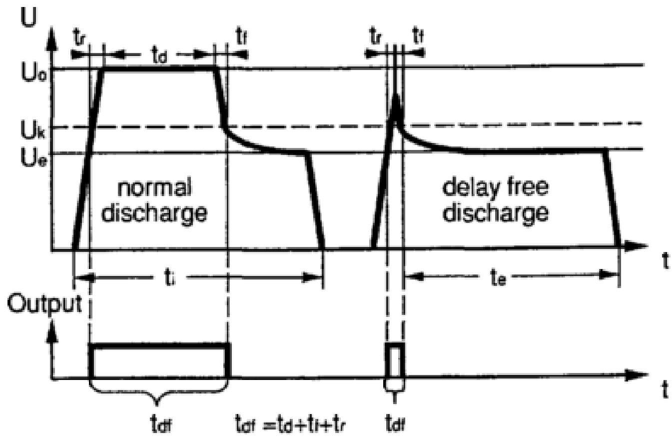

Figure 2.19: Measurement of the ignition delay time [30]

The on-time and off-time used for the experiments were 112.5 µs and 43 µs respectively. A threshold t_{df} of 20 µs was used for discriminating between arcs and sparks. All pulses with a t_{df} lower than 20 µs were designated as arcs. It was determined that lower the t_{df}, the higher the electrode wear (Figure 2.20). Dauw determined that discharges with a low t_f, have a very steep rise and absolute value of current at the start of the discharge [31]. Therefore, this relationship between t_{df} and the electrode wear could be due to the fact that discharges with a low or no t_{df} have a very low or no fall time, which could cause the current to be so high at the start of the discharge that the material evaporates rather than melts as in the case of a normal discharge.

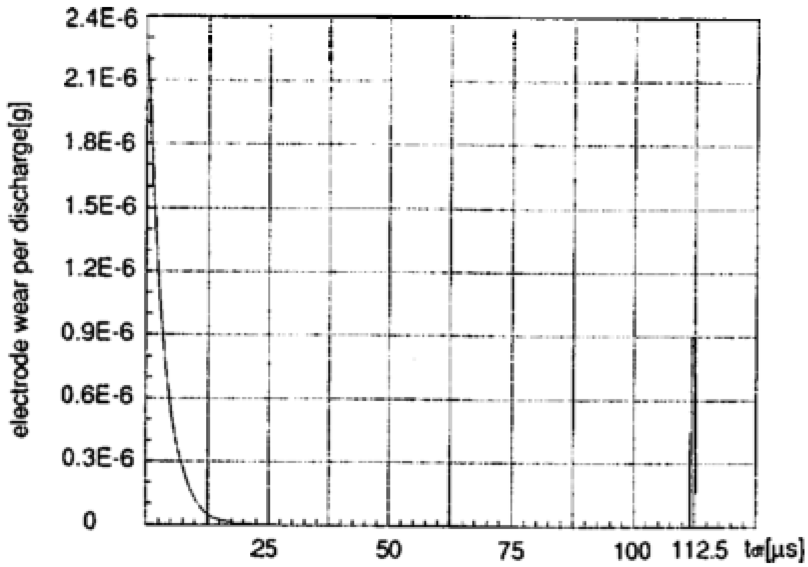

Figure 2.20: Electrode wear per single discharge with different t_{df} [30]

2.4.3 Radio Signals

Bhattacharyya and El-Menshawy [32] investigated the use of radio signals as a process monitoring technique in EDM. By analyzing the radio frequency signals, discrimination between sparking, arcing, open circuits and short circuits could be made. A normal radio receiver and antenna were used and the best machining condition showed the most intense emission as shown in Figure 2.21. The radio frequency emission intensity was shown to be proportional to the material removal rate.

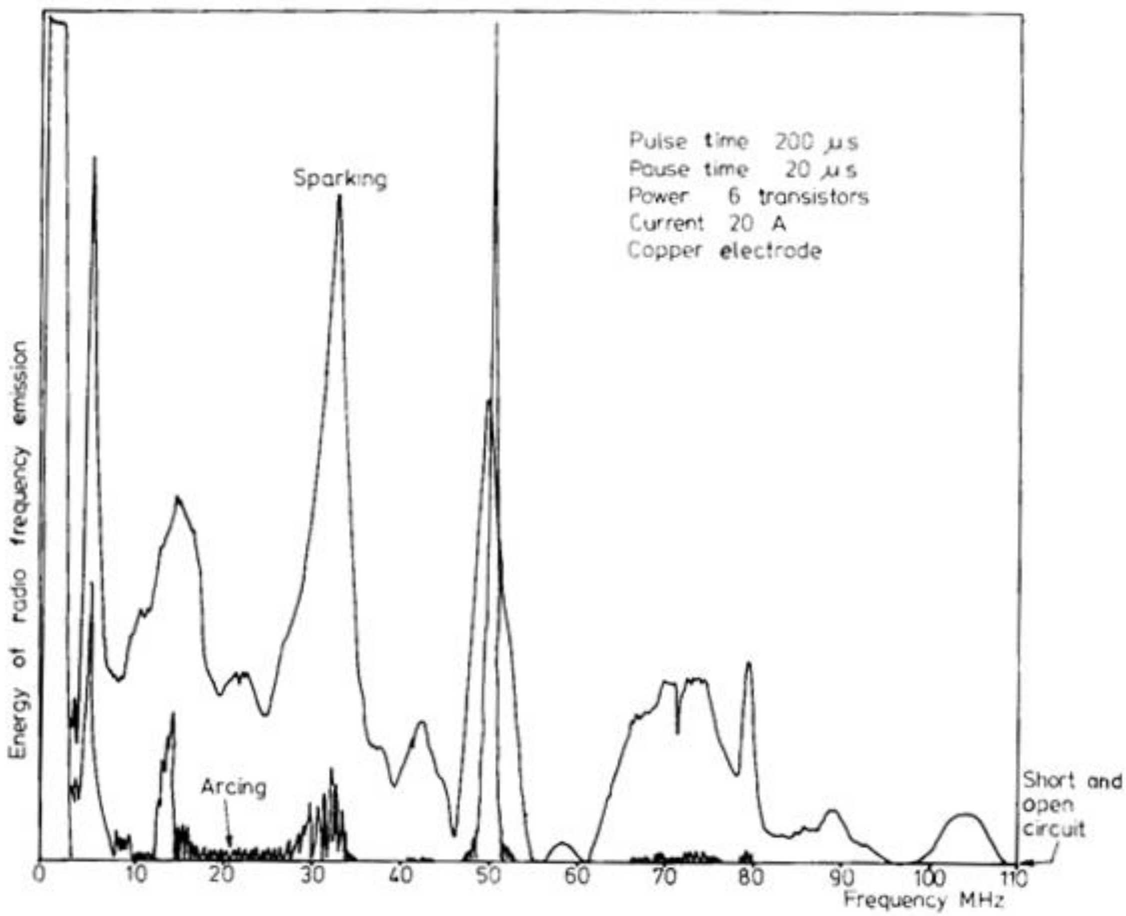

Figure 2.21: Radio spectra during the EDM process [32]

The emitted radio frequency signal was measured at various machining frequencies by changing the spark on-time (duration of a single discharge). No major change was seen in the radio frequency signal when the on-time was changed. As well, the radio signal was recorded at different machining currents, and again very little variations to the signal were observed. From this, it can be concluded that the radio frequency signal can be utilized to monitor the stability of the process; however it cannot be used as a tool to detect unexpected changes in EDM parameters such as on-time and current.

2.4.4 Acoustic Emission Signals

Mahardika et al. [12] investigated the relationship between the discharge pulse energy in the μ-EDM of polycrystalline diamond (PCD) and the AE signals. An important aspect of μ-EDM is accuracy and therefore the stability of the EDM process becomes of great importance to prevent discharge localization. Mahardika et al. found the highest amplitude AE signals during μ-EDM of PCD to be proportional to the discharge pulse energy (Figure 2.22). However, the μ-EDM utilized a resistor-capacitor circuit to generate the discharge pulses, which resulted in the highest amplitude AE signals occurring at the first few discharges of the process, when the capacitance is still fully charged. This reading is not the best representation of process stability, as discharge localization will arise once debris starts to form which transpires long after the first discharge.

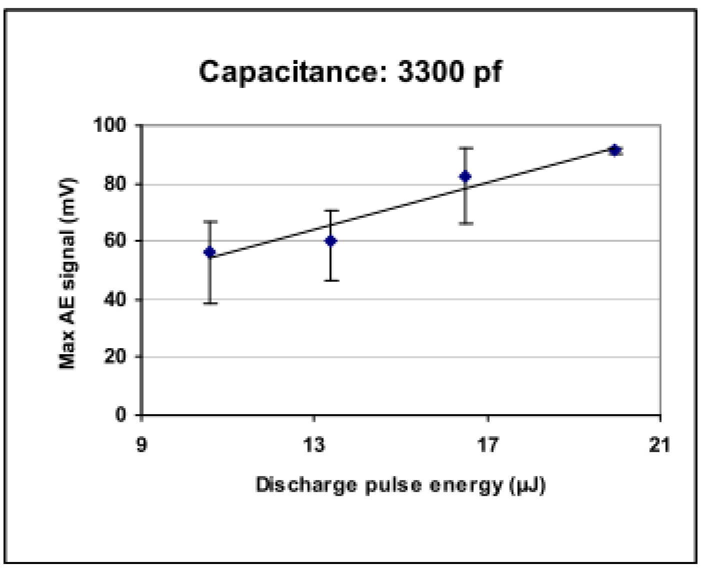

Figure 2.22: Highest amplitude AE signal during PCD machining [12]

Mahardika et al. also state that "disturbances due to EMI are negligible" [12], which is not a true assumption in all cases. As discussed in the introduction section, in the case of a low amplitude AE signal, the amplitude of the EMI can match or even be larger than the AE wave.

This can occur under specific EDM conditions and can also depend on sensor placement. The EMI should be filtered out rather than neglected to ensure a consistent representation of the AE signal while data processing.

Smith and Koshy [33] used acoustic emission in EDM as a way to map the locations of the discharges. Shown in Figure 2.23 are the AE signals from two sensors placed at specific distances away from a single discharge. The EMI marks a frame of reference for the instance of discharge and therefore it can be seen that the AE signal takes longer to arrive at sensor 2 than sensor 1.

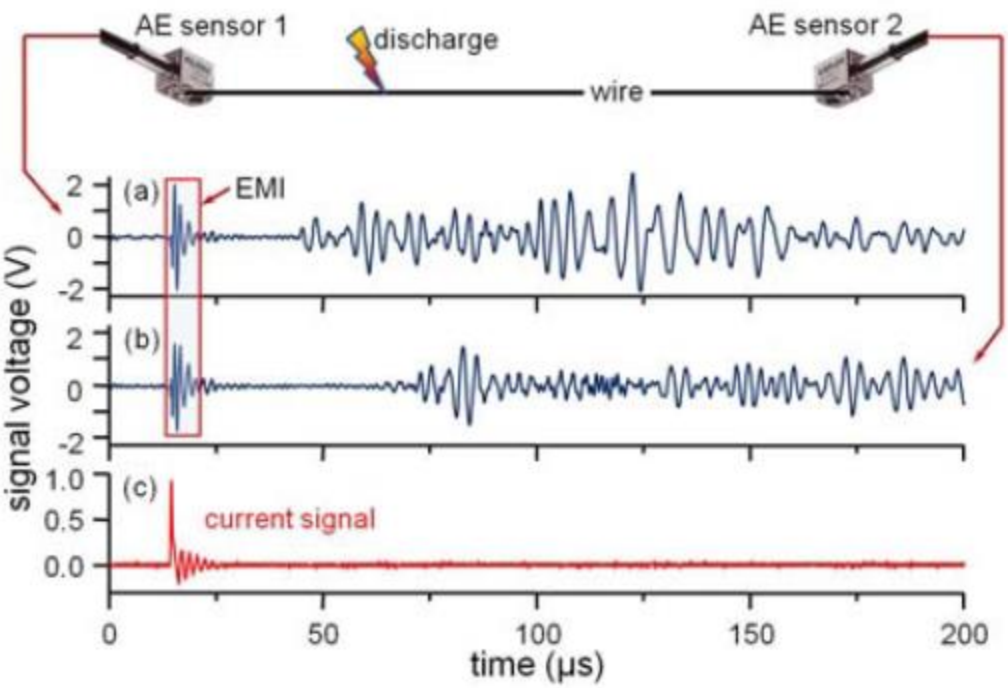

Figure 2.23: AE for single discharge location
a) Sensor 1 AE signal, b) Sensor 2 AE signal, c) Current signal [33]

Using a Short Time Fourier Transform (STFT) of the signal, the peak on the acoustic portion shown in Figure 2.24 is used as a consistent reference on the acoustic wave. Using the time lag between the EMI and the acoustic peak the speed of sound in the wire can be calibrated. Once the speed of sound in a material is calibrated using this method, realistic EDM conditions would have electrical discharges occurring much closer together which would significantly convolute the signal.

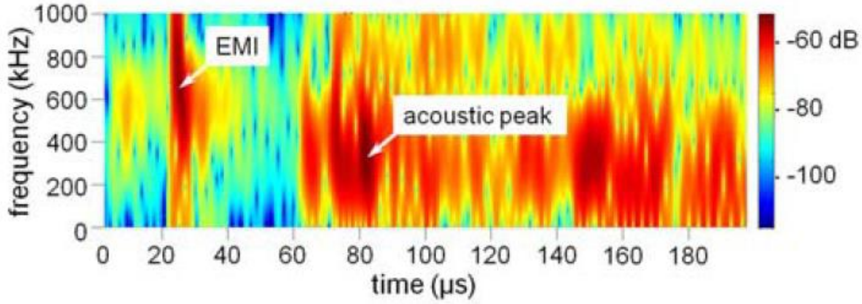

Figure 2.24: Spectrogram of a typical AE signal

An example of two discharges occurring 12.9 µs apart can be seen in Figure 2.25a. Using the same spectrogram technique (Figure 2.25b) and looking at the power spectral density at the dominant 300 kHz frequency (Figure 2.25c), a time difference of 12.7 µs can be determined. Using the calibrated speed of sound, the error of 0.2 µs corresponds to a location inaccuracy of just 0.07 mm.

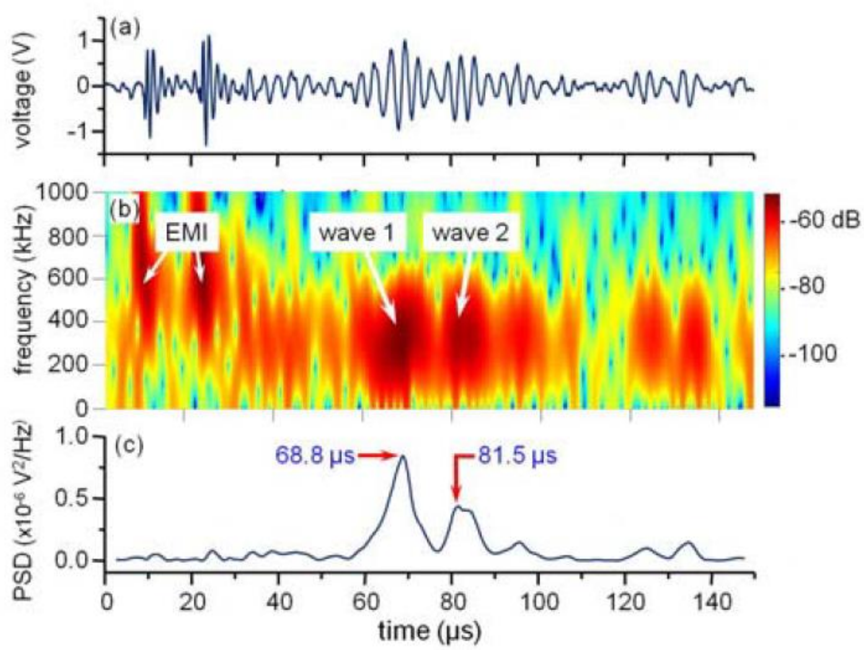

Figure 2.25: Spatial mapping of two close discharges
a) AE signal from 2 discharges 12.9 µs apart, b) Spectrogram, c) Power spectral density at 300 kHz

By successfully mapping electrical discharges, the results have an application for the respective identification of electrode length and workpiece height in fast-hole EDM and wire EDM. While the mapping of electrical discharges requires thorough investigation into single sparks, this thesis will focus on the larger picture. Using the knowledge learned from the state-of-the-art flushing techniques, a reliable and repeatable experimental setup will be created. Using this setup, the value of using acoustic emission in EDM will be determined as compared to the current process monitoring techniques that were discussed above. The success of acoustic emission in other machining processes and applications gives an optimistic outlook for acoustic emission in EDM.

3 Experimental

Experiments were performed on a sink EDM machine to determine the efficacy of using an acoustic emission sensor as a monitoring tool. A setup was created with a rotating electrode to ensure a consistent and quantifiable level of flushing. Experiments were run at various EDM parameters including flushing, electrode material, on-time, electrode polarity, gain, current and voltage which would simulate EDM conditions that would apply in an industry setting.

3.1 Machine Setup

The experiments were performed in the Machining Systems Laboratory (MSL) at McMaster University. The machine used for these experiments was an AGIETRON Impact 2 Ram-type EDM System and can be seen in Figure 3.1 below. The software is windows-based Agievision 2 control. The machine has 4 servo controlled axes, a 72 A power generator, a maximum rotational speed of 60 RPM, and uses an oil based dielectric.

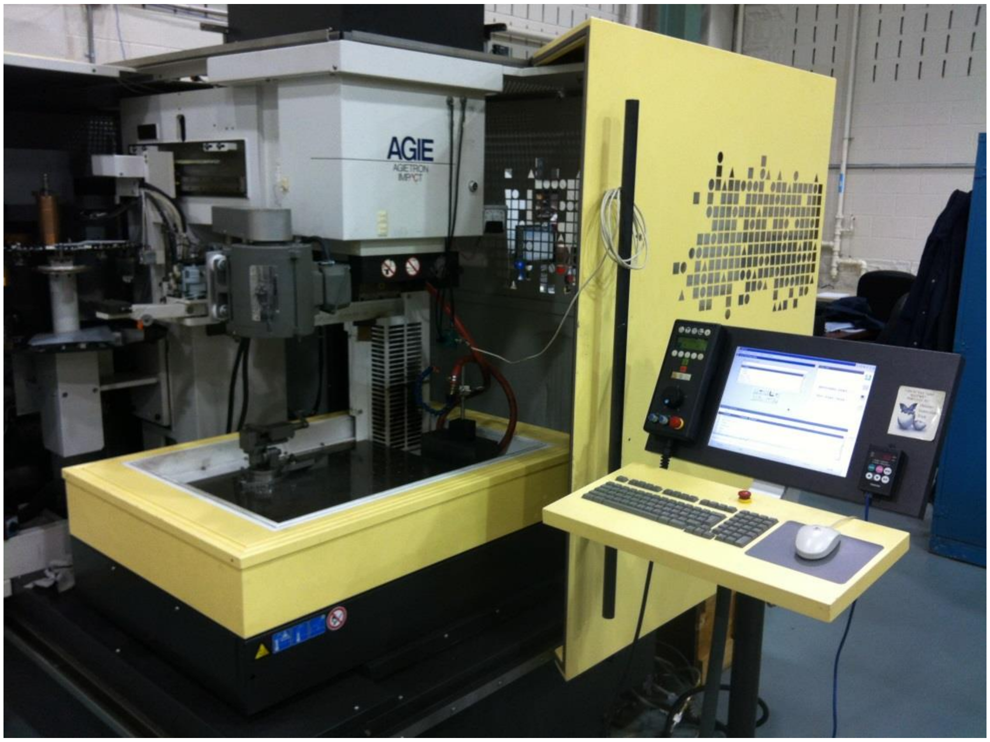

Figure 3.1: AGIETRON Impact 2

The electrode used in the experiments was a copper disk that was rotated against a mild steel workpiece which was slightly thinner than the copper disk. By rotating the copper disk at a constant speed and feeding the disk into the steel workpiece, the speed of the copper disk can be a representation of the level of flushing. Due to the extremely small gap width in EDM and the no-slip condition of the dielectric fluid, the surface speed of the outer surface of the copper disk can be seen as the rate that the debris is being flushed out of the gap.

3.1.1 Low Electrode Rotational Speed Setup

A 152.4 mm diameter copper disk with a thickness of 6.35 mm was manufactured as the tool electrode for the low electrode rotational speed setup. A 152.4 mm diameter was chosen to maximize the surface speed of the electrode as the C-axis rotation on the AGIETRON Impact 2 is only capable of 60 RPM. Therefore the range of electrode surface speeds using this setup was from 0 - 28.73 m/min. The workpiece had a width of 25.4 mm and a thickness of 3.175 mm. The workpiece was thinner than the electrode to ensure the electrode could not cut a groove into the workpiece and thus ensuring machining on just the circumferential surface. As well with a thinner workpiece, any face run-out of the electrode disk was of little concern. Although the electrode wear is considerably lower than that of the workpiece, the outer surface of the electrode was still trued using the C-axis on the EDM machine after several tests to remove any ‘steps’ created by the workpiece and to ensure close to zero radial run-out on the disk. The setup can be seen in Figure 3.2. The acoustic sensor was attached to the end of the workpiece with a nut and bolt through a hole in the workpiece. Copper was chosen as the electrode material as it is a common electrode material choice used in industry today. Copper is desirable due to its high electrical conductivity and its high thermal diffusivity [1].

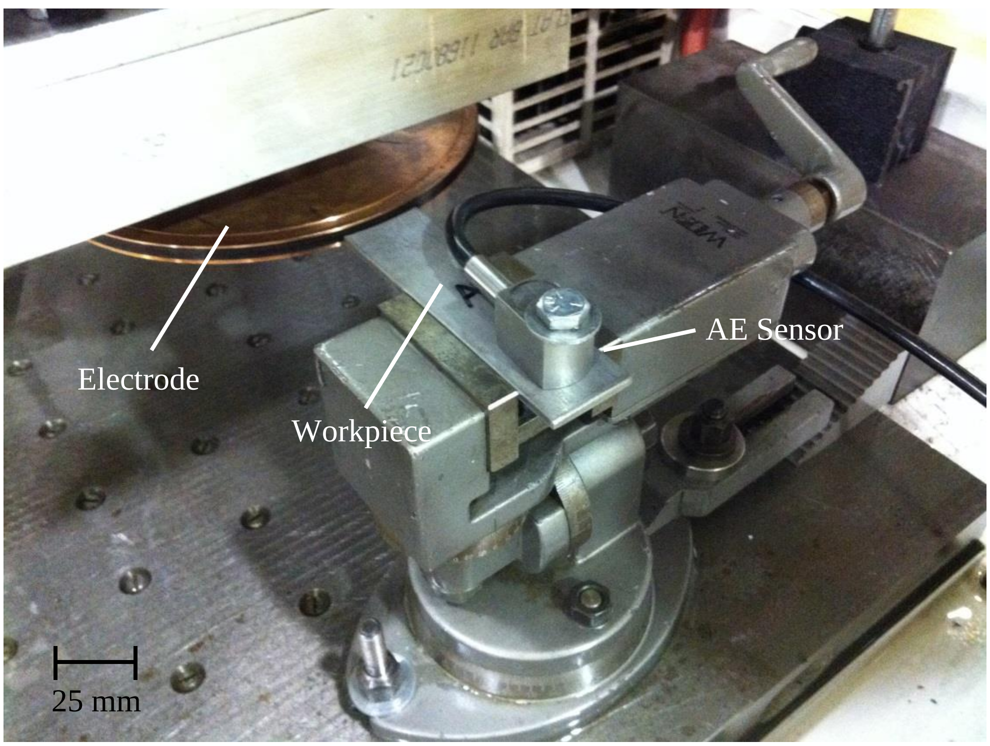

Figure 3.2: Low electrode rotational speed setup

3.1.2 High Electrode Rotational Speed Setup

To create high electrode surface speeds, the capabilities of the AGIETRON Impact 2 are not adequate. An apparatus designed and manufactured at McMaster University was attached to the machine. The apparatus can be seen in Figure 3.3 below, and mounts on the quill. It consists of a sturdy aluminum frame, a 3 phase 1 horsepower induction motor, and a pulley system that runs from the motor to the main shaft. The copper electrode is attached to the bottom of the main shaft which can be seen in Figure 3.3.

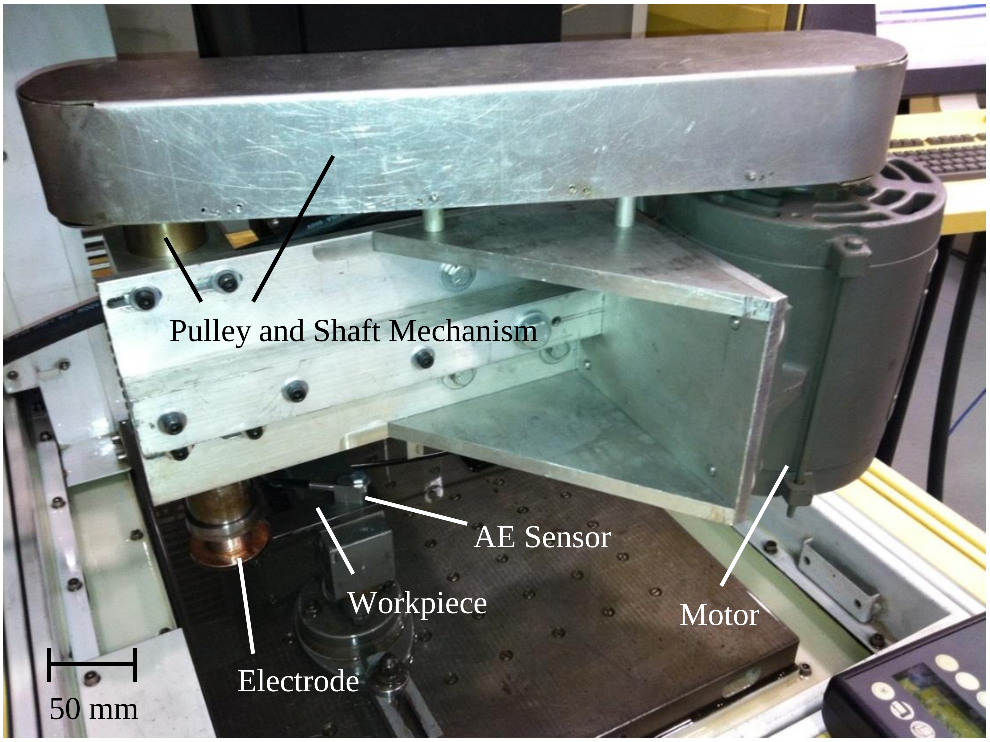

Figure 3.3: High electrode rotational speed setup apparatus

The electrode for the high electrode rotational speed setup is again a 6.35 mm thick copper disk. With this setup the disk was reduced in diameter to 54.6 mm because the motor is capable of speeds much higher than what was required for EDMing, and a smaller disk is easier to machine. The workpiece is the same as the low electrode rotational speed setup and can be seen in Figure 3.4.

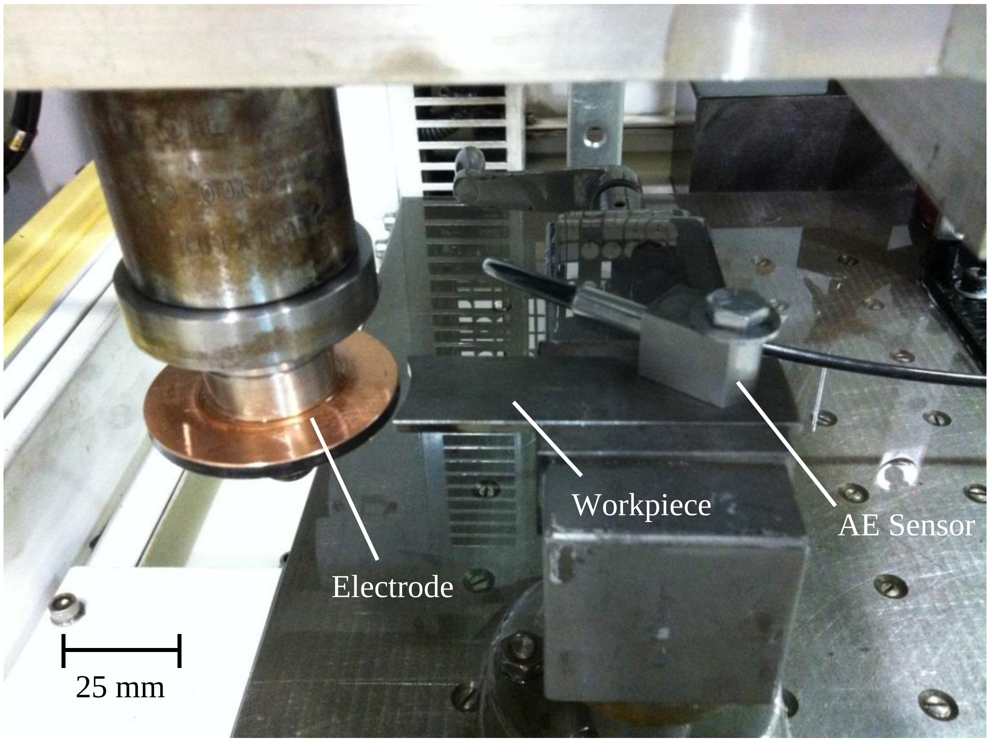

Figure 3.4: High electrode rotational speed setup

3.1.3 Multi-Material Electrode Setup

To investigate the effect of different electrode materials on the acoustic signal, an innovative electrode design was implemented (Figure 3.5). The design utilizes four different common electrode materials: copper, brass, graphite, and copper-infused graphite. A ¼ circle of each material with a thickness of 6.35 mm and a radius of 76.2 mm was manufactured. The four pieces were placed together to make a complete 152.4 mm diameter circle and then sandwiched between two aluminum plates to hold them firmly together. This complex design raises the question as to why four full disks, each made from one of the four materials were not used? With four separate electrodes, the process would have to be interrupted during testing to switch out electrodes, negatively affecting the repeatability of the testing procedure. Another design could be to manufacture four full disks, each made from one of the four materials and then stack them. This design would eliminate interrupting the process, however to interact each material with the workpiece, the z-axis would need to be varied during the process along with the c-axis and the servo controlled gap width maintaining axis (y-axis or x-axis). Adding the use of an additional axis in the process increases the sources of errors. With the chosen design, one test can be run without interruption, by using only two axes on the machine and it can provide equal length data about each electrode material.

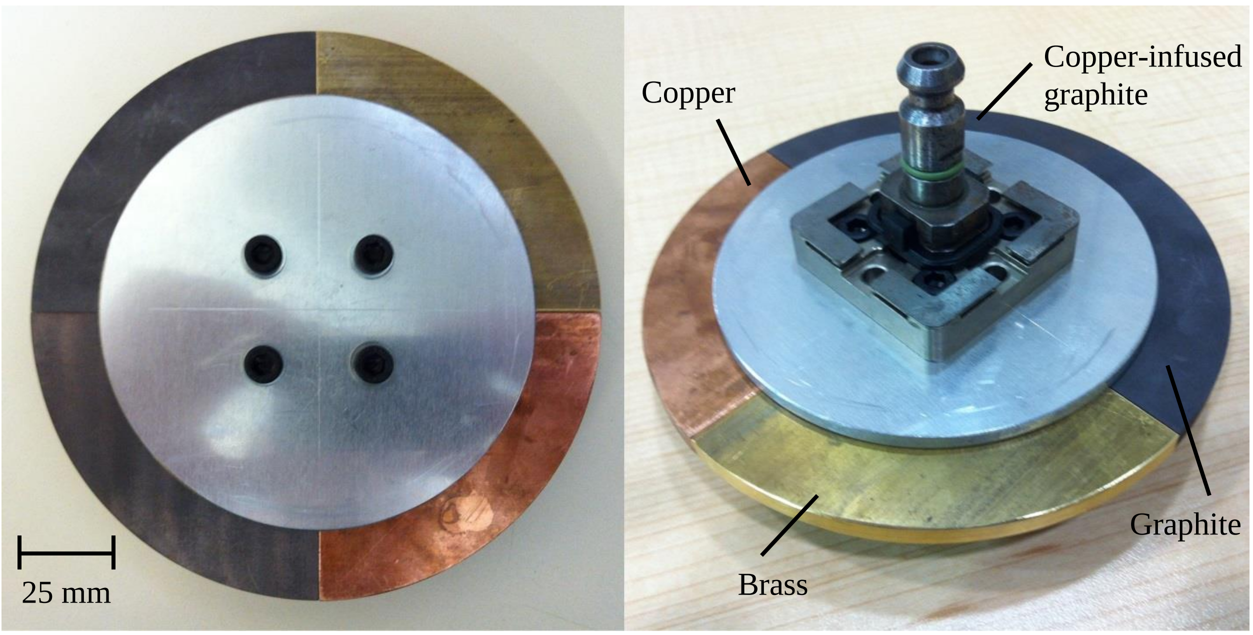

Figure 3.5: Multi-material electrode

Copper and graphite were chosen as electrode materials because they are the most common EDM electrode materials used today. As mentioned earlier, copper has many desirable properties including its high electrical conductivity, high thermal diffusivity, and copper is sometimes preferred over graphite because of the “untidiness” nature of machining graphite [34], and due to its structural integrity, copper can usually produce finer finishes than graphite [35]. Graphite is however the preferred electrode material for 90% of all sinker EDM applications [34]. Graphite has a melting point approximately 2500°C higher than copper making it a desirable electrode material. By controlling graphite properties such as particle size and density, EDM surface finishes can be improved to match that of copper. Graphite also has a very low coefficient of thermal expansion providing geometrical stability and has a density 5 times lower than copper which means lighter electrodes [36]. A graphite electrode infused with copper was chosen because it combines the advantages of both copper and graphite electrodes. The graphite is manufactured with a controlled amount of porosity which is then infiltrated with copper in a furnace by capillary action [34]. Brass was chosen as it was one of the first EDM electrode materials due to its low cost and easy machinability. Brass is seldom used in sink EDM applications in today's industry, although it is still a common choice for wire and fast hole EDM applications. Brass is also an alloy of copper and zinc so it was chosen to examine if there were any similarities in the brass and copper acoustic signal.

3.2 Acoustic Emission Setup

The acoustic sensor used was a Kistler Piezotron® Sensor type 8152B2 (Figure 3.6), a commercially available sensor. The sensing element is made of piezoelectric ceramic and is mounted on a thin steel diaphragm. The surface of the diaphragm protrudes slightly from the sensor housing to ensure a precisely defined coupling force when mounted. The sensor was mounted with a M6 bolt that is torqued to 9±1 N·m [37]. Alternatively, the sensor can be mounted with a magnetic clamp in the case where the workpiece needs to remain unaltered. The tightening torque along with Sonotech Soundsafe® ultrasonic couplant between the coupling surfaces ensure reproducible coupling. The sensor is designed so that the sensing element is acoustically isolated from the housing, protecting it from external noise.

Figure 3.6: Kistler acoustic emission sensor [37]

This sensor features a high sensitivity for Rayleigh waves, which as discussed in section 1.2.1, carries majority of the energy associated with an acoustic wave. The sensor used has a frequency range from 100 – 900 kHz as illustrated by the dotted line on the sensitivity plot shown in Figure 3.7.

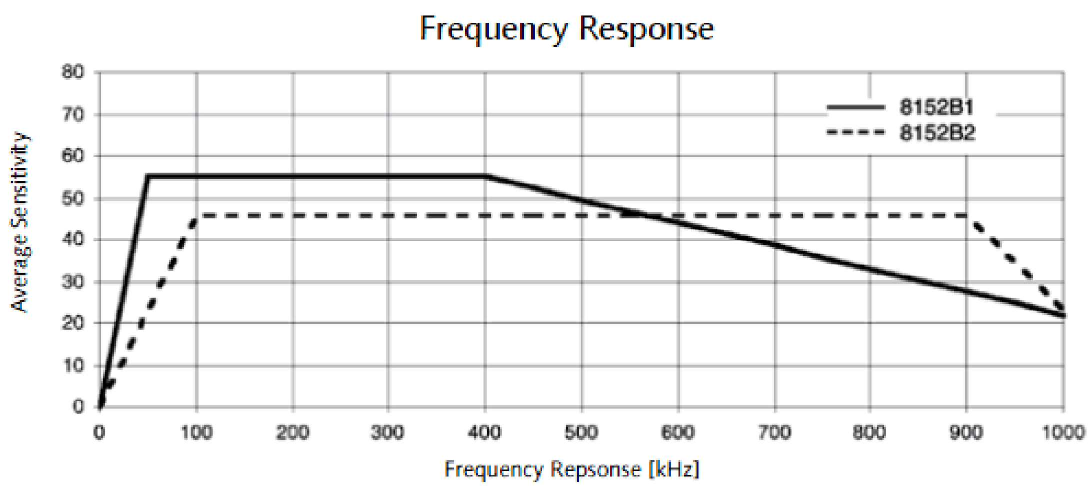

Figure 3.7: Sensitivity plot for Kistler AE sensors [37]

The Piezotron® Sensor is used in conjunction with a Kistler Piezotron® Coupler Type 5125B1. The Piezotron® Coupler is a high frequency amplifier which supplies power to the sensor and processes the AE signal. The amplifier gain can be set to (X1), (X10), or (X100) [38]. It was determined through experiments that with the materials and EDM parameters chosen, a gain of (X100) saturated the signal and therefore a gain of (X10) was used. The amplifier is also equipped with a Butterworth high pass and low pass filter. The high pass filter was set at 50 kHz and the low pass filter was set at 1 MHz, which can be manually set. The high pass and low pass filters were left at these frequencies in order to capture the full frequency range of the sensor.

Data was collected by a National Instruments PCI-6115 S series data acquisition (DAQ) board and a program written in MATLAB. This DAQ board features a maximum sampling rate of 10 million samples per second per channel [39]. Due to the fact that the desired acoustic wave remains in the frequency range below 500 kHz, a 10-fold higher sampling rate of 5 MHz was used. This sampling rate corresponds to a time resolution of 0.2 μs. Due to the high sampling rate used, a solid state hard drive was required to read the data. As well, another issue with the high sampling rate is the memory limitations of the computer. To account for this issue, test samples were collected for no longer than 4 seconds at a time.

Using the experimental setups described above, the following chapter will investigate the benefits of using an acoustic sensor as a real-time monitoring tool for EDM. The experiments will begin by exploring the effect of flushing on the AE signal and subsequently use this knowledge to improve process stability and material removal rates.

4 Results and Discussion

By understanding the state-of-the-art process monitoring methods for EDM, and the benefits of acoustic sensors seen in other machining processes, the results of using an acoustic sensor in an EDM application can now be presented. In this section, a suitable data processing technique will first be established in order to obtain an accurate and repeatable representation of the acoustic signal. The acoustic signal will then be related to various EDM parameters including flushing, machine gain, voltage, current, electrode material, electrode polarity and on-time.

4.1 Analyzing the Acoustic Signal

Collecting an acoustic signal using a commercial sensor is a basic task. The important step is properly analyzing the collected signal. Due to the high sampling rate used for collecting acoustic signals, small timeframes of a signal can reach sizes up to the order of gigabytes. This large volume of data must be analyzed in an efficient way that allows for a timely representation of the acoustic signal, while filtering out any unwanted data.

4.1.1 Filtering the Acoustic Signal

As discussed in section 1.2.3, the EMI component in the acoustic signal is undesired and should be filtered out in order to give a more accurate representation of the desired acoustic wave. The first set of experiments was conducted on the low electrode rotational speed setup described in section 3.1.1. A typical acoustic signal produced from an EDM discharge can be seen in Figure 4.1. The EMI occurs immediately at the point of discharge which is then followed by the acoustic wave. In this case, the distance travelled by the spark location to the sensor is roughly 70 mm, and if we take the speed of the Rayleigh wave in steel to be 3000 m/s [10], the acoustic wave should arrive approximately 23 μs after the EMI.

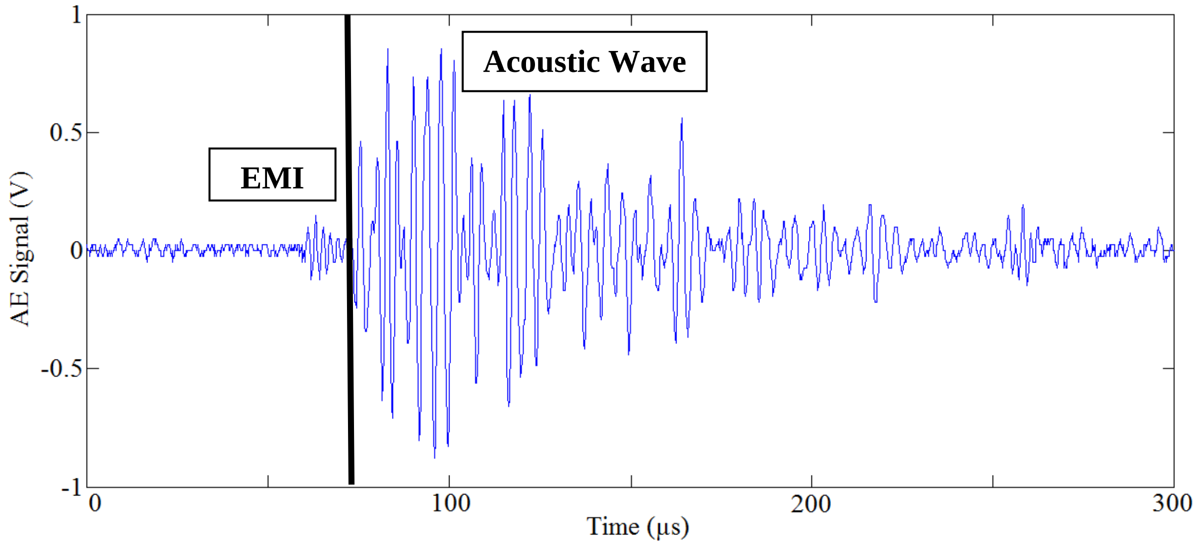

Figure 4.1: Typical acoustic burst signal (before filtering)

The EMI and acoustic wave were analyzed in the frequency spectrum separately which can be seen in Figure 4.2. It can be seen that the acoustic signal has frequency content below 450 kHz while the EMI has a frequency band between 400 and 600 kHz. This agrees with Smith and Koshy [33], who state that the frequency content of the AE wave is "largely confined to the 200-400 kHz interval" and that "the EMI is manifest essentially at frequencies upwards of 500 kHz".

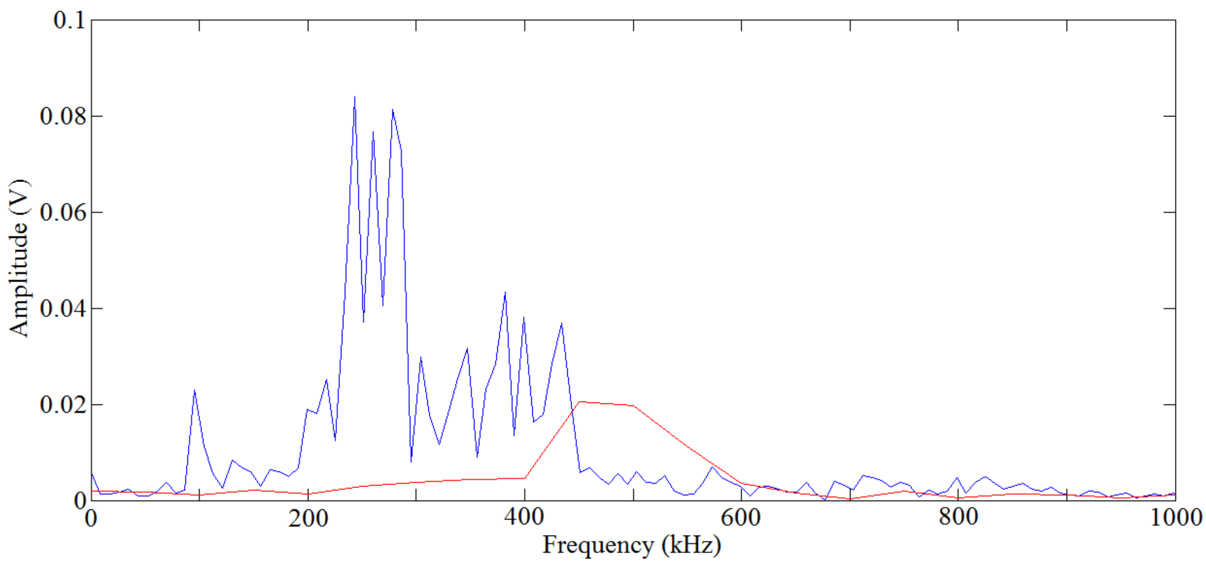

Figure 4.2: Frequency spectrum of EMI and AE waves

For the purpose of this research, the acoustic wave is the only desired component of the AE signal, and therefore the EMI will be filtered out using a Butterworth filter at 450 kHz. The typical signal shown in Figure 4.1 after being filtered, is shown in Figure 4.3. It can be seen that the EMI is not completely removed, but this is due to the fact that the EMI and the acoustic signal have a slightly overlapping frequency range. Nevertheless, the EMI has been reduced. Now with the acoustic signal being received in a desired form, methods of quantifying and comparing the signals may be discussed.

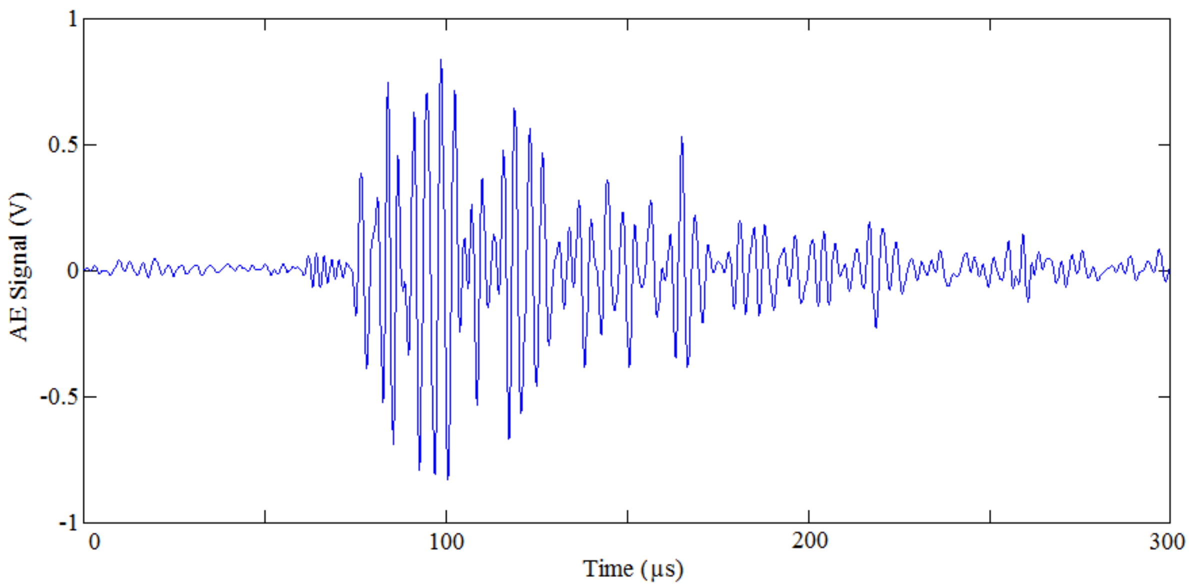

Figure 4.3: Typical acoustic burst signal (after filtering)

4.1.2 FFT of the Acoustic Signal

A fast Fourier transform (FFT) is a useful numerical algorithm that will be used for not only looking at frequencies present in the acoustic signal, but also to compare relative amplitudes between signals. An example can be seen below in Figure 4.4. By doing a FFT, particular frequency bands can stand out when differentiated signals. It can also be used when comparing two different acoustic signals corresponding to thousands of discharges such as in Figure 4.4a and Figure 4.4b, where it can be difficult to tell which is the stronger signal. Once a FFT is taken of the AE signals, it can clearly be seen that signal 2 (Figure 4.4d) is stronger than signal 1 (Figure 4.4c).

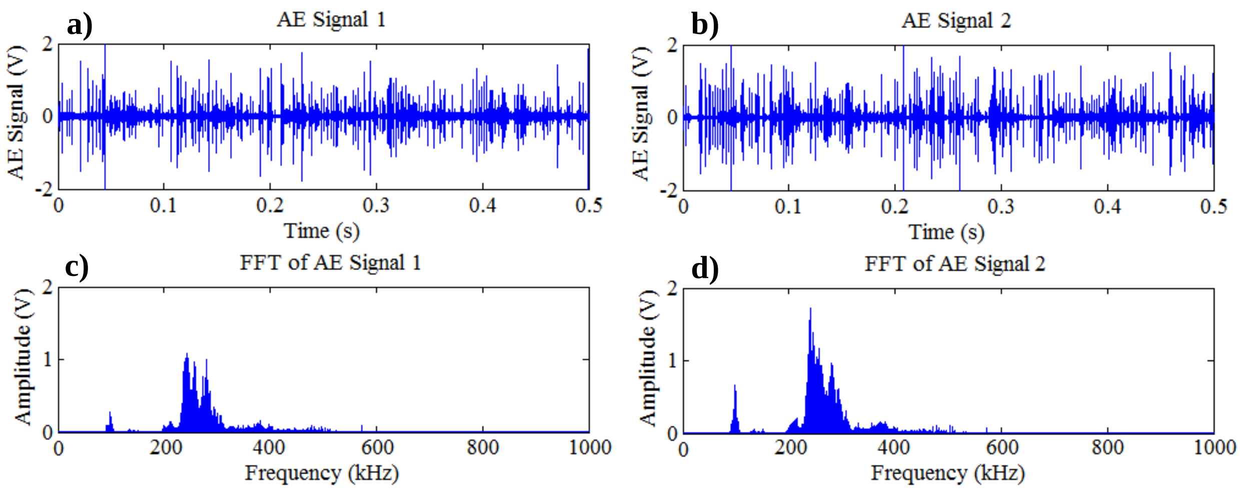

Figure 4.4: FFT comparison of AE signals

4.1.3 Deconvolution

Deconvolution is an algorithm based process used to the remove distortions such as echoes, sensor resonances, and distortions from the bandpass filters. Convolution is the integral of the product of two functions after one is reversed and shifted as described in Equation 4.1 and Figure 4.5 below.

$$(f * g)(t) = \int_{-\infty}^{\infty} f(\tau)g(t-\tau)d\tau \quad \textbf{Equation 4.1}$$

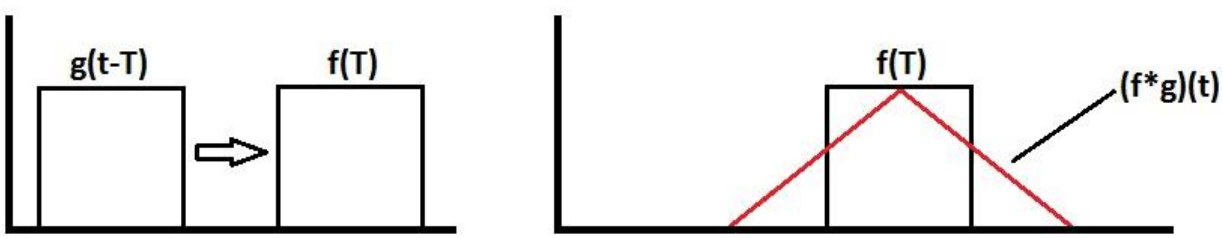

Figure 4.5: Convolution

The object of deconvolution in the processing of AE signals is to find f in the convolution equation (Equation 4.2). The AE signal recorded would be h, and the unwanted signal g will have been convolved with the desired signal f.

$$f * g = h \qquad \textbf{Equation 4.2}$$

The benefit of using a deconvolution technique for this project was investigated. A recursive least square (RLS) filter was used which are useful for separating impulsive signals from distortions such as echoes, sensor resonances, and the type of bandpass filtering used [15]. When filtering a signal with an RLS filter, an appropriate filter length must be determined. Too short of a filter will result in degraded echo cancellation performance and too long of a filter will result in a slow convergence time [40]. Using Matlab, an RLS filter was applied to a sample signal that spanned 0.5 seconds. From the sample, one acoustic burst was isolated and can be seen in Figure 4.6. Figure 4.6a shows the acoustic burst before the RLS filter was applied. Figure 4.6b shows the acoustic burst after an RLS filter with a filter length of 20 coefficients was applied and Figure 4.6c is with a filter length of 400 coefficients. It can be seen that the RLS filter provides a cleaner signal, and when the filter length is increased to 400, the signal improves just very slightly. The issue with this filter is the time required for the filtering process to take place. For the sample duration of 0.5 seconds, the RLS filter takes several minutes when using a filter length of 20, and takes over an hour when using a filter length of 400. Shown in Figure 4.7 are the FFTs of the three corresponding AE signals. For each case, the filter does not change the FFT drastically other than slightly reducing the amplitude at every frequency. The advantages and disadvantages of the RLS filter was weighed, and it was decided that for the time taken to filter the AE signal, the benefit is not significant enough to justify filtering the AE signal. For the remainder of the data presented in this project, RLS will not hence be applied.

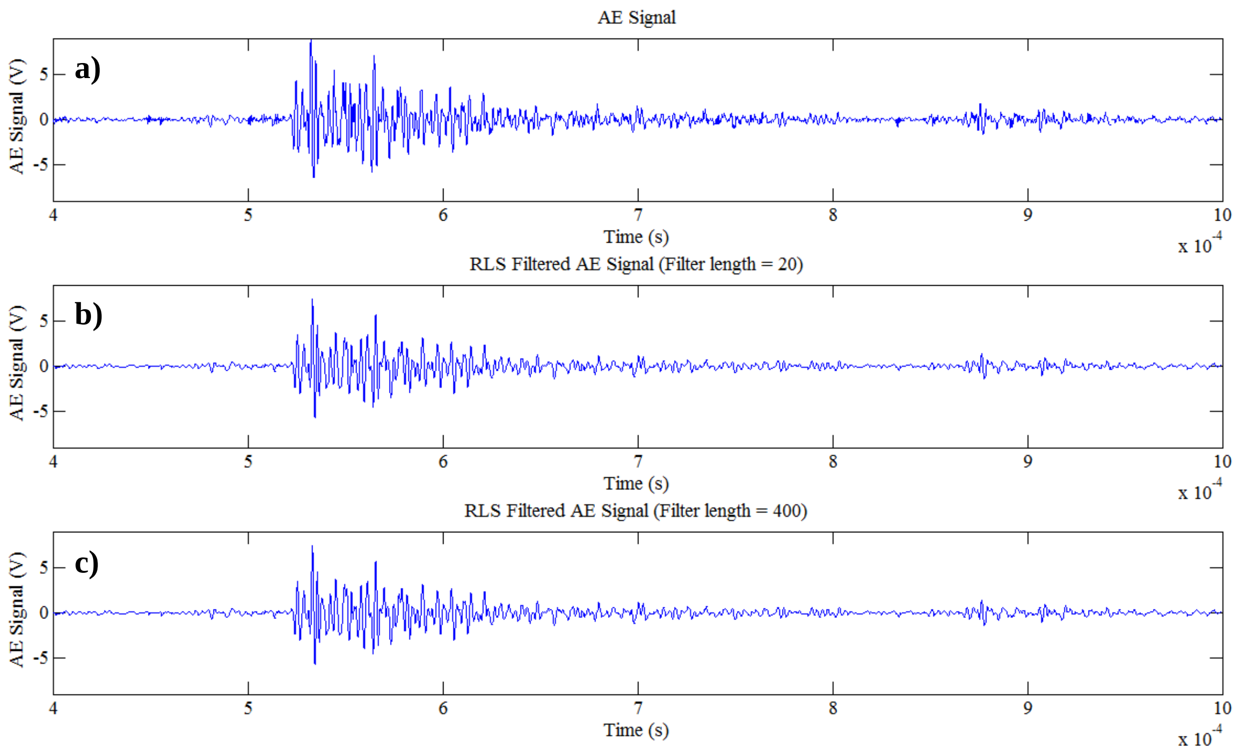

Figure 4.6: RLS filtering of AE signal
a) AE Signal (no filtering), b) Filter with length of 20, c) Filter with length of 400

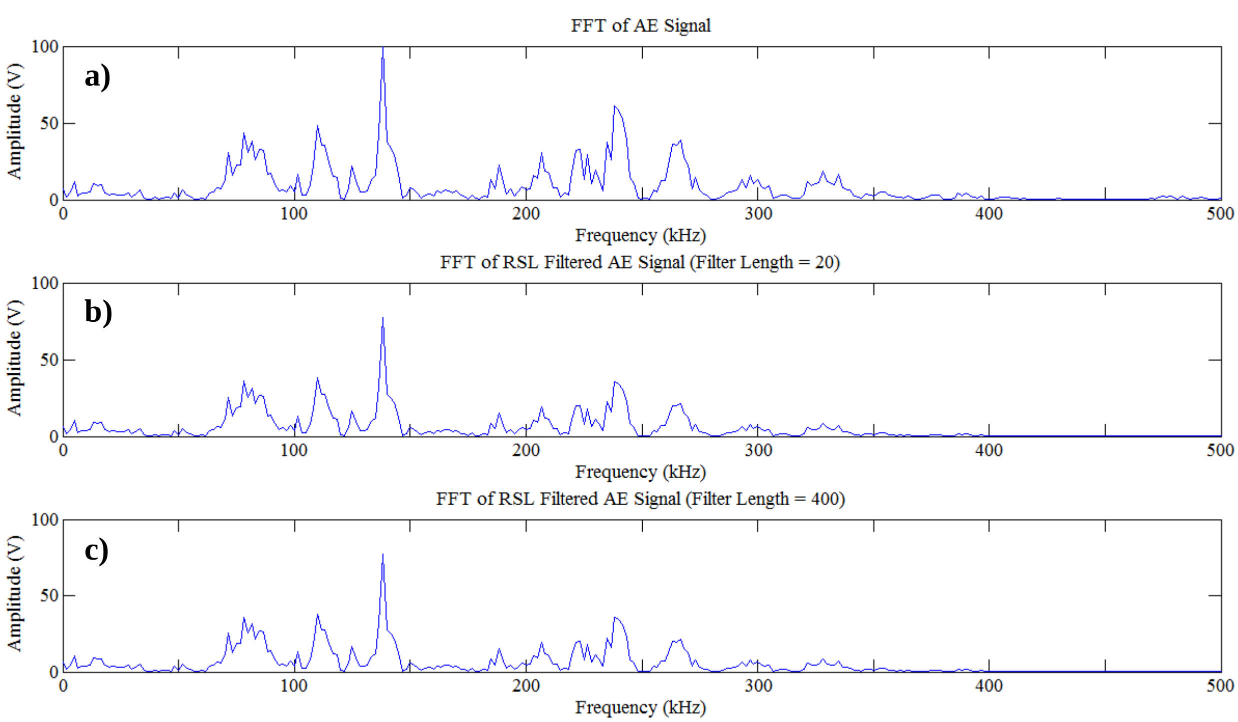

Figure 4.7: FFTs of RLS filtered AE signal
a) AE Signal (no filtering), b) Filter with length of 20, c) Filter with length of 400

4.1.4 RMS of the Acoustic Signal

Calculating the root mean square (RMS) is another useful tool when comparing two different AE signals. Although typical AE RMS time constants generally range between 0.1 and 100 milliseconds [41], the time constant used in this project may not fall in that range due to its different purpose. Typical AE RMS signals are a time-averaged value, calculated over a small interval and reported as a voltage. The main advantage of using the RMS signal over the raw signal is the increased simplicity due to the lower sampling rates and is useful for monitoring varying amplitudes in the raw AE signal. For this research project, the RMS will be used to quantify the overall strength of the AE signal. The RMS is calculated as follows:

$$x_{RMS} = \sqrt{\frac{\sum_{i=1}^{n} {x_i}^2}{n}} \qquad \textbf{Equation 4.3}$$

Where n is the number of data points included in a constant time interval and x refers to individual data points. A reliable and repeatable value of the RMS is desired for this research in order to get a quantifiable representation of the AE signal. Therefore a time constant will be chosen that provides a consistent value with low variability.

A test was conducted in order to determine a suitable time constant. A typical raw AE signal (Figure 4.8) was obtained using the setup described in section 3.1.1. RMS values were then calculated from this signal using various time constants. For each time constant, five values of RMS were calculated across the signal, which were then averaged and plotted as shown in Figure 4.9. From this plot, a RMS time constant of 200 milliseconds was chosen as this is the point where the RMS value appears to converge. When the RMS time constant is too small, there is more variability because the section that is averaged may only span a section of instability or a section of only ideal sparks. The RMS time constant needs to be larger to include more discharges to get a better representation of the data. All RMS values calculated for the remainder of this research will use a time constant of 200 milliseconds.

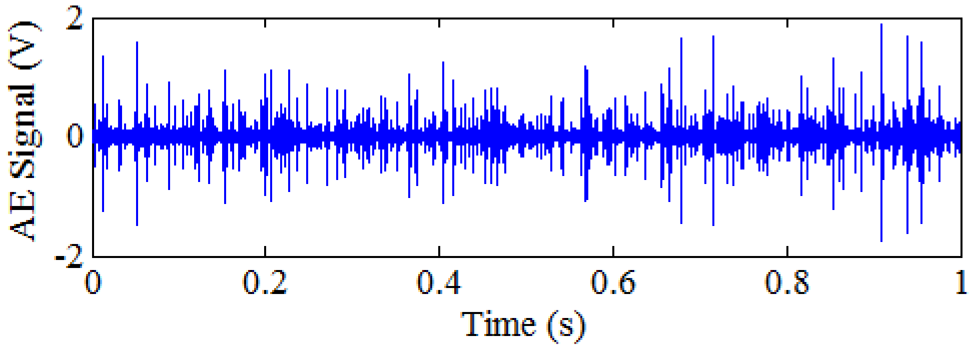

Figure 4.8: Sample raw AE Signal for RMS time constant test

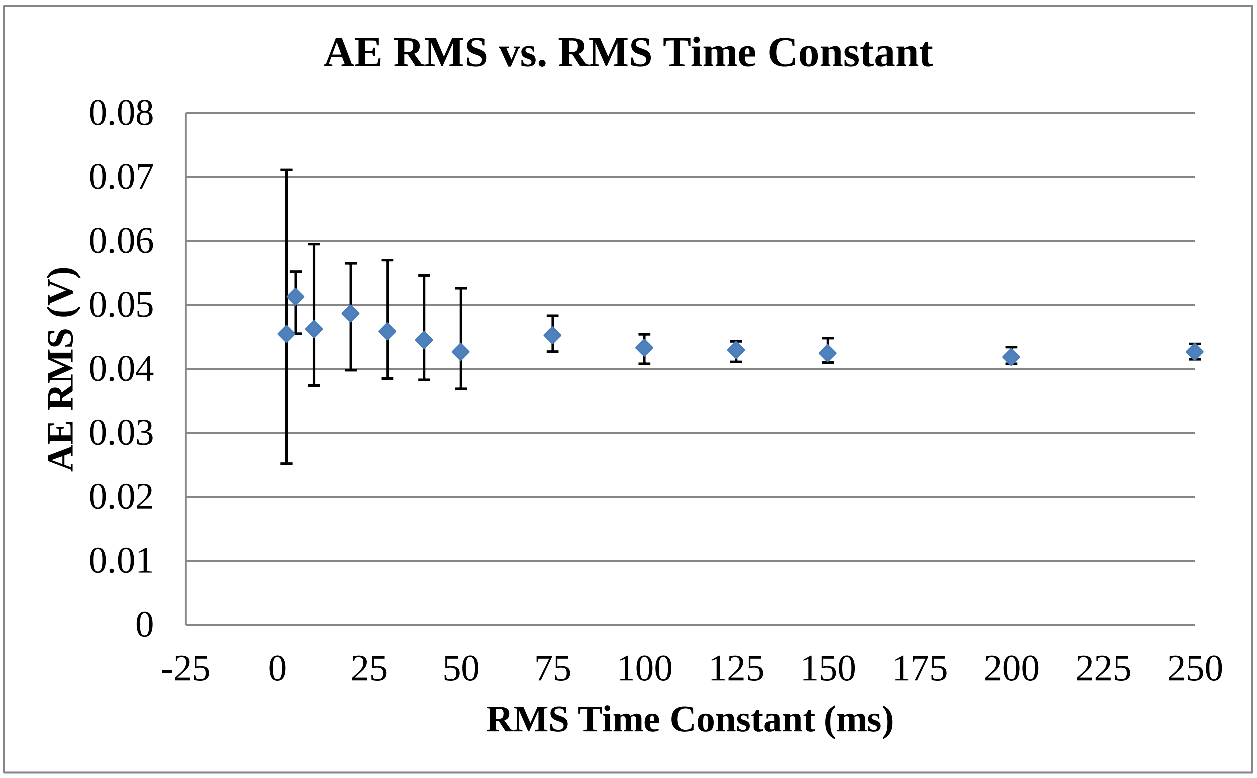

Figure 4.9: Determination of RMS time constant

Now that suitable data processing techniques have been established, tests can be conducted and the results can be analyzed in an accurate and repeatable fashion. AE data can be filtered and then analyzed in its raw form, in the frequency spectrum, or by calculating RMS values of the data.

4.2 Effect of Flushing

Using the setup described in section 3.1.1, tests were conducted to determine the effect of flushing on the acoustic emission signal. During the EDM process, the copper disk was rotated at 1, 5, 15, 30, and 60 RPM, which with a 152.4 mm diameter disk equates to peripheral speeds of 0.48, 2.4, 7.2, 14.4, and 28.7 m/min. AE samples were collected at each speed. As discussed in section 3.1, the peripheral speed of the disk is a representation of the level of flushing. The EDM parameters used for this test can be found in Table 4.1. The parameter ‘gain’ refers to the speed at which the servo control feed adjusts to maintain the gap width. The parameter ‘compression’ refers to the gap width which has a direct influence on the delay time. These EDM parameters were one of the manufacturer's recommended parameter sets when machining steel with a copper electrode. Only the current was lowered in order to conserve material and to have a less aggressive machining environment.

Table 4.1: EDM Parameters (Flushing)

On-time	154 μs
Off-time	37 μs
Current	2.4 A
Open Circuit Voltage	100 V
Electrode Polarity	Positive
Gain	15
Compression	18
AE Sampling Rate	5,000,000 samples/second
Sample Length	1 second

Frequency plots were created from the 1 second test samples, which can be seen in Figure 4.10 below. It is very clear that as the level of flushing increases, the strength of the AE signal increases as well. With a rotation speed of 1 RPM, the process has inadequate flushing and has relatively no acoustic signal (Figure 4.10a), whereas with a rotation speed of 60 RPM, the process has adequate flushing and has the strongest acoustic signal (Figure 4.10e). It is also important to note that the acoustic wave remains in the same frequency range at each level of flushing.

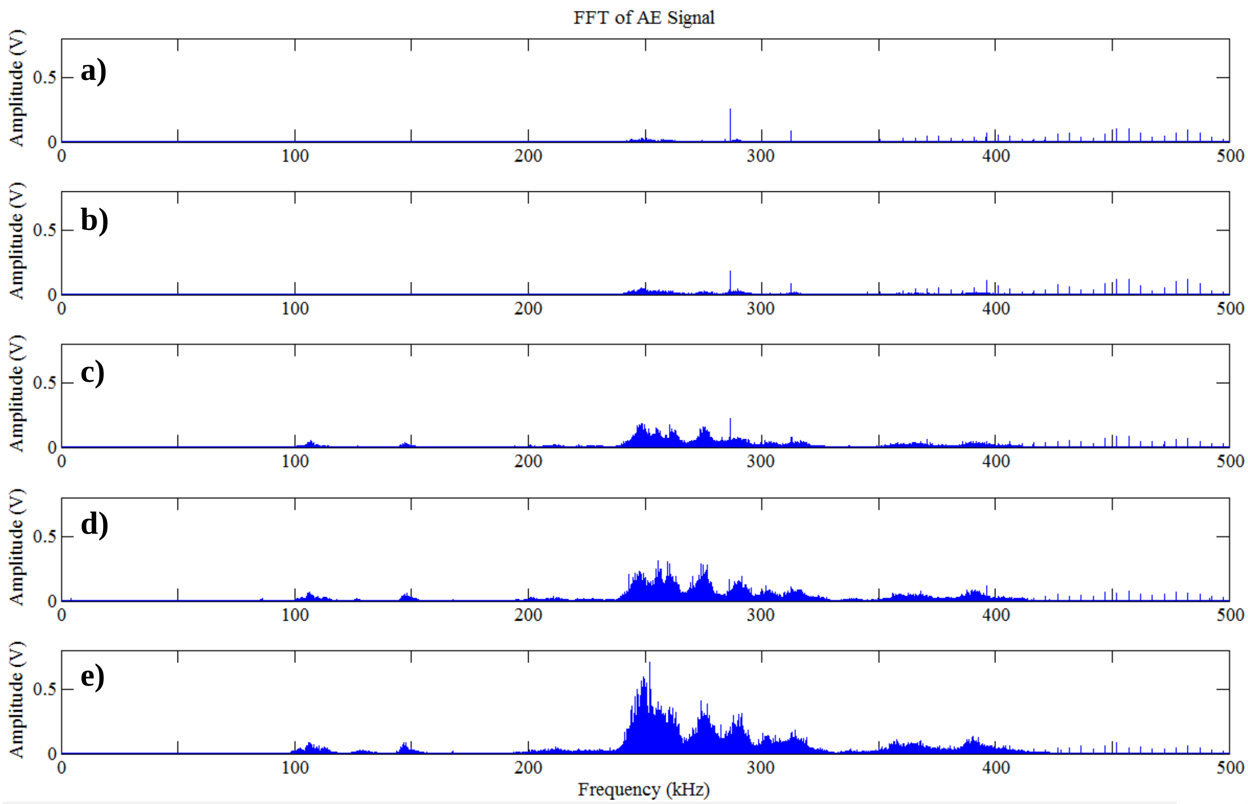

Figure 4.10: Frequency plots of AE signals for various flushing levels
a) 0.48 m/min, b) 2.4 m/min, c) 7.2 m/min, d) 14.4 m/min, e) 28.7 m/min

To verify that the trend that is seen is actually the effect of flushing, a test was run using jet flushing, which was explained in section 2.1.1. An external nozzle was placed over top of the gap between the copper electrode and steel workpiece (Figure 4.11).

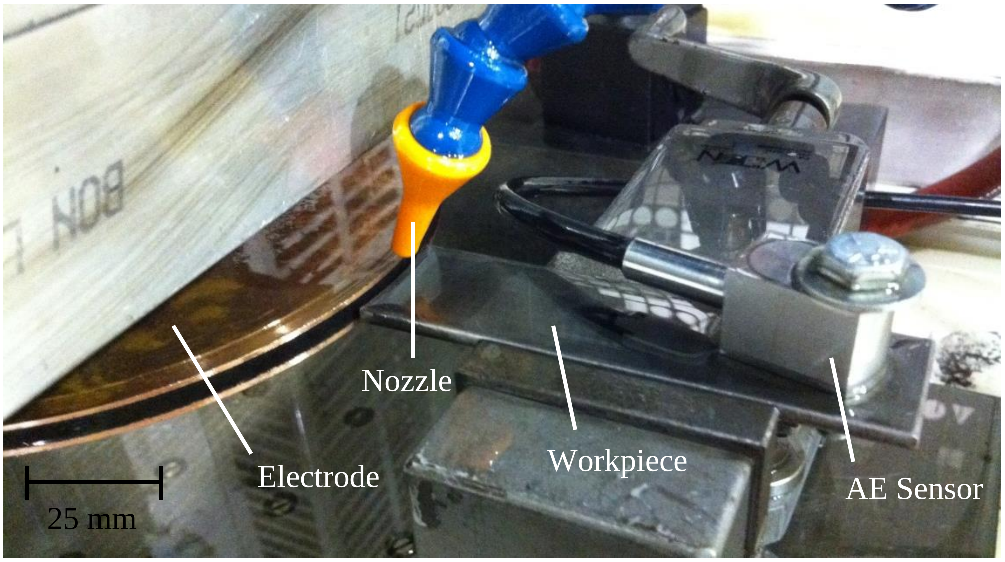

Figure 4.11: External flushing setup

The copper disk was rotated at 5 RPM or 2.4 m/min in order to set a baseline, and then jet flushing was applied through the external nozzle and through the gap at pressures of 0.25 and 0.5 bar. Frequency plots of the 1 second samples were created and can be seen in Figure 4.12 below. It can be seen that as the pressure is increased, the strength of the AE signal increases as well. The fluid pressure on the machine has some degree of variability however, and does not ensure consistent flushing through the gap, which is why the rotating disk is used for this research.

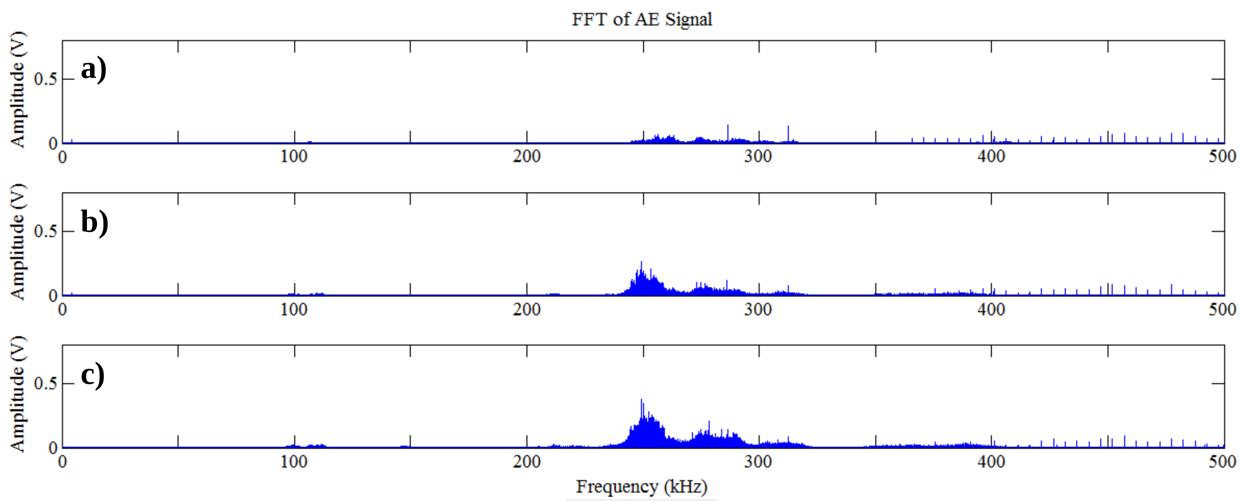

Figure 4.12: Frequency plots of AE signals with external flushing
a) 0 bar, b) 0.25 bar, c) 0.5 bar

As discussed in section 4.1.4, the RMS value of the AE signal can also be useful for quantifying the AE signal. For each rotation speed of the copper disk, 1 second samples were collected at five separate instances, and then using the time constant of 200 milliseconds, twenty five RMS values could be calculated for each speed. The resulting averaged RMS values along with their standard deviations are plotted below in Figure 4.13. By plotting the acoustic emission RMS values, the trend becomes more apparent. The AE RMS values increase with the electrode speed; however it appears that the AE RMS values will eventually reach a maximum value.

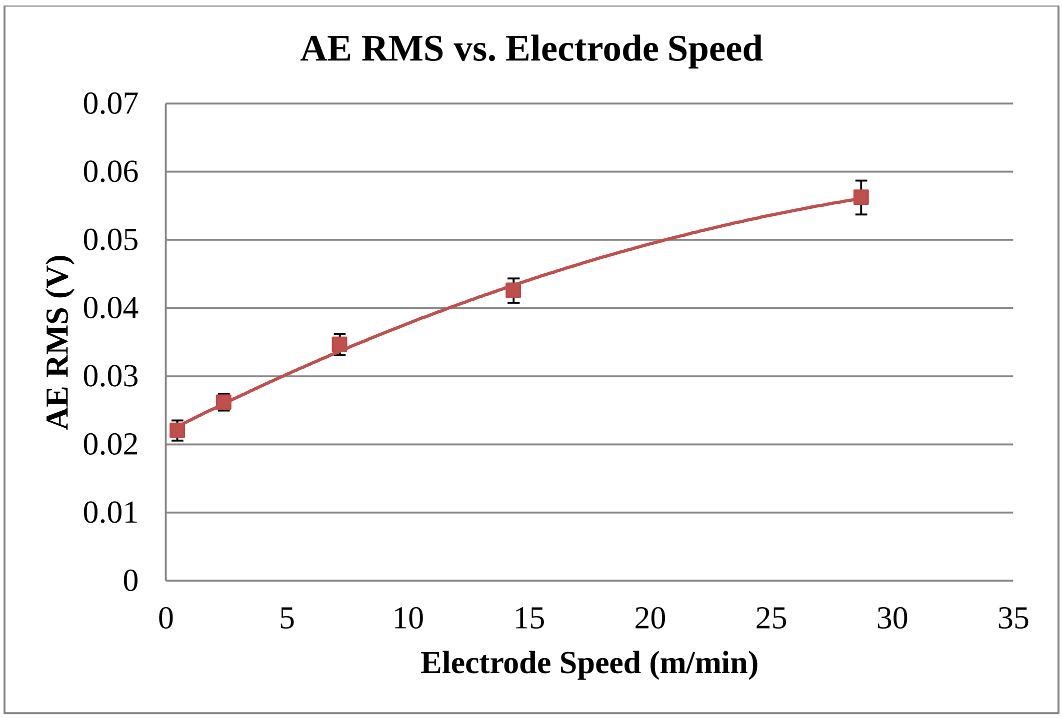

Figure 4.13: AE RMS versus electrode speed (low electrode rotational speed setup)

To investigate the trend of the AE RMS value at higher speeds, the higher electrode rotational speed setup described in section 3.1.2 was required. The tests were run on the new setup using the same EDM parameters and the same AE collection method as with the low electrode rotational speed setup. The AE RMS results can be seen in Figure 4.14. The disk was rotated at speeds in order to obtain data every 25 m/min. It can be seen that the AE RMS increases with the surface speed and then decreases as speed increases further. The results from the low rotational electrode surface speed setup were also plotted on the same graph to show that with the same parameters, the AE data is repeatable across two different setups.

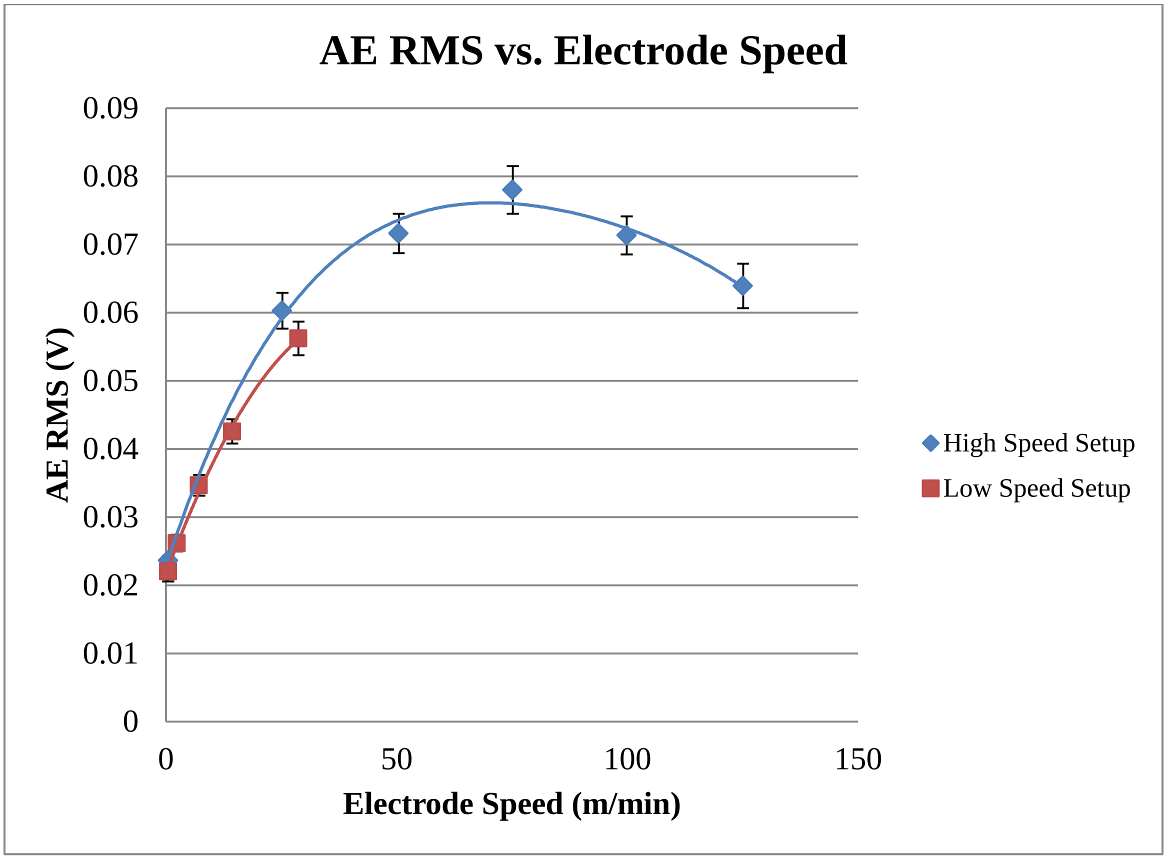

Figure 4.14: AE RMS versus electrode speed (high rotational speed setup)

4.2.1 AE Relationship to MRR

The trend of the AE RMS with the high speed setup plot in Figure 4.14 resembles the trend expected of the material removal rate. In the EDM process, as the level of flushing increases, more debris is removed reducing the chances of arcing and short circuiting which increases the number of effective discharges. Also, better flushing will help aid the removal of the molten material from the crater left by the discharge and reduce the chances of the material resolidifing on the workpiece. Alternatively, with too much flushing the dielectric becomes too clean and is not given enough time to ionize before it is flushed away, reducing the number of effective discharges. Some level of debris is advantageous as it promotes the initiation of a spark. Therefore, just as the AE RMS trend shows, the MRR will have the maximum value at an optimal level of flushing.

To further investigate the relationship between the AE RMS value and the MRR, the material removal rates were measured immediately following the acoustic emission readings. The workpiece sample was initially weighed before it was placed in the EDM machine to be machined with a certain electrode speed for a duration of 10 minutes, and then weighed again. The 1 second AE signals were collected at minutes 2, 4, 6, 8, and 10. The material removal rates were calculated from the material removal over those 10 minutes and plotted along with the AE RMS values in Figure 4.15 below. It can be seen that the AE RMS and MRR have similar trends and both have an optimal flushing level at 75 m/min.

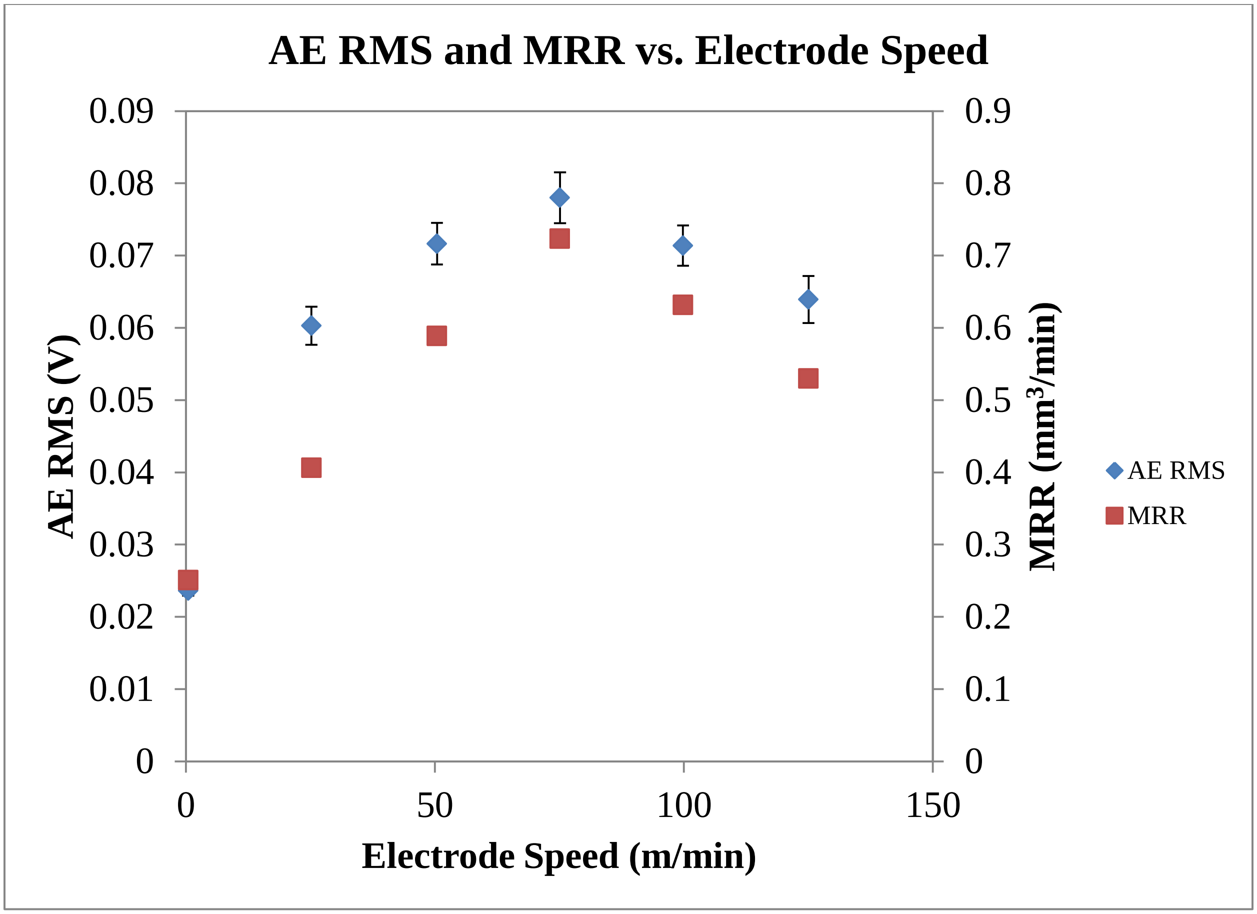

Figure 4.15: Relationship of AE RMS and MRR

The direct comparison between the AE RMS values and the MRR values is shown in Figure 4.16. Using the AE RMS as a representation of the MRR offers a huge benefit for the in-process optimization of the EDM process. For example, in an industry setting, if an operator wants to find the optimal flushing level using just the MRR as an indicator, it would be a very time consuming process. They would need to weigh the sample, fix the sample in the machine, start machining at one specific flushing level for several minutes, stop the machine, remove the sample, weigh the sample, and then repeat this process numerous times. Whereas, using the AE RMS as an indicator, the operator would need to fix the sample and AE sensor once in the machine, start machining and then as the flushing is adjusted, take a 1 second AE reading at each level of flushing. The time taken to conduct the MRR method would take hours, whereas the AE RMS method would take just several seconds.

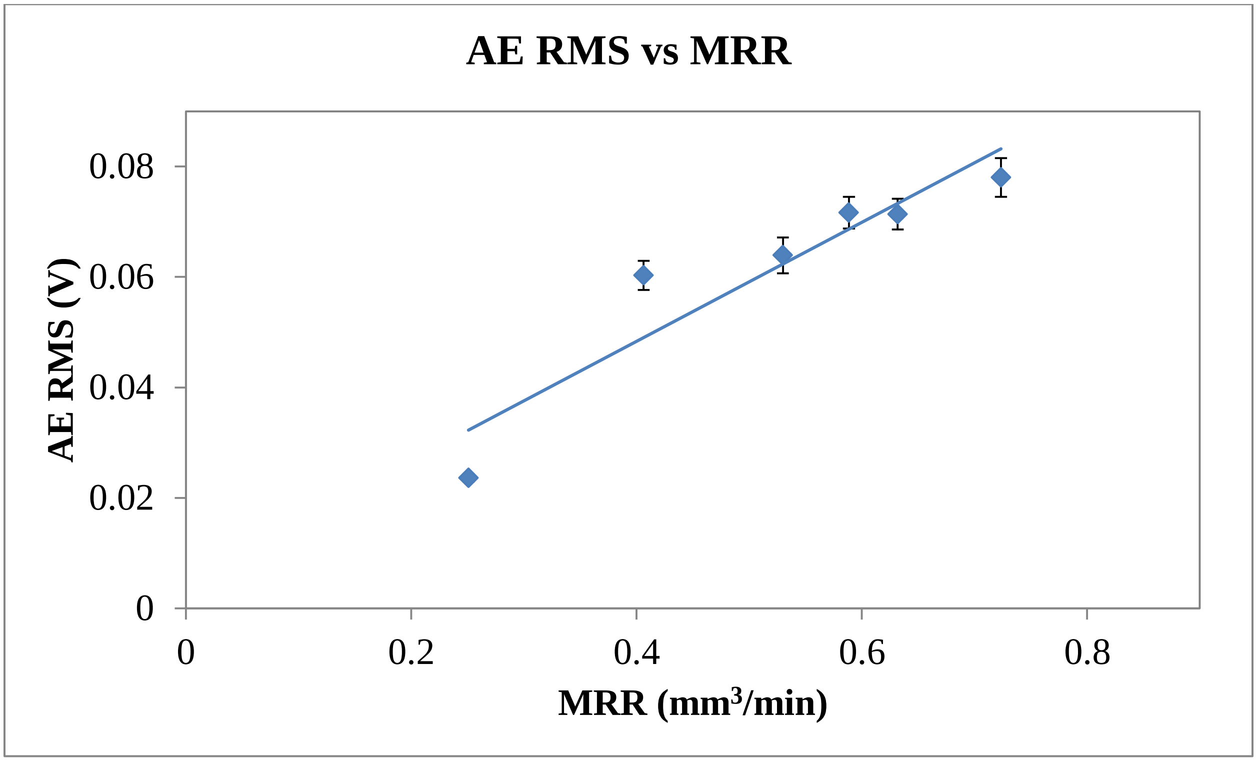

Figure 4.16: AE RMS versus MRR

Weingärtner et al. used electrode surface speeds up to 80 m/s [42] whereas the optimal surface speed in this research was found to be only 75 m/min. This discrepancy can be explained by looking closer at the parameters used in each case. Weingärtner et al. used a low on-time of 1.2 µs, which with a surface speed of 80 m/s equates to a relative displacement of 96 µm between the electrode and workpiece. Now if the higher on-time used in this project (154 µs), was calculated with that relative displacement of 96 µm, the surface speed equates to a much lower 37.4 m/min. Using the same relative displacement, one can compare the MRR results from Weingärtner et al. (Figure 4.17), and the AE RMS results from this project (Figure 4.18) and see that they are quite similar. The relative displacement may be a more representative value of the flushing rather than the surface speed. For example, in wire EDM with a typical wire speed of 20 m/min and discharge duration of 0.5 µs, the wire only moves 0.5 µm throughout the discharge. This 0.5 µm is very little compared to the size of the craters, and in the case of high discharge energies, the crater sizes can be hundreds of times larger, meaning the 0.5 µm of surface movement will not adequately flush out the crater.

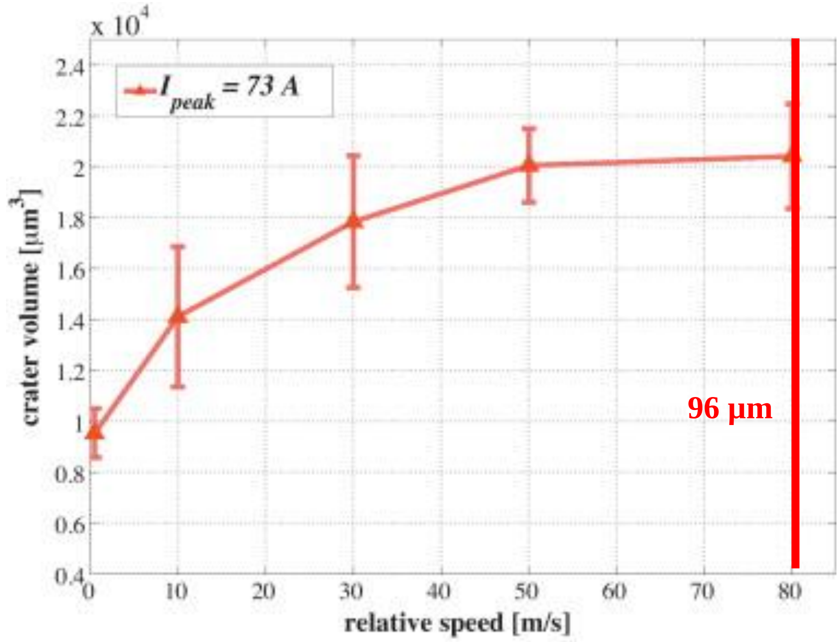

Figure 4.17: Influence of relative speed on eroded volume of single craters [42]

The results from Weingärtner et al. appear to be reaching a maximum at a relative displacement of 96 µm, but that cannot be confidently concluded without higher speeds being tested. The results shown in Figure 4.18 also appear to be reaching a maximum at 96 µm, but as proven earlier, the maximum is reached at a surface speed of 75 m/min or a relative displacement of 192.5 µm.

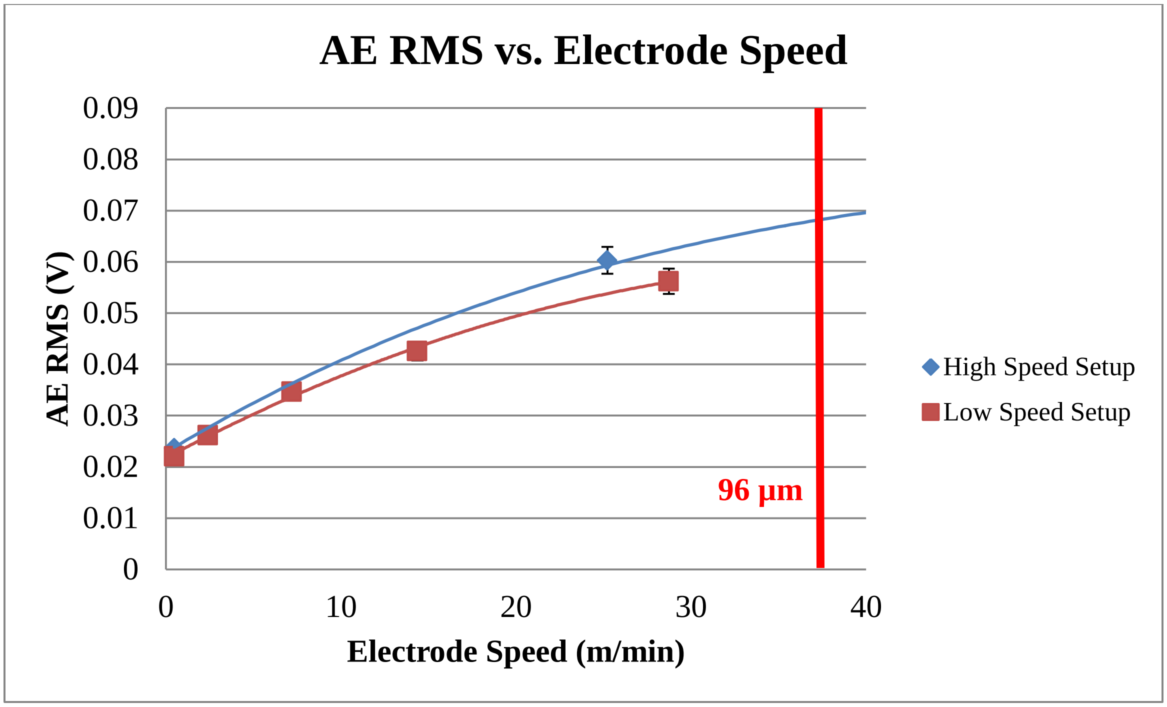

Figure 4.18: Influence of relative speed on AE RMS

4.2.2 Effect of Flushing on the Current Signal

To investigate if the AE signal carries any unique process information as it relates to Figure 4.15, the current signal was collected under the same parameters as the AE signal. To measure the current signal, a Pearson current monitor model 411 was used [43], allowing the current signal to be collected using the same data acquisition system as the AE signal. RMS values of the current signal were calculated using a time constant of 200 milliseconds, just like the AE RMS. The current signal RMS values are plotted versus the electrode speed in Figure 4.19. It can be seen that the current signal RMS values remain relatively constant as the electrode speed increases. This is likely due to the similar current waveforms of an arc and a spark as discussed in section 1.1. The RMS values appear to be declining slightly at higher electrode speeds which is expected because when there is too much flushing, open circuits would occur which have no current waveform. The highest current signal RMS value appears at 25 m/min, however this does not mean that this is the highest MRR. At 25 m/min, the occurrence of arcs could raise this RMS value, and also it is more likely that the amount of material removed per spark is higher for a better level of flushing.

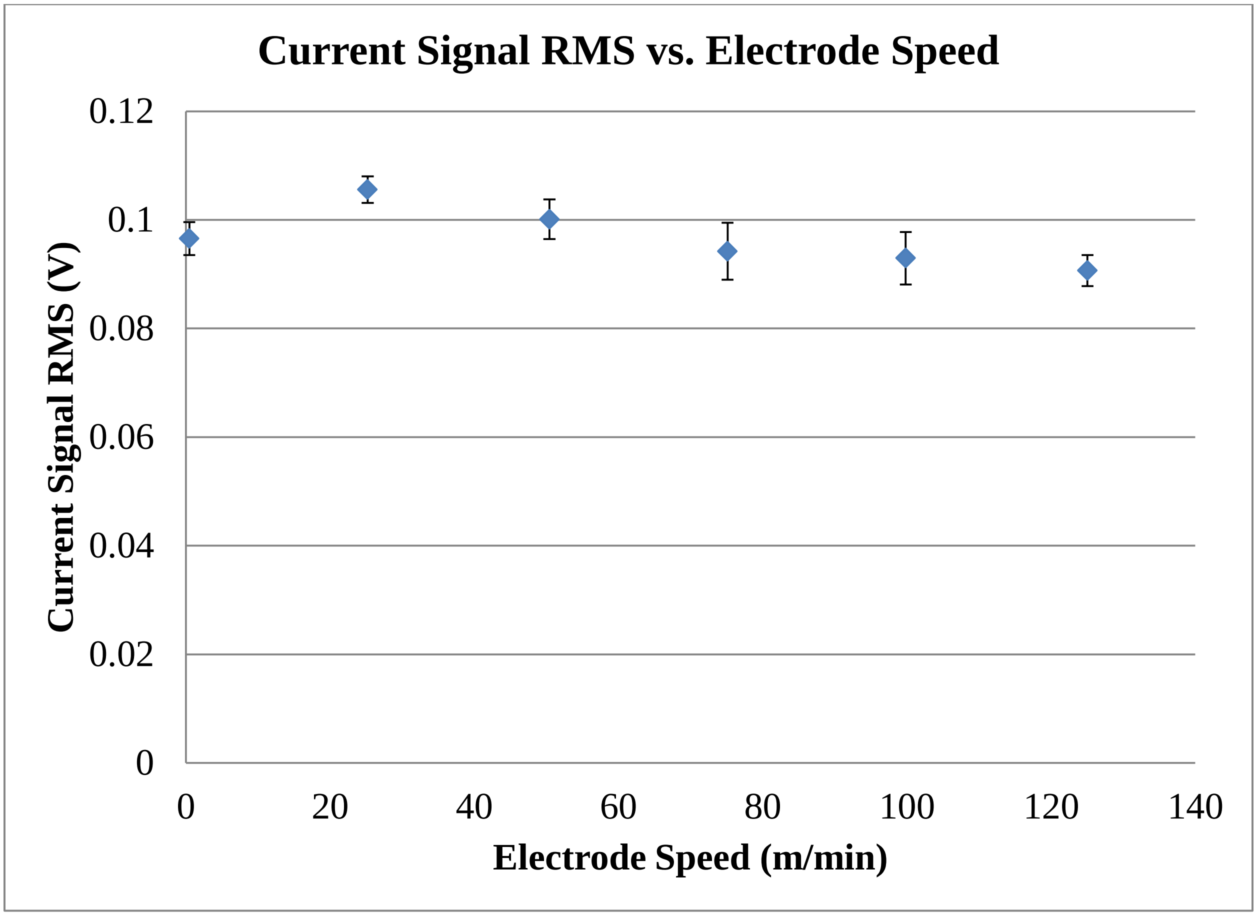

Figure 4.19: Effect of flushing on current signal

4.2.3 Effect of Adding Metallic Debris to the Process

The theory that weaker AE signals are a result of too much debris in the gap due to inadequate flushing is supported by the next test. Fine iron powder was purchased that had a diameter of 44 microns or a volume of approximately 4.5 x 10^{-5} mm^3. This falls into the range of EDM debris size (10^{-6} – 10^{-4} mm^3) that was discussed in section 1.1. The tests were conducted using the low electrode rotational speed setup described in 3.1.1 and a plastic container in order to separate a small volume of dielectric from the rest of the EDM tank (Figure 4.20). A low electrode surface speed of 7.2 m/min was chosen as a baseline and then debris was added directly above the gap between the copper electrode and steel workpiece.

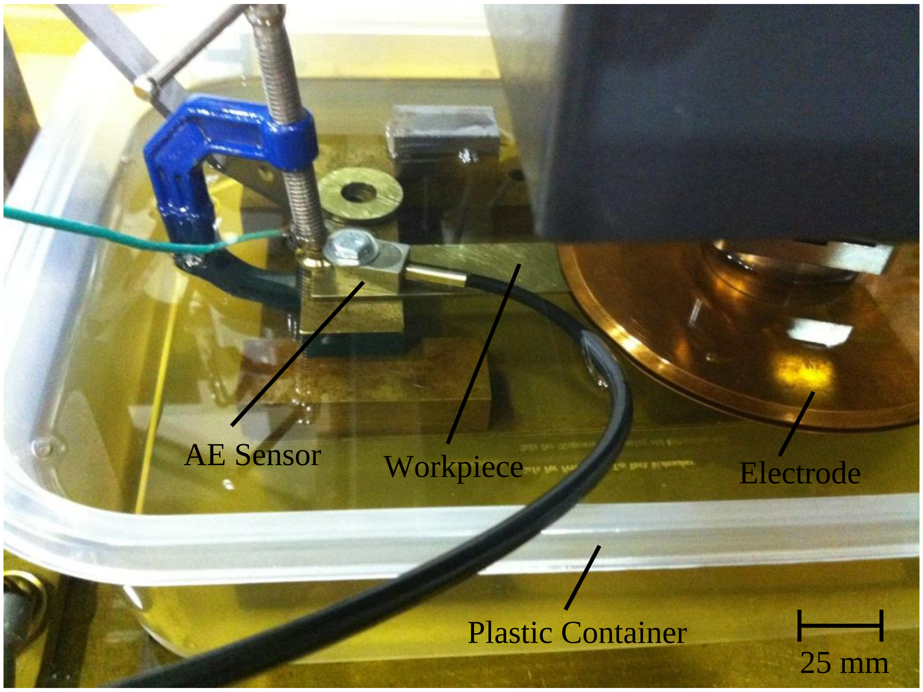

Figure 4.20: Setup used to contaminate small amount of dielectric

Before the debris was added, clean dielectric was added into the plastic container, the EDM process was started, and an AE signal was collected (Figure 4.21a) in the first few seconds before too much debris had been formed. 100 grams of the iron powder was then added into the system and another AE signal was collected within a few seconds (Figure 4.21b). The process was very clearly unstable as only occasional sparks could be seen through the pile of debris over the gap. After a couple minutes, however, the powder in the area closest to the gap was cleared away from the movement of the electrode and another AE signal was collected (Figure 4.21c).

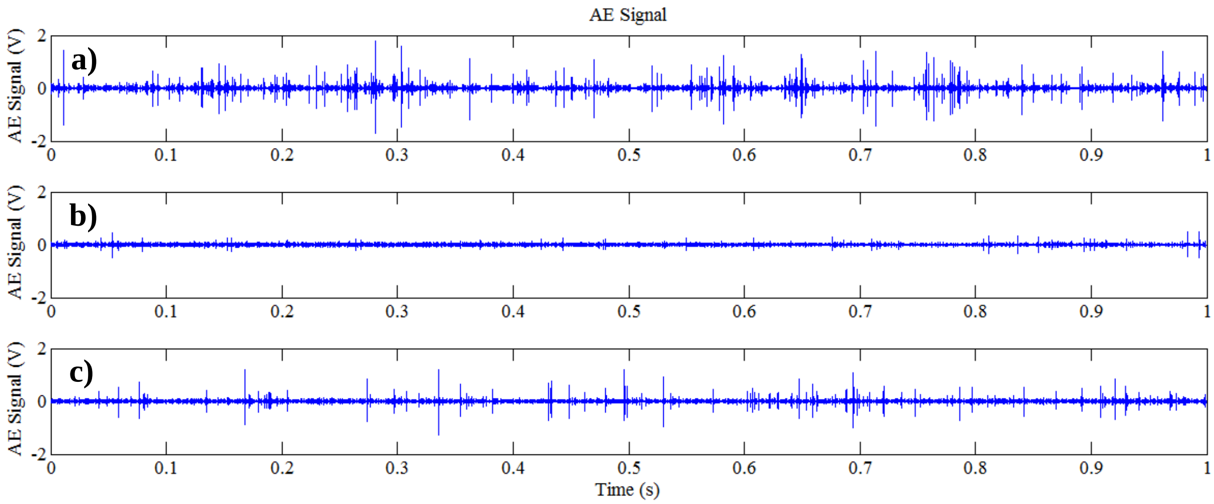

Figure 4.21: AE signal for debris contamination tests
a) Clean dielectric, b) 100 g debris (immediately), c) 100 g debris (after 2 minutes)

FFTs were computed of the three AE signals, which are shown in Figure 4.22 below. It can be seen that the AE signal in the clean dielectric is the strongest (Figure 4.22a). When the iron powder is first entered into the system, the AE signal is almost non-existent (Figure 4.22b). As the electrode's rotation clears away some of the iron powder, the AE signal increases again (Figure 4.22c). The AE signal is not as strong as with the clean dielectric, but there is some sparking activity evident.

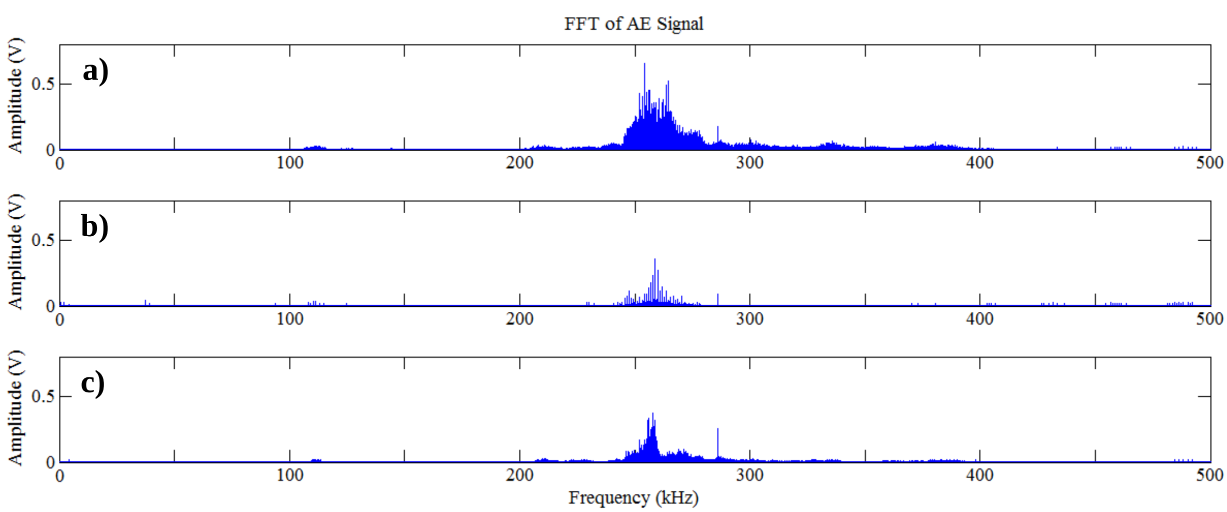

Figure 4.22: Frequency plots of AE signal for debris contamination tests
a) Clean dielectric, b) 100 g debris (immediately), c) 100 g debris (after 2 minutes)

4.3 Effect of Dielectric in EDM

The relation between the material removal rate and the AE signal is strengthened when we look at the effect of the dielectric in EDM. Dielectric fluid is used as an insulating medium that also helps avoid electrolysis effects on the electrode and workpiece. The EDM process however can occur without the use of a dielectric fluid and is usually accompanied with a high velocity gas flow to flush out the molten material. Using the high electrode rotational speed setup described in section 3.1.2, AE signals were collected for both dry and wet EDM conditions and the material removal rate was also measured. The disk electrode was rotated at 43 m/min which was an acceptable level of flushing in the wet EDM case. The resulting workpiece surfaces can be seen in Figure 4.23. In the dry EDM case (Figure 4.23a), it is very evident that the process was unstable. Evidence of arcing can be seen by the workpiece burn and also a recast layer is apparent, meaning the molten material was not removed efficiently. In the wet EDM case (Figure 4.23b), the process appears to be stable. The surface has no burn marks, and craters can be seen meaning the molten material has been ejected from the craters.

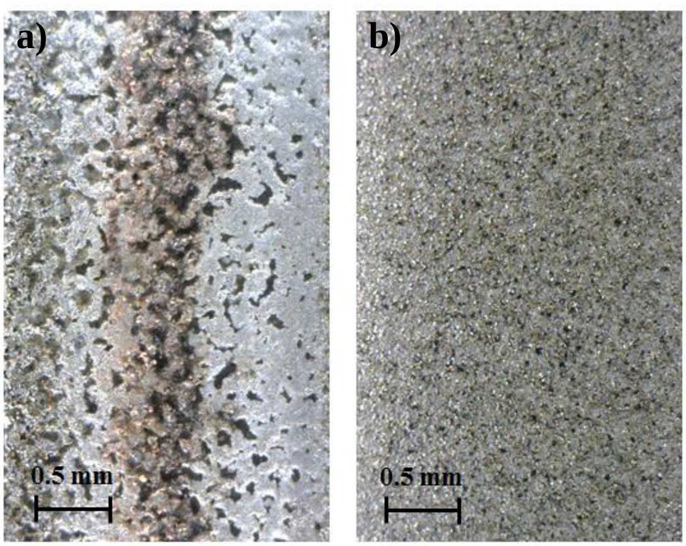

Figure 4.23: Workpiece surface finish
a) Dry EDM, b) EDM with dielectric

The material removal results are shown in Table 4.2. Due to the large amounts of arcing and recast in the dry EDM case, the material removal is negligible. In the wet EDM case, however, the material removal was significant and was calculated to be 0.484 mm^3/min.

Table 4.2: Dry and wet EDM: Removal rate comparison

EDM Condition	Initial Weight (g)	Final Weight (g)	Material Removed (g)	MRR (mm^3/min)
Dry	44.5008	44.5004	0.0004	0.005
Wet	56.3043	56.2663	0.0380	0.484

The AE signals collected (Figure 4.24) agree with the theory that the AE signal is a representation of the MRR. For the dry EDM condition shown in Figure 4.24a, the AE signal has no acoustic burst signals, and no dominant frequencies register on the corresponding FFT (Figure 4.24c). Therefore with a set of parameters that result in no material removal, such as this dry EDM condition, the AE signal is non-existent. For the wet EDM condition, where material is removed during the process, the AE signal appears to be a strong signal (Figure 4.24b), which is supported by the corresponding FFT (Figure 4.24d). This suggests that AE waves are only created once the molten debris is ejected from the discharge crater.

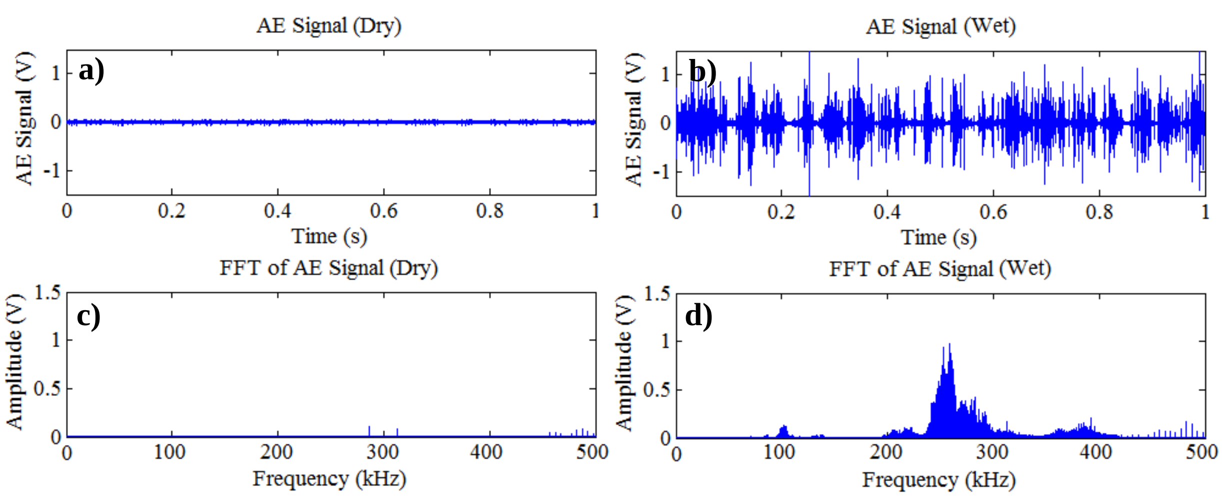

Figure 4.24: Dry and wet EDM acoustic signal comparison

4.4 Effect of Machine Gain

During the EDM process, the gap width between the electrode and workpiece is servo controlled. The electrode jumps back and forth to maintain the proper gap width and to also avoid further arcing and short circuiting when they occur. A machine parameter called, “gain”, that can be manually set controls the rate at which the electrode moves. The machine manufacturer recommends a gain value for a specific set of parameters. Using the high electrode rotational speed setup described in section 3.1.2, AE signals were collected at various gain values, including the manufacturer recommended value of 15. A few resulting AE signals are shown in Figure 4.25 for gain values of 1, 15, and 75 respectively, at the optimum level of flushing. It can be seen in Figure 4.25b that the gain value of 15 gives a slightly more uniform signal than the gain value of 1 in Figure 4.25a. By increasing the gain further to 75, it can be seen in Figure 4.25c that the process becomes unstable.

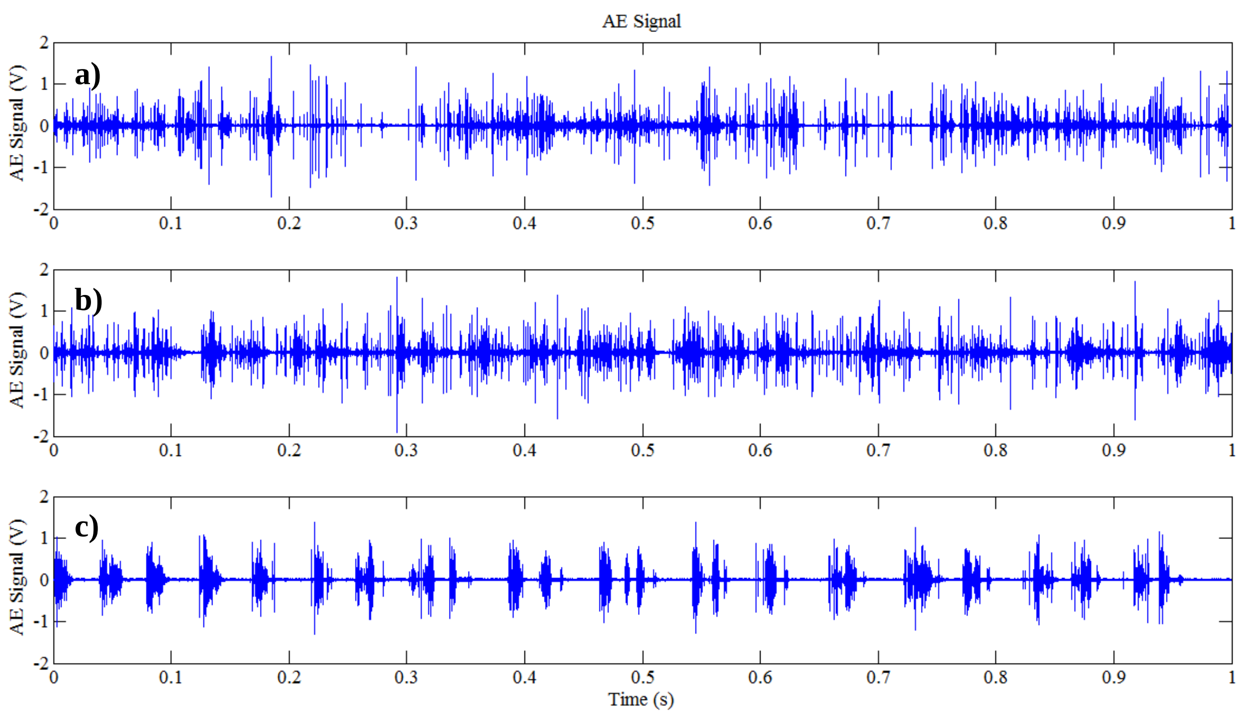

Figure 4.25: Effect of machine gain on acoustic signal
a) Gain = 1, b) Gain = 15 (Manufacturer recommended), c) Gain = 75

The gain tests were performed at three different surface speeds to represent three different levels of flushing: a slow speed (7 m/min), the optimum speed (75 m/min), and past optimum speed (125 m/min). 1 second samples were collected at five separate instances, and then using the time constant of 200 milliseconds, twenty five RMS values were calculated for each machine gain. The resulting averaged RMS values can be seen in Figure 4.26. Although the AE RMS values do not change drastically with gain, information can still be gained from these results. For the optimum and past optimum levels of flushing, the maximum AE RMS values occur at a gain value higher than the recommended gain of 15. When the gain is increased too high however, the AE RMS value drops back down again because the process becomes unstable as was shown in Figure 4.25c. For the poor level of flushing, the AE RMS value continues to increase with the gain. This could be due to the fact that with a high gain value, the quick ‘jumping’ motion of the electrode induces debris movement, which would assist with the flushing.

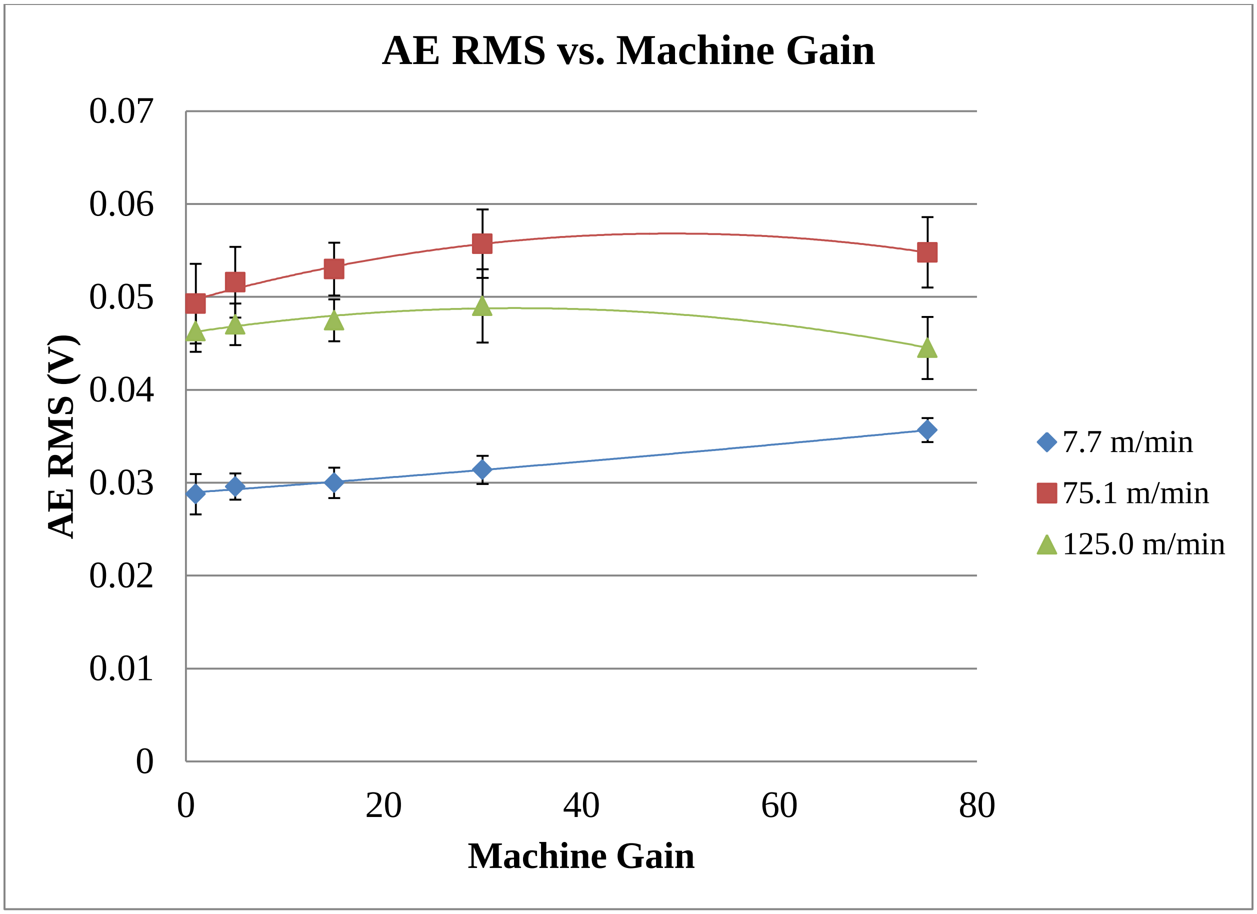

Figure 4.26: AE RMS versus machine gain

Using the same methodology as the above test, the optimum gain value for an EDM machine in industry for a specific set of parameters can quickly be determined. Determining the optimum gain value will encourage process stability and ultimately make the EDM process more efficient.

4.5 Effect of Voltage and Current

Now that the relationship between the acoustic signal and flushing has been established, it may also be useful to investigate the effect of the pulse voltage and pulse current on the acoustic signal, considering the voltage and current have an effect on the MRR and surface finish. Using the high electrode rotational speed setup described in section 3.1.2, tests were run using the same EDM parameters that were used for the flushing tests listed in Table 4.1, excluding the voltage and current which will be varied. The disk electrode was rotated at a constant peripheral speed of 40 m/min for all of the tests to ensure a consistent level of flushing. The results of varying the voltage while keeping a constant current can be seen in Figure 4.27. The voltage that is manually set on the machine is the open circuit voltage. After the spark delay time, the voltage drops to a working voltage for the remainder of the spark. The current was kept at 4.4 A and it can be seen that as the open circuit voltage is increased up to the machine’s maximum of 250 V (along with its corresponding working voltage), the AE RMS increases as well. This means the AE signal could be influenced by the discharge energy.

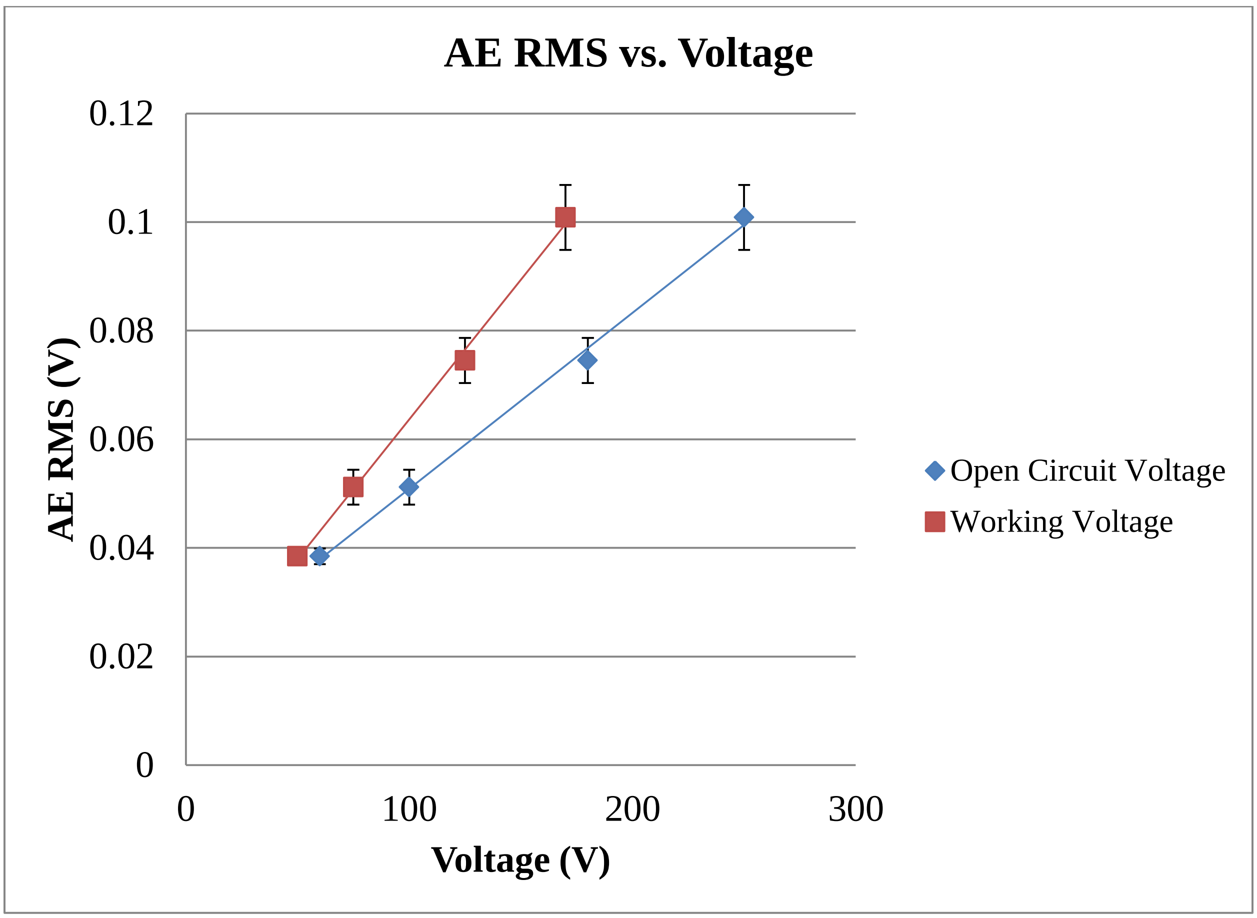

Figure 4.27: Effect of voltage on acoustic signal

The relationship between the AE RMS and the voltage agrees with Mahardika et al. [12] who state that "improving the discharge pulses energy will increase the material removal rate and the fractures energy captured by AE sensor". Varying the pulse current was the next parameter to be tested, and after the outcome of the voltage relationship, it was hypothesized that the AE RMS would increase as the current increased. Also, it is a well-known fact in EDM that as the current is increased, the MRR increases up to a maximum. Bayramoglu and Duffill [44] show this effect for different machining areas (Figure 4.28).

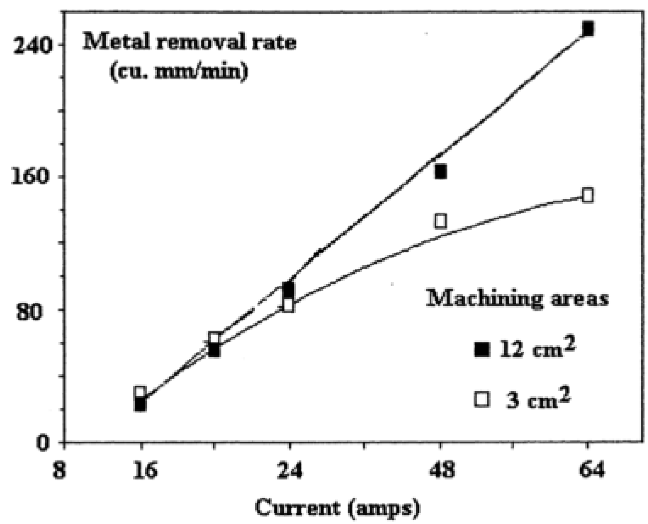

Figure 4.28: The effect of current on MRR for two constant machining areas [44]

For the present test, the AE signal was measured at 1.8, 4.4, 10, and 17 A. The AE signal was measured at open circuit voltages of 60, 100, 180, and 250 V to see if the relationship was the same for each voltage. The results of the AE RMS versus the pulse current can be seen in Figure 4.29 below. The AE RMS values actually follow the opposite trend of what was hypothesized. As the current is increased, the AE RMS values decrease at a decreasing rate.

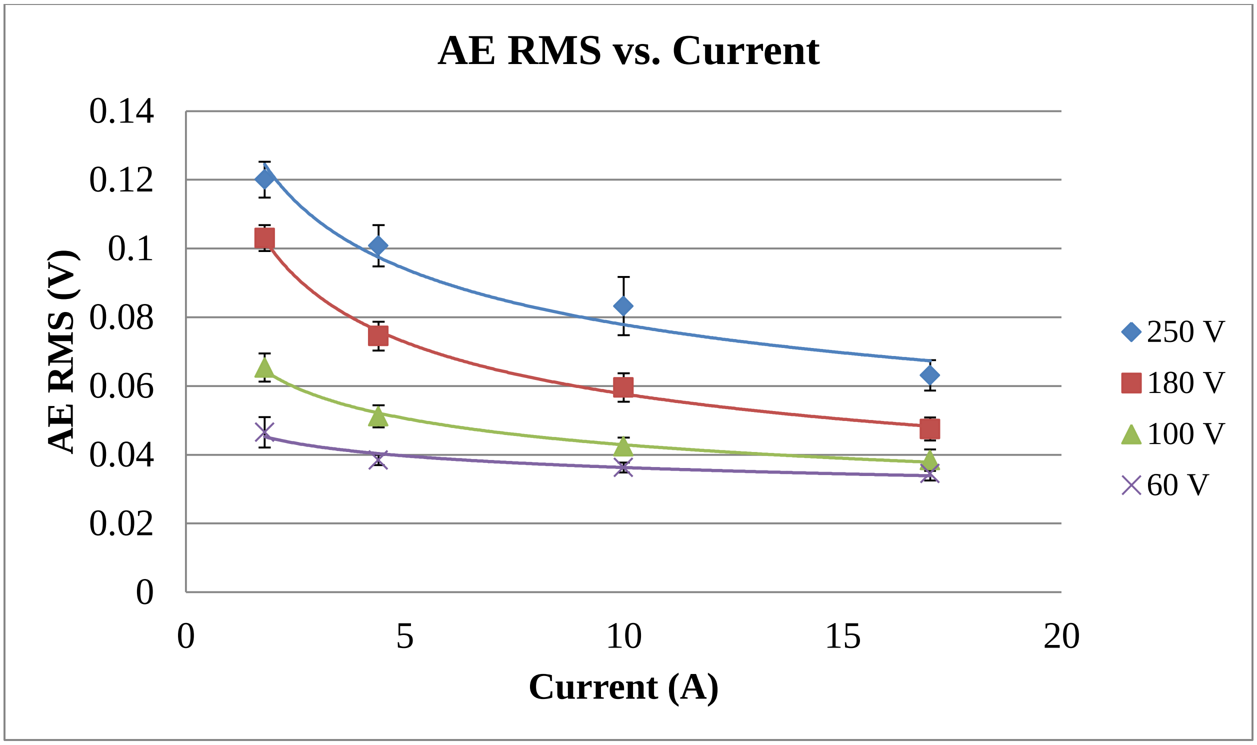

Figure 4.29: Effect of current on acoustic signal

This unexpected result was investigated further by varying the pulse on-time. The open circuit voltage was kept constant at 100 V, and four different pulse on-times were tested at varying currents (Figure 4.30). It can be seen that as the on-time becomes lower, the expected trend becomes apparent. The AE RMS switches from a decreasing to an increasing trend with a drop in the on-time. At roughly an on-time of 21 μs, the AE RMS appears to be constant with an increase in current. The higher values of the AE RMS at the same current for varying on-times will be explained in a later section.

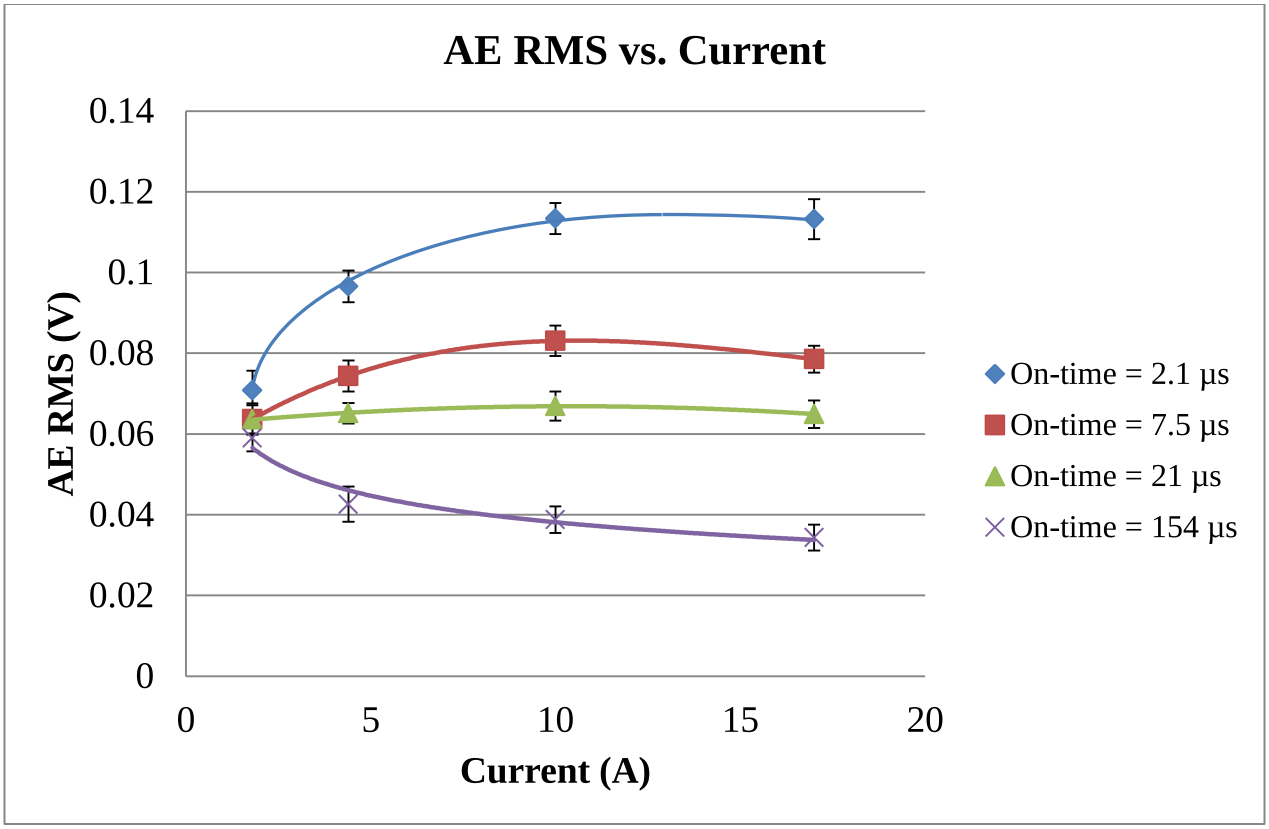

Figure 4.30: Effect of current on acoustic signal using different on-times

In order to explain this phenomenon between the on-time, current, and acoustic signal, a closer look into the effects of on-time and current on the plasma channel is warranted. Based on the Equation 4.4 determined by Saito et al. [45], assuming the heat source diameter is equal to the discharge crater diameter, the heat source diameter, *d(t)*, is a function of the on-time, *t*, and the current, i_e.

$$d(t) = 2.4 \times 10^{-3} \times t^{0.4} \times {i_e}^{0.4} \qquad \textbf{Equation 4.4}$$

Using Equation 4.4 and the various current and on-time combinations used in the above test, the AE RMS values can be plotted against the crater diameter as shown in Figure 4.31. It can be seen that as the crater diameter increases, the AE RMS values decrease. This suggests that the acoustic signal may be more useful when looking at the power density per spark rather than the current or on-time individually. This leads to the next set of tests in this thesis which investigate the effect of current density on the acoustic signal.

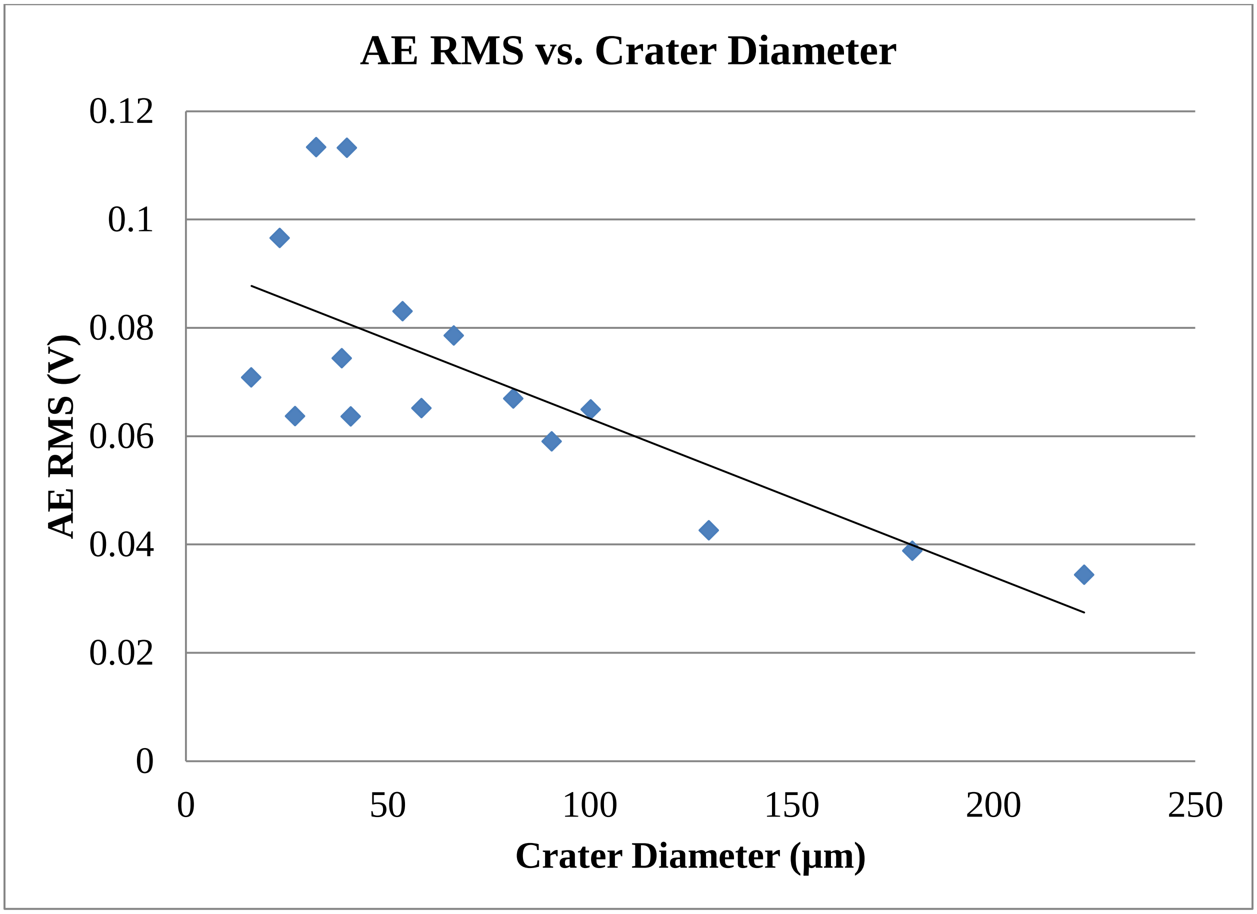

Figure 4.31: Effect of crater diameter on acoustic signal

4.6 Effect of Current Density

For all of the previous tests, the electrode frontal area has remained the same. The electrode area is the area in which discharges can occur in at any given time during the EDM process. By changing the electrode area, the current density will change. The current density may be a more useful parameter to investigate rather than just the current. By only changing the current, the concentration of sparks is not considered. Similar to the level of flushing, there is an optimal current density for the EDM process. Blatnik et al. [46] found that the optimal current density which provides the maximum MRR before the stability of the process becomes compromised is 0.1 A/mm^2 or 10 A/cm^2. It can be seen in Figure 4.32 that with a larger area, A1, the current must be increased in order to reach the optimal current density and therefore the MRR (V_w) is higher.

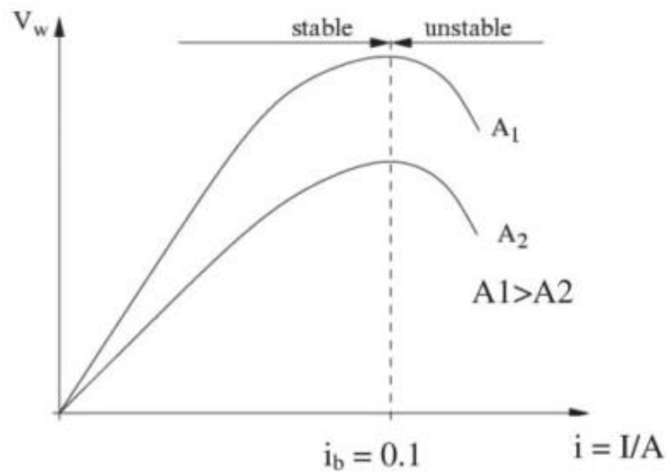

Figure 4.32: MRR versus the current density for two eroding surfaces [46]

To investigate the effect of the current density on the acoustic signal, tests were completed using various workpiece sizes in order to obtain different electrode contact areas. Six different contact areas were used: 0.251, 0.440, 0.635, 0.839, 1.056 cm^2, and the corner of one of the workpieces to obtain a line contact (Figure 4.33). A current of 4.4 A was chosen for the tests so that the optimal current density found in literature of 10 A/cm^2, could be achieved with the workpiece shown in Figure 4.33ii. The other parameters used for the test are the same as the previous parameters found in Table 4.1.

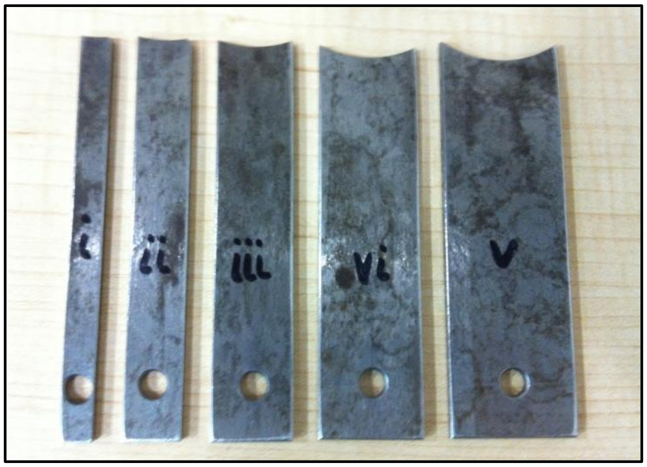

Figure 4.33: Workpieces used to obtain various electrode contact areas
i) 0.251 cm^2, ii) 0.440 cm^2, iii) 0.635 cm^2, iv) 0.839 cm^2, v) 1.056 cm^2

The tests were done using the high electrode rotational speed setup from section 3.1.2 and three levels of flushing were used for each of the workpieces. The optimal electrode surface speed determined in section 4.2 (75.1 m/min), a low level of flushing (14.4 m/min), and a zero flushing case (0 m/min) were used. The AE RMS values were calculated using the same method as the previous tests and can be seen in Figure 4.34. In the case of optimal flushing (top line), the results agree with the literature by going through an optimal current density at 10 A/cm^2. In the case of low flushing (middle line), the AE RMS continues to increase with a decreasing current density but appears to be reaching an optimal value. This is most likely because with the low level of flushing, the debris that is produced at 10 A/cm^2 is not adequately removed, and the flushing can only keep up with the debris produced by much lower current densities. When the current density increases, more debris is created in that area and therefore if adequate flushing is not achieved, the process will be unstable due to discharge localization. The condition with zero flushing is the extreme case in which the current density has little to no effect on the AE RMS signal because debris is not being removed effectively.

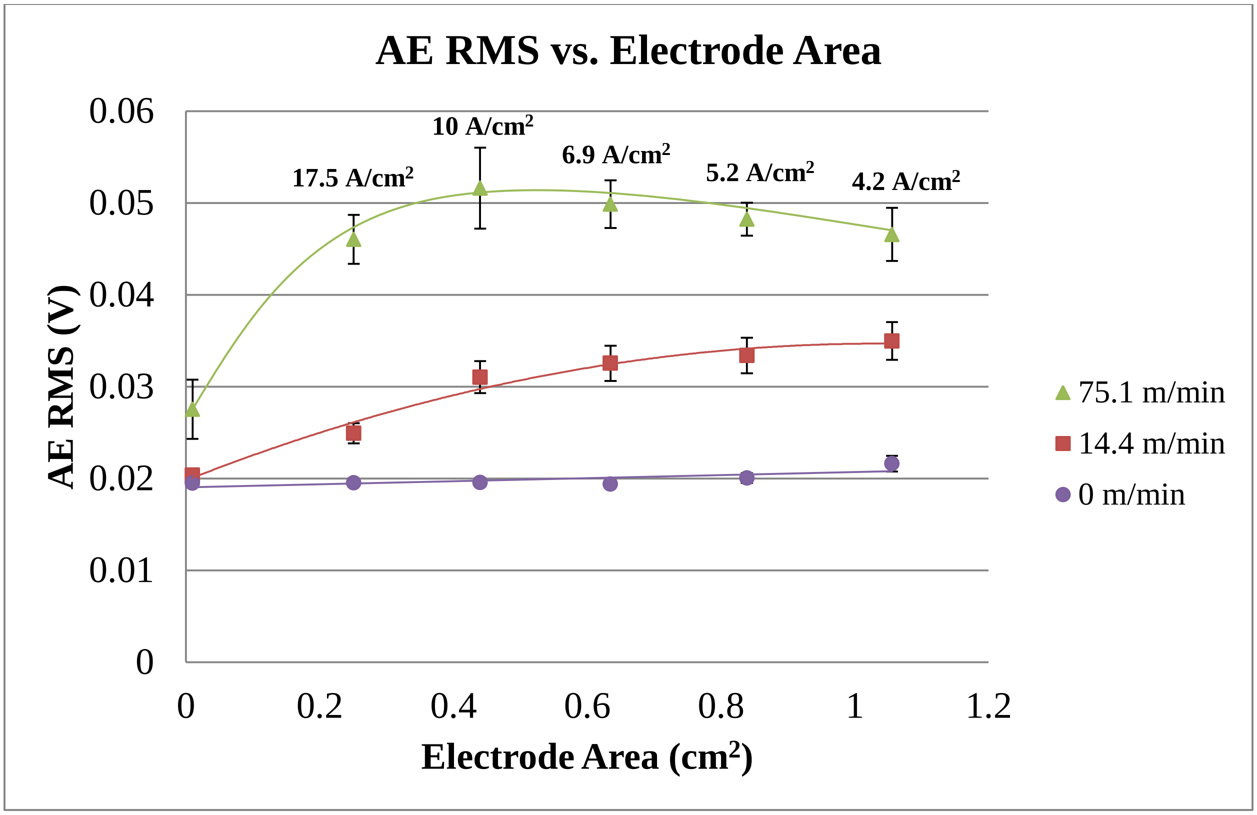

Figure 4.34: Effect of current density on AE signal

4.7 Effect of Electrode Material

Another parameter that has been kept constant in all of the previous tests has been the electrode material. Copper has been used for the previous tests because it is one of the most commonly used EDM electrode materials used in industry due to its high electrical conductivity and high thermal diffusivity. Depending on the situation however, other electrode materials are desirable, such as the use of brass wires in wire EDM [47]. To investigate the effect of the electrode material on the acoustic signal, the multi-material electrode setup described in section 3.1.3 was used. The different electrode materials were arranged into a disk, so the same workpiece and AE sensor mounting could be used. The rotary axis of the EDM machine would spin the multi-material electrode in the clockwise direction so the mild steel workpiece would be exposed to brass, graphite, copper/graphite, and copper, in that order. A 12 mm wide slot was filed into the peripheral surface of the disk at the intersection of copper and brass in order to have a reference point on the acoustic signal. The disk was rotated at 30 RPM (14.4 m/min) and AE signals were collected for 4 seconds, which would allow the disk to make two full rotations. One of the signals collected can be seen in Figure 4.35 below. Knowing that there is a slot at the intersection of copper and brass, the point on the acoustic signal where the signal disappears can be taken as the end of the copper section and the start of the brass section. With the rotation speed of 30 RPM, each material will be exposed to the workpiece for 0.5 seconds, and the acoustic signal can therefore be separated for each electrode material as shown in Figure 4.35. A RMS value for each material was calculated and is displayed at the bottom of each corresponding material in Figure 4.35.

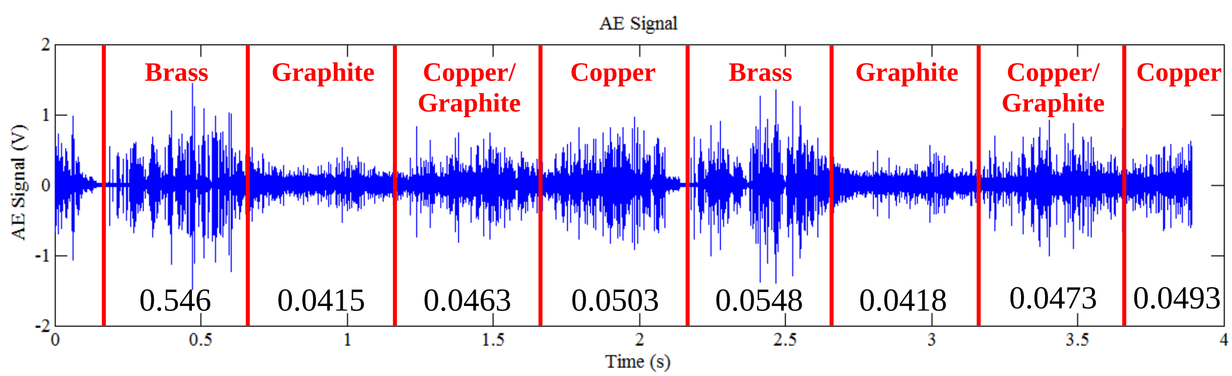

Figure 4.35: Multi-material electrode acoustic signal (with RMS values)

By looking at the acoustic signal, it appears that brass has the strongest acoustic signal while graphite has the weakest acoustic signal. This observation is verified by the RMS values and also by taking the FFT of each material as shown in Figure 4.36. Brass has the strongest AE signal followed by copper, copper/graphite, and graphite. It is also interesting to note that the frequency span of the AE signal for each material is the same. These results are specific to the EDM parameters and material properties used for these tests such as the on-time, pulse current, workpiece material, etc. Using the same AE measurement method and changing certain parameters could result in graphite having the strongest signal and brass having the weakest signal.

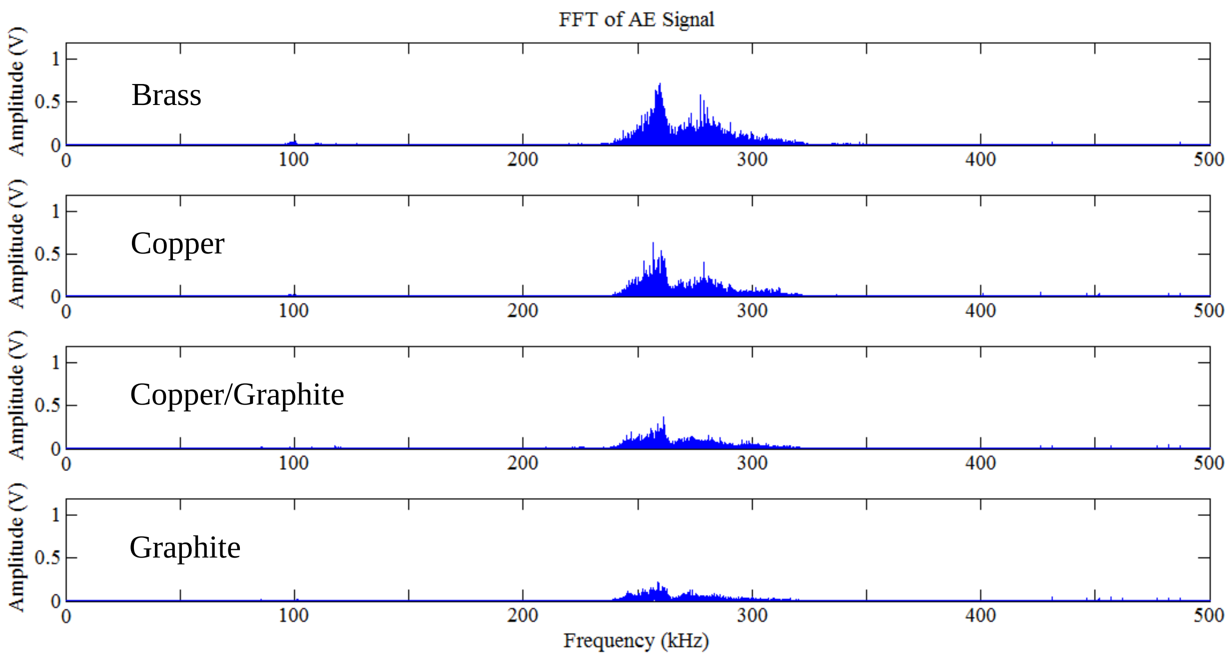

Figure 4.36: FFT of multi-material electrode AE signal

4.7.1 Effect of Electrode Polarity

The polarities of the electrode and workpiece used in EDM are dependent on several factors, such as the combination of electrode and workpiece materials. Whether the process is a roughing or finishing operation also has an influence on the polarity because the material removal rate and electrode wear can drastically change with polarity. When machining steel, a graphite electrode is generally used in positive polarity for a roughing operation [36], and for a copper electrode, the machine manufacturer of the sink EDM machine used for this project recommends a positive polarity for a roughing operation and a negative polarity for a finishing operation [48]. To investigate the effect of the polarity on the AE signal, tests were run using the multi-material electrode keeping all parameters constant and changing the electrode polarity. Tests were run using a long on-time and off-time suggested by the machine manufacturer to simulate a roughing operation and a low on-time and off-time to simulate a finishing operation. For the roughing operation, an on-time of 154 μs and an off-time of 37 μs were used. Once the acoustic signal was collected and separated into sections by its corresponding electrode material, an RMS value was calculated for each material section. It can be seen in Figure 4.37, that the RMS values agree with the FFT results where brass has the strongest signal and graphite has the weakest. When the polarity is switched to negative, the material trend remains the same but the amplitude of the RMS values decrease. This agrees with the sink EDM machine manufacturer's manual which says that when machining steel in a roughing operation, an electrode with a positive polarity is recommended [48].

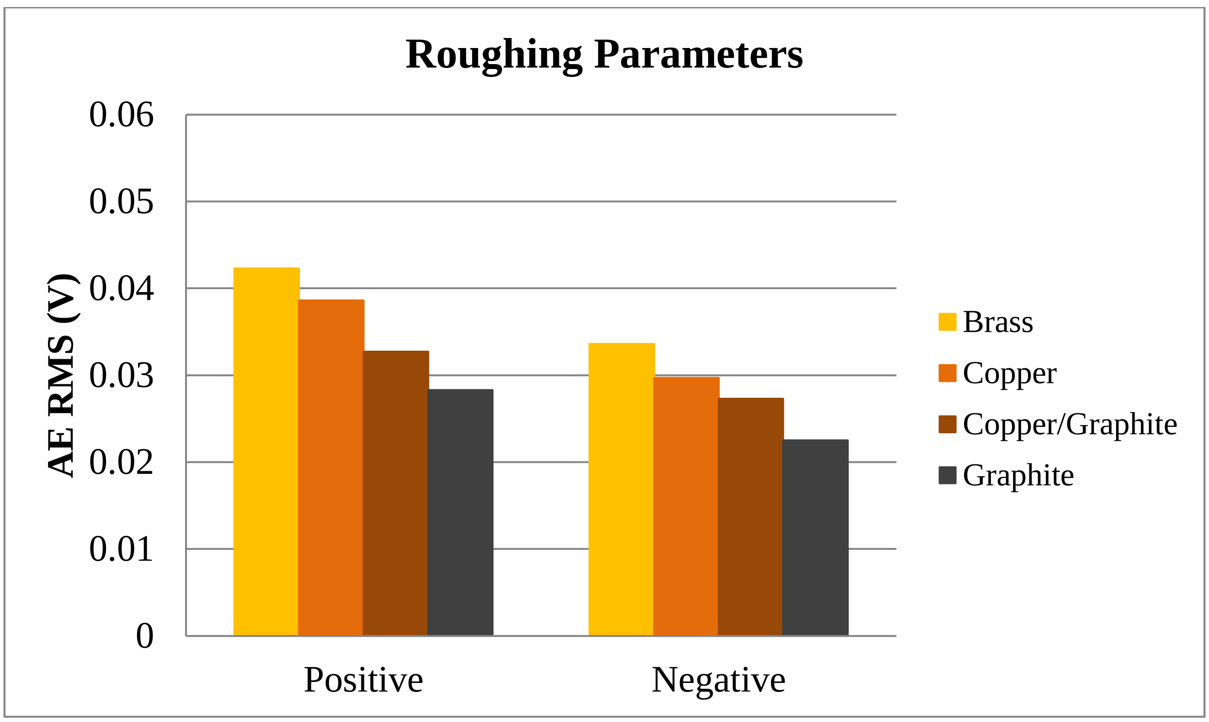

Figure 4.37: Effect of electrode polarity for roughing on-time

For the finishing operation, an on-time of 2.4 μs and an off-time of 7.5 μs were used. The AE RMS results can be seen below in Figure 4.38. The material trend for both the positive and negative case again agrees with the frequency plots. Unlike the roughing operation, when the electrode polarity is switched to negative, the amplitude of the RMS values increase. This again agrees with the literature that recommends when machining steel with a low on-time, a negative polarity should be used for the electrode.

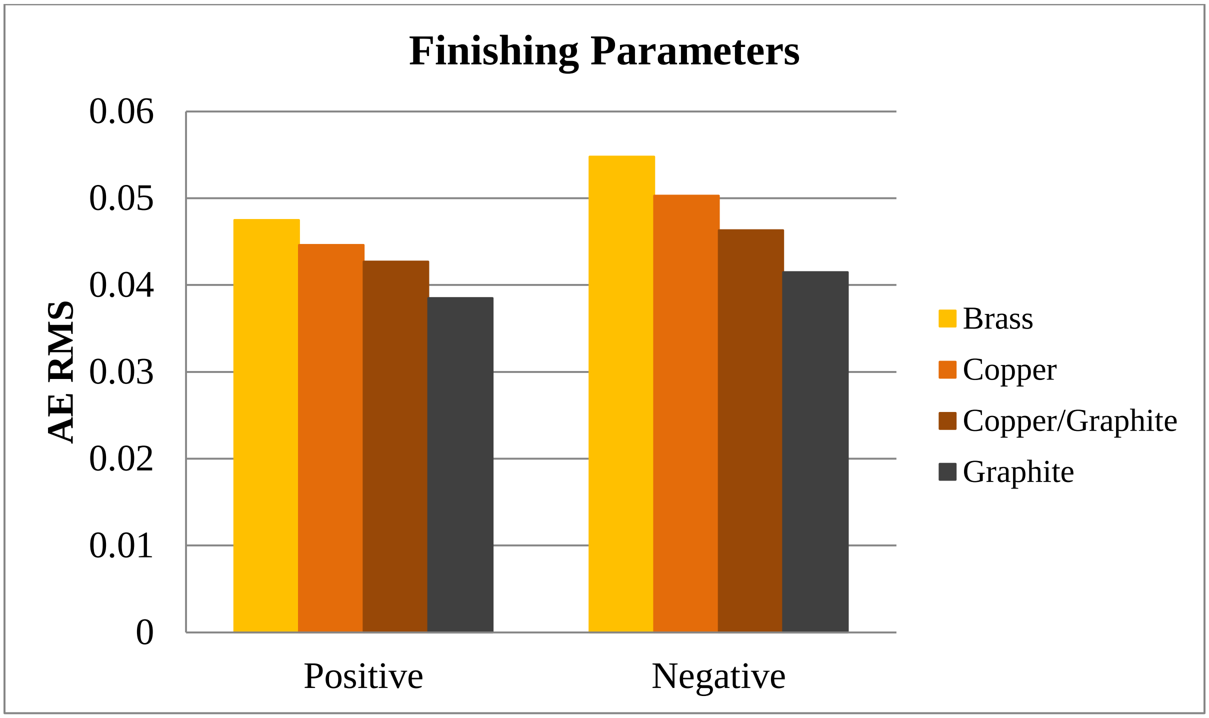

Figure 4.38: Effect of electrode polarity for finishing on-time

Kunieda et al. explains why the polarity changes with the on-time for a copper electrode [1]. Due to the thermal dissociation of the dielectric oil, a carbon layer is deposited on the anode surface protecting it from wear. When the on-time is long, the carbon layer is thick and provides a low wear ratio for a positive tool electrode. However, with a low on-time the carbon layer is scarce and therefore the polarity is switched because the energy dissipation into the anode is greater than into the cathode.

If one were to compare the RMS values between the roughing operation (Figure 4.37) and the finishing operation (Figure 4.38), it would be determined that the RMS values for the finishing operation are much higher than the roughing operation. This is due to the lower on-time, similar to what was seen in Figure 4.30 when the effect of current for various on-times was being investigated. The reason for this will be explained in the next section.

4.8 Effect of Pulse Duration

It has become apparent in several of the previous tests that the acoustic signal is significantly affected by the on-time. To investigate this phenomenon, tests were run using the high electrode rotational speed setup described in section 3.1.2 and parameters listed in Table 4.3. The duty factor is calculated using the following equation:

$$Duty\ Factor\ (DF) = \frac{T}{T+P} \qquad \textbf{Equation 4.5}$$

Where T refers to the pulse on-time and P refers to the pulse off-time. For the first set of tests, the duty factor was held constant at 0.667, meaning the energy going into the system would remain the same for all on-times used. The AE RMS results can be seen below in Figure 4.39. It can be seen that the AE RMS value is the highest when the on-time is the lowest. This suggests that the acoustic signal is proportional to the number of sparks and not necessarily a representation of the crater size or plasma diameter. In the EDM process, when the on-time is increased the diameter of the plasma channel increases leaving behind a larger diameter crater [49].

Table 4.3: EDM Parameters (On-time)

Current	4.4 A
Voltage	100 V
Duty Factor	0.667
Electrode Polarity	Positive
Gain	15
Compression	18
Electrode Peripheral Speed	43 m/min
AE Sampling Rate	5,000,000 samples/second
Sample Length	1 second

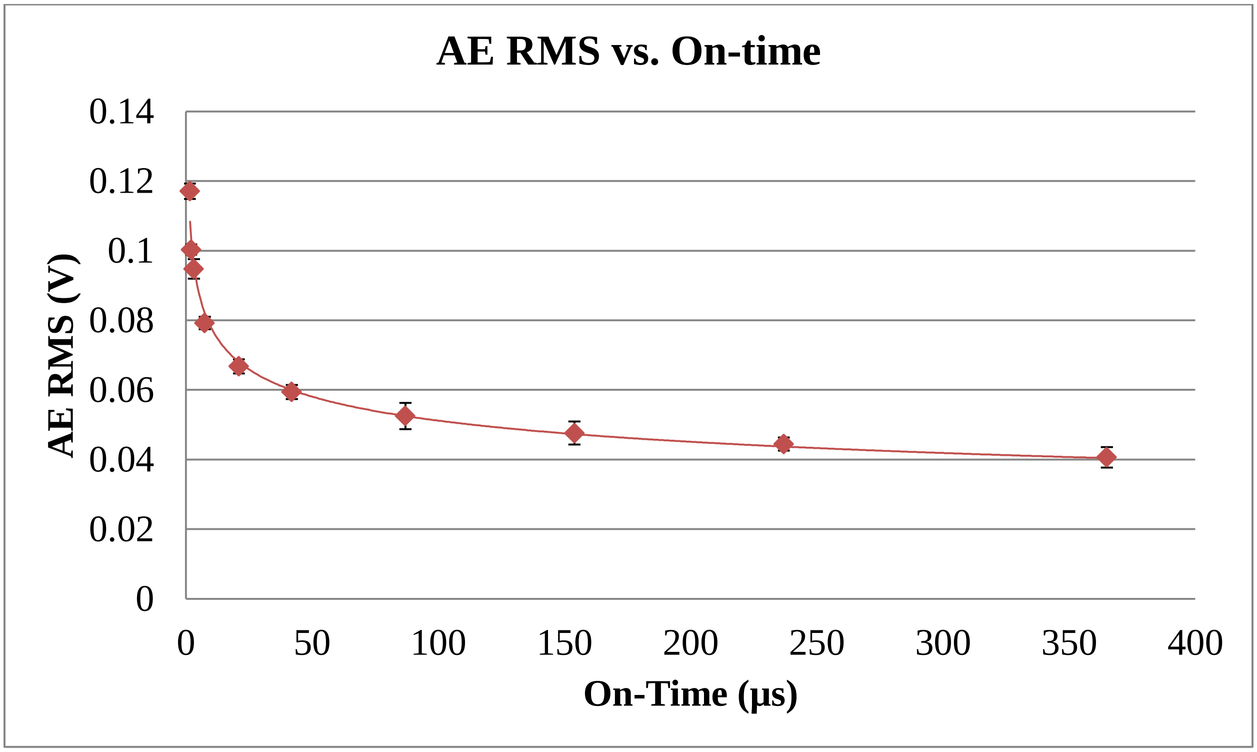

Figure 4.39: Effect of on-time

Another test was run varying the duty factor and keeping the on-time constant. The duty factors used were 0.333, 0.5 and 0.667, which means the energy going into the process for the 1 second timeframe would total to be 0.333, 0.5, and 0.667 seconds, respectively. By increasing the duty factor while keeping the on-time constant means the off-time would have to decrease which would consequently increase the number of expected discharges in the 1 second measurement timeframe. The results from this test are shown in Figure 4.40, and agree with the theory that the AE signal is proportional to the number of discharges. As the duty factor is increased, the AE RMS value increases slightly.

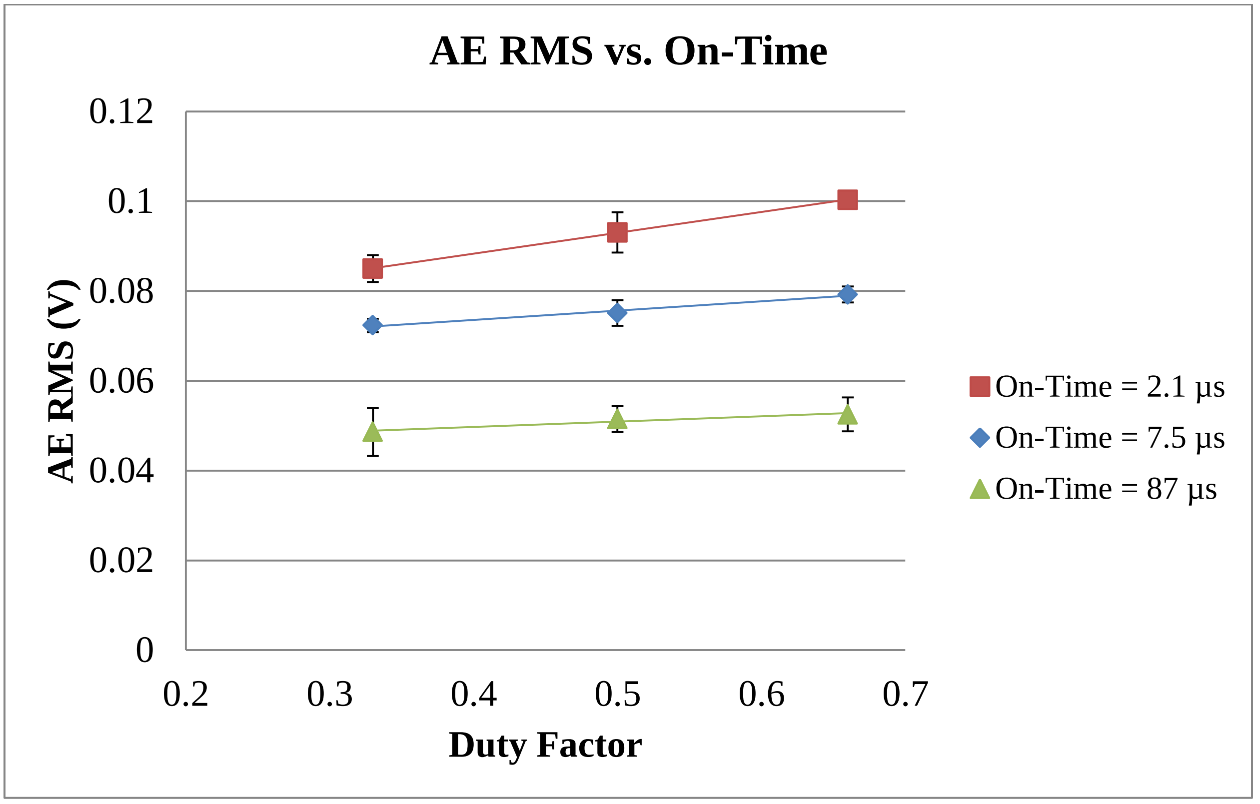

Figure 4.40: Effect of duty factor

4.9 Understanding the Acoustic Emission Signal

Now that the acoustic signal has been related to several EDM parameters it may be useful to understand more about how the individual acoustic waves are affected by the EDM process. The source of the acoustic signal in the EDM material removal mechanism is still unknown. By comparing three different flushing levels, we can obtain three very different AE signals. As shown in Figure 4.41, a very low flushing condition (0.48 m/min), an intermediary level of flushing (28.7 m/min), and the optimal level of flushing (75.0 m/min) were chosen. It can be seen that the amplitude of the AE bursts increases with increased flushing, however there are still AE bursts in each flushing case that have similar amplitudes.

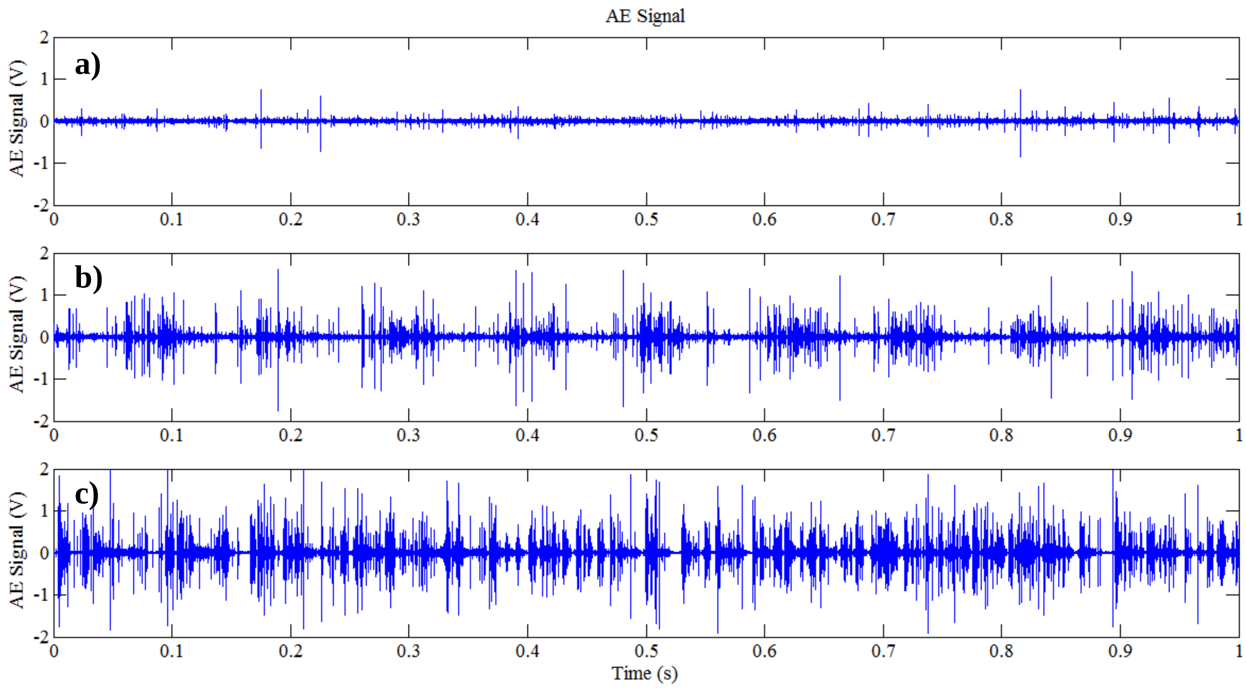

Figure 4.41: AE signals with different flushing levels
a) 0.48 m/min, b) 28.7 m/min, c) 75.0 m/min

A histogram of the AE signals was created showing the frequency of AE bursts, depending on their amplitude (Figure 4.42). The case with the best flushing reaches amplitudes that the other two conditions do not. As well, at low amplitudes such as 0.5 V, the occurrences of the 0.5 V signal is considerably higher when the flushing level is better. This suggests that as the level of flushing is increased, the amount of discharges increases as well as the efficiency of the discharges.

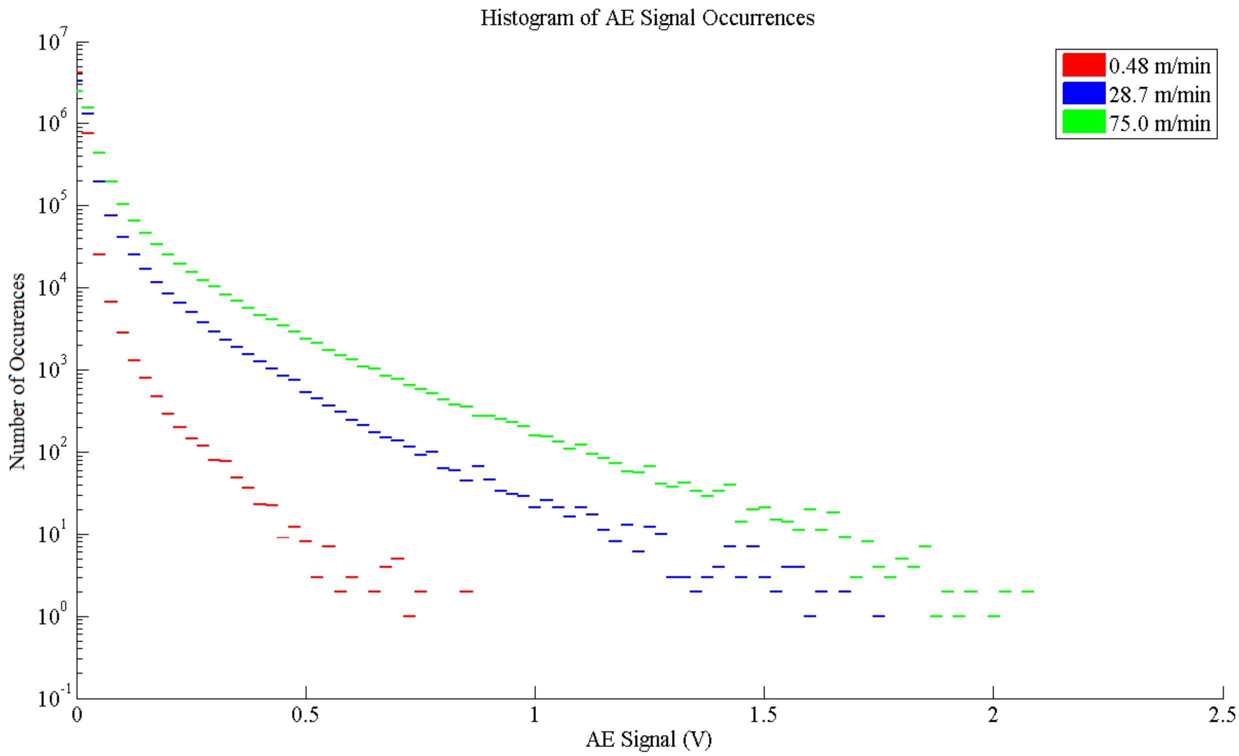

Figure 4.42: Histogram of AE signal occurrences

4.9.1 Single Spark Tests

An aspect of the acoustic wave that has not been investigated yet is the length of the acoustic wave. To ensure the AE signal seen is in fact a burst signal, AE signals were collected at various pulse on-times. Three signals of similar amplitudes were compared, each one having a different pulse on-time (Figure 4.43). Figure 4.43a shows a spark with an on-time of 15 µs, Figure 4.43b shows a spark with an on-time of 100 µs, and Figure 4.43c shows a spark with an on-time of 274 µs. Regardless of the different on-times, the sparks have a very similar shape and all have the exact same length, meaning the discharges are burst signals that attenuate over 200 – 300 µs.

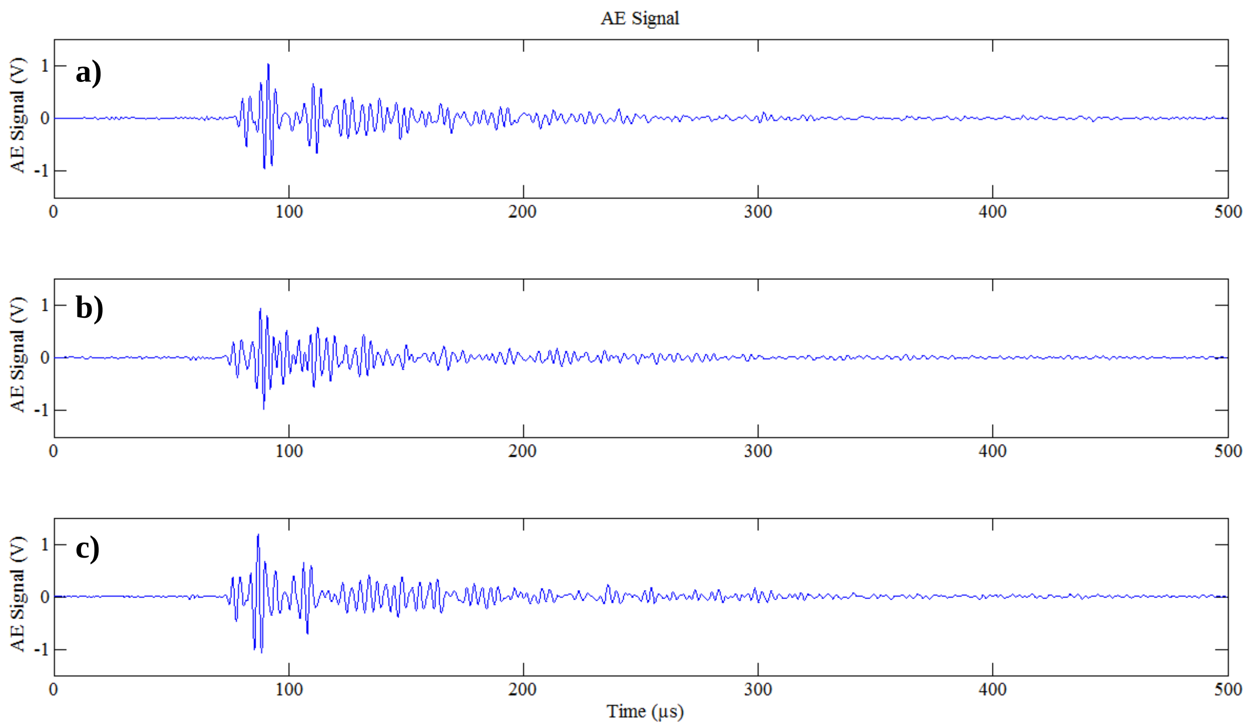

Figure 4.43: Single spark test for different on-times
a) On-time = 15 µs, b) On-time = 100 µs, c) On-time = 274 µs

Considering the AE RMS value increases with increased flushing when the MRR increases, it would be logical to assume that the AE bursts are a result of the debris being extracted from the crater that is formed during the discharge. As described in section 1.1, it is in the final stages of the electrical discharge in the EDM process that the plasma channel implodes and ejects material from the molten pool. To determine the exact source of the AE burst, a test was done by collecting both the voltage and AE signal in a single spark test. Using a Tektronix P5200 high voltage differential probe [50], the voltage signal was collected using the same data acquisition system as the AE signal. A pulse on-time of 100 µs was chosen in order to get a definitive separation between the start and end of the spark. Shown below in Figure 4.44a is the AE signal for a single spark and the corresponding voltage signal of this spark is shown in Figure 4.44b. It can be seen that the AE burst does not start until after the voltage waveform is complete. Recalling from section 4.1.1, with the 70 mm length between the spark and the AE sensor, the AE signal should take approximately 23 µs to reach the sensor. Knowing that the pulse on-time is 100 µs, it can be concluded that the AE burst does not come from the start of the voltage waveform, but rather the end of the voltage waveform. The end of the voltage waveform is the same point where the current flow stops and therefore the plasma channel implodes, ejecting the molten metal from the crater that was just formed. This also supports the dry EDM case that was looked at in section 4.3. In this dry EDM case, a recast layer was formed because no molten metal was ejected from the craters. In this case, the acoustic signal showed no acoustic bursts at all.

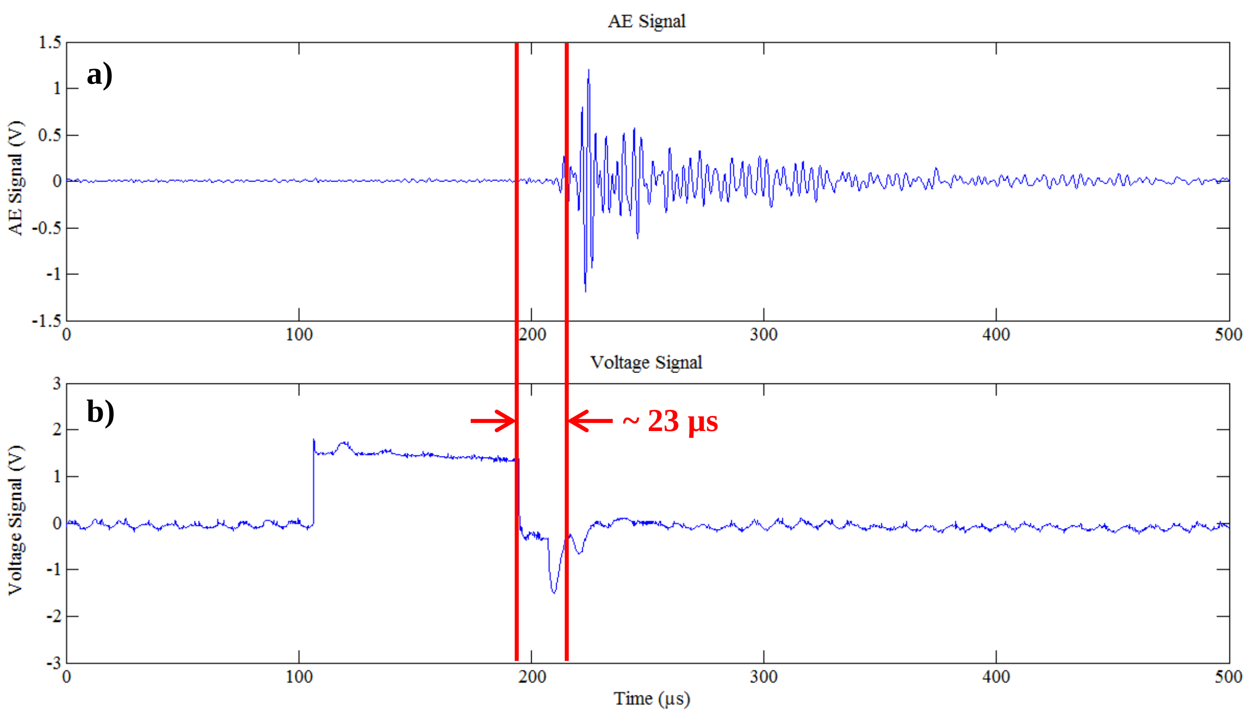

Figure 4.44: Determining the source of the AE burst
a) AE signal, b) Voltage signal

By looking at the AE signal for individual sparks along with the voltage and current signal, a much better understanding of the AE signal can be learned. The AE signal has been used to monitor several EDM parameters in realistic machining conditions, but more research investigating individual sparks is warranted to better understand characteristics such as signal source, shape, and amplitude.

5 Conclusions and Future Work

Several benefits and capabilities of using an acoustic emission sensor as a monitoring tool for the EDM process have been presented. Due to the limited amount of research done on acoustic sensors in EDM, many of the areas explored in this thesis allowed for new and exciting results. This section will outline the conclusions drawn from this thesis and will recommend ideas for future research.

5.1 Conclusions

The motivation for this project was fuelled by the lack of research done on acoustic emission in EDM and the success of using acoustic emission sensors in other machining processes. This research was focused on the EDM process as a whole, relating the acoustic signal to electrical parameters, tool materials, flushing effectiveness and some process modifications such as dispersing metallic powder into the gap. Emphasis was placed on the material removal rate and achieving process stability. Increasing the material removal rate is always a benefit in machining applications, but process stability is of particular importance when it comes to wire EDM. If process stability can be achieved, wire breakage due to arcing can be eliminated and productivity will consequently increase. The main results of this research are summarized as follows:

1. Filtering the unwanted electromagnetic interference out of the acoustic signal can be done using a Butterworth filter. After the EMI has been filtered out, the acoustic signal can be represented accurately with a fast Fourier transform. A repeatable and quantifiable representation of the acoustic signal can be done by calculating the root mean square value using a time constant of 200 milliseconds.

2. Using a rotating disk shaped electrode to control the level of flushing, the effect of flushing on the stability of the process can be measured using an acoustic sensor. As the level of flushing increases, the AE RMS value increases up to a peak value where it then begins to decrease. The trend of the AE RMS value replicates the trend of the material removal rate as flushing is increased. A significant benefit of using an acoustic sensor to monitor the process can be seen here. Measuring the material removal rate requires the process to be interrupted and the workpiece to be removed whereas the acoustic sensor can take readings in real-time as the EDM process is happening. The ability to use the AE data as a representation of the MRR cannot easily be accomplished by using the current signal.

3. When machining a workpiece in the absence of a fluid, and without a high velocity gas flow to flush out the molten metal, no material removal is possible. The process can become so unstable that large amounts of arcing occur, and the sparking that does occur creates a recast layer when the molten metal is not removed. In this extreme case, the acoustic signal shows absolutely no acoustic bursts.

4. By monitoring the AE signal while altering the machine gain, process stability can be improved. When low levels of flushing are present, a higher gain may be required to induce movement of the machined debris. The optimum gain can be quickly determined for a specific set of parameters using AE data.

5. Altering the open circuit voltage or the working voltage, the AE RMS value increases proportionally with the voltage. Altering the current on the other hand, results in a more complicated phenomenon. With a high pulse on-time, the AE RMS value decreases with an increase in current. With a low pulse on-time, the AE RMS value increases with an

increase in current. A pulse on-time exists between the higher and lower on-times that result in a constant AE RMS value for an increase in current. The AE RMS value relates to the crater diameter which is a function of both current and on-time.

6. Keeping the current at a constant value and altering the workpiece contact area, the current density can be changed. An optimal AE RMS value was found when using a current density of 10 A/cm^2 and the optimal level of flushing that was determined earlier. This current density of 10 A/cm^2 agrees with the optimal current density found in the literature. When a lower flushing level is used however, the EDM process is not stable at 10 A/cm^2 and the optimal current density becomes much lower, where the flushing can handle the lower concentration of debris. When no flushing is applied, the current density appears to have no effect on the acoustic signal.

7. Regardless of electrode material, the frequency range of the acoustic signal remains the same and only the amplitude of the signal varies. Testing electrode materials, brass, copper, copper infiltrated graphite, and graphite, it was seen that when using a roughing pulse on-time, a positive electrode polarity showed higher AE RMS values. When using a finishing pulse on-time, a negative electrode polarity showed higher AE RMS values. In an EDM process that is gradually altering parameters from roughing to finishing, by using the acoustic signal, the exact moment when to switch the polarity can be pinpointed.

8. By varying the pulse on-times, it was concluded that the acoustic signal was highly representative of the number of discharges occurring in a specific time frame and not the crater sizes left from the discharges. The acoustic signal does not occur until the plasma channel implodes ejecting the molten metal from the crater, which was discovered by

seeing that the acoustic burst signal for a single discharge occurs after the voltage waveform is complete.

Investigating the benefits of using an acoustic sensor as a real-time monitoring tool for the EDM process has produced significant results that give a better understanding of the EDM process and can be used to improve process monitoring. Using an acoustic sensor to measure process stability, productivity will be greatly increased by reducing wire breakage in wire EDM and ultimately increase efficiency in all EDM processes by maximizing material removal rates.

5.2 Future Work

This section will provide suggestions for further development in using acoustic emission sensors for process monitoring of EDM. It is expected that the work completed in this thesis and the proposed further work will provide a complete fundamental basis for identifying and controlling the process state in EDM. Continuing research will help support the implementation of acoustic emission sensors in industry.

5.2.1 Effect of Crater Size

The pulse on-time and pulse current have a direct relationship with the plasma channel diameter and therefore the crater size [49]. Tests should be performed to investigate the relationship between plasma channel sizes, crater sizes, and the acoustic signal. Conducting more extensive single spark experiments, while collecting the acoustic signal, voltage signal, and current signal simultaneously could be useful. Comparing the acoustic signal, against different cases that are seen in the voltage and current waveforms (such as breaks in the pulse) can give more insight into the exact source of the acoustic signal. The occurrence of acoustic bursts have been investigated in this thesis, however a better understanding of the acoustic wave's source, shape, and amplitude is warranted. Examining the surface topography of the workpiece can be a method to relate crater size to the acoustic signal.

5.2.2 Workpiece Material

For this thesis, all of the experiments reported were conducted using mild steel as a workpiece. Therefore the speed in which the Rayleigh sound waves travelled through the workpiece was always constant and it was not surprising that the frequency range of the acoustic signal remained the same. Using a material with different properties would change the way in which the acoustic waves are produced and how they propagate through the material. It would be interesting to see how the acoustic signal responds to materials with very low or very high melting points. It would also be useful to investigate the use of other workpieces that are common in EDM such as carbide, tool steels, Inconel, and titanium.

Due to the different material properties, the AE data obtained would relate to the specific material. Further work could be done specifically to characterize the AE data as a function of the workpiece material.

5.2.3 Sensor Placement

One of the main focuses of this research was the material removal rate, and therefore the sensor was placed on the workpiece. The fact that the electrode used for this research was rotating, placing an acoustic sensor on the electrode was not a simple task, and was not investigated because it was not an area of interest in the scope of this thesis. In order to receive the full benefits of using AE sensors, it may be worth investigating the placement of a sensor on the electrode. A large concern in EDM deals with electrode wear as it is an important aspect in the reproduction of corners. For example, it was seen in section 4.7 that brass provided the strongest AE signal (or highest MRR), however brass is very seldom used in today's industry due to its higher wear rate [34]. When using the multi-material electrode in section 4.7, a lot more information could be obtained by placing sensors on the electrode as well.

The work done in this thesis shows a broad spectrum of the capabilities and benefits of acoustic emission sensors in EDM. From the several successful results obtained, it is believed that acoustic emission sensors have a promising future in the EDM industry. Continuing research in this area will provide several opportunities to gain practical knowledge of acoustic emission in EDM.

6 References

[1] M. Kunieda, B. Lauwers, K. Rajurkar, and B. Schumacher, “Advancing EDM through Fundamental Insight into the Process,” *CIRP Annals - Manufacturing Technology*, vol. 54, no. 2, pp. 64–87, 2005.

[2] K. Albinski, K. Musiol, A. Miernikiewicz, S. Labuz, and M. Malota, “The temperature of a plasma used in electrical discharge machining,” *Plasma Sources Science Technology*, vol. 5, no. 4, pp. 736–742, Nov. 1996.

[3] K. Ho, “State of the art electrical discharge machining (EDM),” *International Journal of Machine Tools and Manufacture*, vol. 43, no. 13, pp. 1287–1300, Oct. 2003.

[4] Y. F. Luo, “An evaluation of spark mobility in electrical discharge machining,” *IEEE Transactions on Plasma Science*, vol. 26, no. 3, pp. 1010–1016, Jun. 1998.

[5] O. Yilmaz and M. A. Okka, “Effect of single and multi-channel electrodes application on EDM fast hole drilling performance,” *The International Journal of Advanced Manufacturing Technology*, vol. 51, no. 1–4, pp. 185–194, Apr. 2010.

[6] C. B. Scruby, “An introduction to acoustic emission,” *Instrument Science and Technology*, pp. 946–953, 1987.

[7] C. Grosse and M. Ohtsu, *Acoustic Emission Testing: Basics for Research - Applications in Civil Engineering*, 1st ed. Berlin: Springer-Verlag, 2008.

[8] NDT Resource Center, “Introduction to Ultrasonic Testing.” [Online]. Available: www.ndt-ed.org/EducationResources/CommunityCollege/Ultrasonics/cc_ut_index.htm. [Accessed: 04-Jun-2013].

[9] L. Braile, “Seismic Waves and the Slinky: A Guide for Teachers,” *Purdue University*. [Online]. Available: http://web.ics.purdue.edu/~braile/edumod/slinky/slinky.htm. [Accessed: 04-Jun-2013].

[10] B. Muravin, “Acoustic Emission Wave Propagation and Source Location,” *Acoustic Emission Presentations*. [Online]. Available: www.muravin.com. [Accessed: 04-Jun-2013].

[11] A. Descoeudres, “Characterization of Electrical Discharge Machining Plasmas,” Ph.D. dissertation, Ecole Polytechnique Federal de Lausanne, 2006.

[12] M. Mahardika, K. Mitsui, and Z. Taha, “Acoustic Emission signals in the micro-EDM of PCD,” *Materials Research*, vol. 37, pp. 1181–1186, 2008.

[13] C. Smith, “Acoustic Emission Mapping of Discharges in Spark Erosion Machining,” M.S. Thesis, McMaster University, 2012.

[14] P. S. Pai and P. K. R. Rao, "Acoustic emission analysis for tool wear monitoring in face milling," *International Journal of Production Research*, vol. 40, no. 5, pp. 1081–1093, Jan. 2002.

[15] J. Webster and I. Marinescu, "Acoustic Emission for Process Control and Monitoring of Surface Integrity during Grinding," *CIRP Annals - Manufacturing Technology*, vol. 43, no. 1, pp. 299–304, 1994.

[16] A. W. Momber, R. S. Mohan, and R. Kovacevic, "On-line analysis of hydro-abrasive erosion of pre-cracked materials by acoustic emission," *Theoretical and Applied Fracture Mechanics*, vol. 31, no. 1, pp. 1–17, Feb. 1999.

[17] T. Masuzawa, X. Cui, and N. Taniguchi, "Improved Jet Flushing for EDM," *CIRP Annals - Manufacturing Technology*, vol. 41, no. 1, pp. 239–242, 1992.

[18] T. Masuzawa and C. J. Heuvelman, "A Self-Flushing Method with Spark-Erosion Machining," *CIRP Annals - Manufacturing Technology*, vol. 32, no. 1, pp. 109–111, 1983.

[19] P. Koshy, V. K. Jain, and G. K. Lal, "Experimental investigations into electrical discharge machining with a rotating disk electrode," *Precision Engineering*, vol. 15, no. 1, 1993.

[20] S. M. Markalous, S. Tenbohlen, and K. Feser, "Detection and Location of Partial Discharges in Power Transformers using acoustic and electromagnetic signals," *Dielectrics and Electrical Insulation*, vol. 15, no. 6, pp. 1576 – 1583, 2008.

[21] A. Cichon, "The Application of the Selected Time – Frequency Descriptors Detection of the Acoustic Emission Signals Generated by Multisource Partial Discharges," *ACTA Physica Poloncia A*, vol. 116, no. 3, pp. 290–293, 2009.

[22] Bharat Heavy Electricals Limited, *Transformers*. New York: McGraw-Hill, 2005.

[23] I. Inasaki, "Application of acoustic emission sensor for monitoring machining processes," *Ultrasonics*, vol. 36, pp. 273–281, 1998.

[24] H. V. Ravindra, Y. G. Srinivasa, and R. Krishnamurthy, "Acoustic emission for tool condition monitoring in metal cutting," *Wear*, vol. 212, pp. 78–84, 1997.

[25] H. Kayaba and I. Inasaki, "Detection of the Rotating Cutting Tool Failure with an Acoustic Emission Sensor," *The Japan Society of Mechanical Engineers*, vol. 60, no. 580, pp. 4374–4379, 1194.

[26] M. Wakuda, I. Inasaki, K. Ogawa, and M. Takahara, "Monitoring of the Grinding Process with an AE Sensor Integrated CBN Wheel," *Japan Society for Precision Engineering*, vol. 59, no. 02, pp. 275–280, 1993.

[27] A. Hase, H. Mishina, and M. Wada, “Correlation between features of acoustic emission signals and mechanical wear mechanisms,” *Wear*, vol. 292–293, pp. 144–150, 2012.

[28] J. Y. Kao and Y. S. Tarng, “A neutral-network approach for the on-line monitoring of the electrical discharge machining process,” *Journal of Materials Processing Technology*, vol. 69, no. 1, pp. 112–119, 1997.

[29] K. Ter Pey Tee, R. Hosseinnezhad, M. Brandt, and J. Mo, “Pulse Discrimination for Electrical Discharge Machining With Rotating Electrode,” *Machining Science and Technology*, vol. 17, no. 2, pp. 292–311, Apr. 2013.

[30] M. Weck and J. M. Dehmer, “Analysis and adaptive control of EDM sinking process using the ignition delay time and fall time as parameter,” *CIRP Annals - Manufacturing Technology*, vol. 41, no. 1, pp. 243–246, 1992.

[31] D. Dauw, “On-line Identification and Optimization of Electro-discharge Machining,” Ph.D. dissertation, K.U. Leuven, Belgium, 1985.

[32] S. K. Bhattacharyya and M. F. El-Menshawy, “Monitoring the E.D.M. process by radio signals,” *International Journal of Production Research*, vol. 16, no. 5, pp. 353–363, 1978.

[33] C. Smith and P. Koshy, “Applications of acoustic mapping in electrical discharge machining,” *CIRP Annals - Manufacturing Technology*, vol. 62, no. 1, pp. 171–174, 2013.

[34] R. Kern, “Sinker Electrode Material Selection,” *EDM Today*, July/August edition, 2008.

[35] P. M. Lonardo and A. . Bruzzone, “Effect of Flushing and Electrode Material on Die Sinking EDM,” *CIRP Annals - Manufacturing Technology*, vol. 48, pp. 123–126, 1999.

[36] Mersen, “Graphite Advantages.” [Online]. Available: http://www.edm.mersen.com/.

[37] Kistler, “Piezotron ® Sensor,” 2007.

[38] Kistler, “Piezotron ® Coupler,” 2006.

[39] National Instruments, “S Series Multifunction DAQ 12 or 16-Bit , 1 to 10 MS / s , 4 Analog Inputs,” 2005.

[40] C. Schüldt, F. Lindstrom, H. Li, and I. Claesson, “Adaptive filter length selection for acoustic echo cancellation,” *Signal Processing*, vol. 89, no. 6, pp. 1185–1194, Jun. 2009.

[41] J. Webster, W. P. Dong, and R. Lindsay, “Raw Acoustic Emission Signal Analysis of Grinding Process,” *CIRP Annals - Manufacturing Technology*, vol. 45, no. 1, pp. 335–340, Jan. 1996.

[42] E. Weingärtner, K. Wegener, and F. Kuster, "Wire electrical discharge machining applied to high-speed rotating workpieces," *Journal of Materials Processing Technology*, vol. 212, no. 6, pp. 1298–1304, Jun. 2012.

[43] Pearson Electronics Inc., "Pearson Current Monitor Model 411," 2002. [Online]. Available: www.pearsonelectronics.com.

[44] M. Bayramoglu and A. W. Duffill, "CNC EDM of linear and circular contours using plate tools," *Journal of Materials Processing Technology*, vol. 148, pp. 196–203, Apr. 2004.

[45] N. Saito and K. Kobayashi, "Machining Principle and Characteristics of Electric Discharge Machining," *Mitsubishi Denki Giho*, vol. 41, no. 10, pp. 1222–1230, 1967.

[46] O. Blatnik, J. Valentincic, and M. Junkar, "Percentage of harmful discharges for surface current density monitoring in electrical discharge machining process," *Proceedings of the Institution of Mechanical Engineers, Part B: Journal of Engineering Manufacture*, vol. 221, no. 12, pp. 1677–1684, Jan. 2007.

[47] J. Kapoor, S. Singh, and J. S. Khamba, "Recent Developments in Wire Electrodes for High Performance WEDM," *Proceedings of the World Congress on Engineering*, vol. II, pp. 2–5, 2010.

[48] Agie, *Agietron Impact, Innovation, Exact*. Losone, 2002.

[49] S. H. Yeo, W. Kurnia, and P. C. Tan, "Critical assessment and numerical comparison of electro-thermal models in EDM," *Journal of Materials Processing Technology*, vol. 203, no. 1–3, pp. 241–251, Jul. 2008.

[50] Tektronix, "High Voltage Differential Probes," 2005. [Online]. Available: www.tektronix.com.